# SNOW AVALANCHES ON THE SAN FRANCISCO PEAKS,

## COCONINO COUNTY, ARIZONA

Leland R. Dexter, Ph.D.

# Preface to the Digitally Reconstructed Edition

1973 was a pivotal year for avalanches and avalanche awareness on the San Francisco Peaks. Sometime in February of that year, an extremely large avalanche fell from the upper southeastern slopes of Humphreys Peak, shot over the high cliff at the base of the southeast face, and ran into Dunnam Canyon tearing out hundreds of mature spruce and fir trees lining both sides of the older and smaller runout zone. The remnants of this huge avalanche remained undiscovered for many days due to the sparse winter recreational use at that time. This event changed the face of the Peaks and fired the awe and imagination of those who saw its aftermath.

However, in the early seventies the winter recreational use pattern on the Peaks was also beginning to change. More and more Alpine skiers were hiking to the Agassiz-Humphreys ridge, skiing out the Inner Basin, and catching a ride back to Flagstaff on Highway 89. Across the U.S., Nordic skiing was being re-popularized with the introduction of lightweight Scandinavian-made ski gear. Everywhere, skiing and mountaineering shops were adding cross-country ski gear, in all of its forms from racing to telemarking, to their winter product mix. Soon skiers and ski tracks could be seen in some of the most remote reaches on and around the Peaks.

In 1973, as part of the requirements for our USFS special use permit for commercial ski-guiding on the Peaks, I attended my first Silverton Avalanche School. I was immediately enamored with the science behind snow avalanches. In the years that followed, several like-minded avalanche enthusiasts from Flagstaff formed the core of what became known as the San Francisco Mountain Avalanche Project (see the history of SFMAP document on the KPAC website). From 1977 through 1981 this group formally studied snow avalanche activity on the Peaks.

In the fall of 1979, I enrolled in the Master's Degree program in Earth Science at Northern Arizona University. After "shopping" numerous departments Dr. Stanley Beus, then in charge of the Earth Science program, was the only one who would listen to such a crazy proposal as studying avalanches on the San Francisco Peaks. After all, this is Arizona and everyone knows avalanches don't happen in Arizona. Along with Dr. Beus, I was also able to enlist the assistance of Dr. Charles C. Avery from Forestry (advisor and committee chair), Dr. Stanley Swarts from Geography, and Dr. Gordon Johnson from Physics/Atmospheric Science to sit on my interdisciplinary committee. While the overall research design was much larger than a single thesis question, one could frame an overarching thesis statement as "do snow avalanches occur commonly in Arizona?". In July of 1981, after two years of hard but interesting work, I successfully defended my research and, based on that work, the answer to the question posed above is a resounding "yes".

Contrary to my expectations, little attention was paid to the final bound document which was made available on the open shelves and in Special Collections at Cline Library. But as the years wore on and more winter recreationists began encountering avalanches on the Peaks, interest in the avalanche phenomenon has grown and I have had numerous requests for the map and even the full thesis document. Even though this work is thirty years old, it still remains the only substantial formal study of snow avalanches on the San Francisco Peaks.

I have finally put in the effort and this .PDF document is a digital reconstruction of that thesis. The original paper was created with an electric typewriter and the figures were hand-drawn or hand-enhanced versions of very simplistic dot matrix computer printout. In creating this digital reconstruction the overall flavor of the original paper is preserved as much as possible. The original figures are used and the text font, page layout etc. is set to mimic the typewritten manuscript with the exception that all landscape format figures and tables are all rotated to portrait format. The paper avalanche zone map included with the original thesis has also been reproduced for inclusion with this document for historical accuracy. The updated GIS-produced 2006 version (optimized for 22 x 34 inch format printing), is included as well.

It is hoped that the digital version of both the map and the thesis will be more widely distributed and will inspire additional avalanche studies on the Peaks.

In the years since the original work was done several notable avalanches have been observed on the Peaks. It may be of interest to add a small set of notes here that recap notable avalanche activity on the mountain. This following summary is a blend of data from my research work and from that of later observers. It covers the period from 1930 to 2005 which marks the formation year of the Kachina Peaks Avalanche Center. Hopefully data like these will continue to be gleaned and recorded from the yearly comments accruing on the KPAC discussion board.

1932 - Widespread avalanching, 4 out of 5 tree-ring monitored paths indicate events on all aspects. Allison Clay and Snowslide Canyon run huge.

1949 - Widespread avalanching, 4 out of 5 tree-ring monitored paths indicate events on all aspects.

1952 - Widespread avalanching, 5 out of 5 tree-ring monitored paths indicate events on all aspects.

1960 - Widespread avalanching, 4 out of 5 tree-ring monitored paths indicate events on all aspects.

1965 - Widespread avalanching, 4 out of 5 tree-ring monitored paths indicate events on all aspects.

1966 - Widespread avalanching, 4 out of 5 tree-ring monitored paths indicate events on all aspects.

1972-73 - Widespread avalanching, 5 out of 5 tree-ring monitored paths indicate events on all aspects. Dunnam Canyon runs huge.

1977-78 - 17 avalanches were reported by SFMAP observers, some as large as class 4.

1978-79 - 17 avalanches were reported by SFMAP observers, some as large as class 4.

1979-80 - 12 avalanches were reported by SFMAP observers, some as large as class 4.

1980-81 - numerous avalanches were reported by SFMAP observers, but formal record keeping had ceased and a total is not available.

1985 - Avalanche cycle in Crossfire.

1993 - Allison Clay runs big from south ridge loading. Numerous trees removed from the south side of the starting zone. Snow remains all year in the runout under tree debris.

1995 - A huge and fatal avalanche in Monte Vista on the “Southside” due to prolonged north wind loading. Human triggered class 5 hard slab during an otherwise unremarkable winter.

2005 - Crossfire runs huge wiping out the upper part of the Aubineau Canyon Trail.

From the above list, it can noted that; 1) very large avalanches occur on every aspect of the San Francisco Peaks, and 2) the only fatal avalanche thus far ran huge on a southern aspect in a relatively mediocre winter!

One other point of interest can be seen the results presented in the thesis. A three to five year avalanche and snowfall cycle is clearly defined in the autocorrelation analysis. El Nino was not known in the avalanche community at the time; but since then the wide-spread effects of El Nino events on the climates of the United States (especially the southern tier states) have become well known. This tree ring work, done in 1981, clearly picked up an El Nino signal in snow avalanche activity.

Leland R. Dexter

Digital preface photos:

Title page – 2 meter crown fracture, January 1995 Monte Vista Path event (Merrianne Etter photo).

Page 1 – Damage to vegetation from the February 1973 Dunnam Canyon Path event (Lee Dexter photo).

Page 5 top – 2 meter blocks litter the starting zone and the crown fracture is visible above, January 1995 Monte Vista Path event (Lee Dexter photo).

Page 5 bottom – View down Aubineau Canyon showing rebound zones, recent damage is from a 2005 event in Crossfire (Art Pundt photo).

Page 6 - View into the upper half of the Monte Vista Path event, January 1995 (Lee Dexter photo).

# SNOW AVALANCHES ON THE SAN FRANCISCO PEAKS,

# COCONINO COUNTY, ARIZONA

---

Graduate Research

Presented to the Graduate Faculty

Northern Arizona University

---

In Partial Fulfillment

of the Requirements for the Degree

Master of Science

(Earth Science)

---

by

Leland R. Dexter

April, 1981

SNOW AVALANCHES ON THE SAN FRANCISCO PEAKS,

COCONINO COUNTY, ARIZONA

---

Graduate Research in Earth Science

In Partial Fulfillment

of the Requirements for the Degree

Master of Science

---

by

Leland R. Dexter

Approved:

Chuck C. Avery

Stanley W Swarts

Stanley S. Beus

Gordon P. Johnson

Date: 28 July 1981

TABLE OF CONTENTS

LIST OF ILLUSTRATIONS

Figure | Page

Figure Page

Figure Page

LIST OF TABLES

ABSTRACT

Sixty-six potential avalanche paths are recognized on the San Francisco Peaks. These paths usually start in basins above timberline which receive abnormally high snow loads. The tracks and runout zones extend well down into heavy timber.

Records of winter weather patterns indicate Pacific storm systems with both cold air and high moisture levels account for most avalanche producing storms. Many times, snowfall from these storms is deposited over a radiation weakened snowpack resulting in very large climax avalanche events. A thaw-related spring avalanche cycle is also found.

Tree ring studies indicate substantial event activity over the past fifty-one years. Very large events occurred in 1932 and 1973. A return time figured for large tree damaging events yields 4.25 years per path.

Recent observations of actual avalanche events by skiers suggest most activity on the Peaks results from either climax or direct action events. An average of 15 events per year was observed. It appears that snow avalanches affect the San Francisco Peaks more frequently and with greater magnitude than was previously thought.

ACKNOWLEDGMENTS

Much of this work would not have been possible without the direct assistance of all members of the San Francisco Mountain Avalanche Project. Especially valuable assistance was provided by Art Pundt and Ken Walters.

Additional assistance was provided by Thor Karlstrom, United States Geological Survey; Frank Ronco, United States Forest Service; Ron Reid, United States Forest Service; Jeffery Dean, Laboratory of Tree Ring Research; Richard and Betsy Armstrong, San Juan Avalanche Project.

The writer wishes to thank Dr. Charles Avery, Dr. Stanley Beus, Dr. Gordon Johnson and Dr. Stanley Swarts for serving as interdisciplinary committee members. Finally, the greatest appreciation of all is extended to my wife Kris for much needed moral support.

# Chapter 1

# INTRODUCTION

## Location and Access

The study was limited to the area above 8,000 feet (2,438 meters) on the San Francisco Peaks, Coconino County, Arizona. The study area covers about 10 square miles (26 square kilometers) on the Peaks centered around the intersection of 35°20' north latitude and 111°04' west longitude, approximately 10 miles (17 kilometers) north of the city of Flagstaff (Figure 1).

Access to the area is via a network of forest roads situated between U.S. Highway 180 on the west and U.S. Highway 89 on the east. Most of these roads are open to vehicles during the dry months but are closed by snow in mid winter.

## Geographic Setting

The San Francisco Peaks consist of several high points situated on the eroded rim of a large volcanic cone. This cone marks the primary vent of the San Francisco Volcanic Field (Robinson, 1913) (Holm, 1974) during Pliocene-Pleistocene time (Pewe and Updike, 1970). The San Francisco Volcanic Field overlies thick Paleozoic sediments (with some remnant Mesozoic sediments) which were broadly uplifted beginning in Late Tertiary time to form the southwestern edge of the Colorado Plateau (Wilson, 1962).

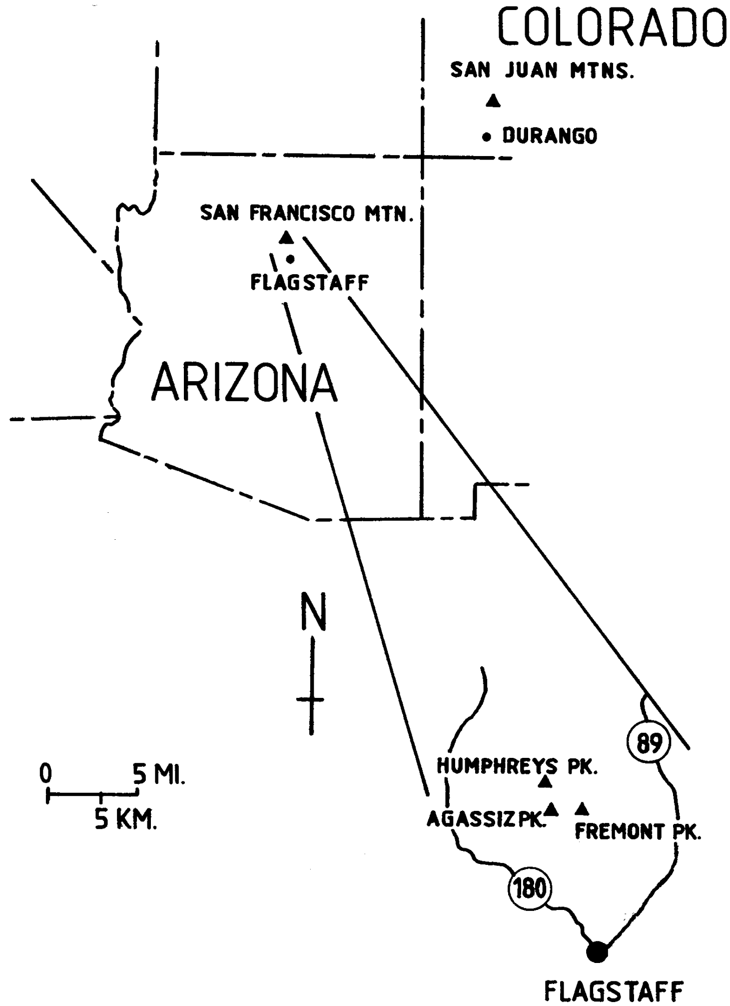


Figure 1. Index map.

The regional topography rises in a series of steps eastward from elevations around 500 feet (152 meters) at the Colorado River, to elevations around 7,000 feet (2,134 meters) on the Coconino Plateau (Figure 2). The San Francisco Peaks rise another 5,000 feet (1,524 meters) to a cumulative elevation of 12,633 feet (3,581 meters) at the summit of Humphreys Peak, the highest point in Arizona. The mountain is a large cone with a central caldera which breaches the crater rim to the northeast. The caldera forms the Inner Basin and Interior Valley which have been modified by Pleistocene glaciation (Pewe and Updike, 1976). The radial drainage from the mountain is redistributed into shallow meandering stream channels following the regional drainage. The north, east, and south slopes drain into the Colorado River via the Little Colorado River. Only a small portion of the west slope drains into the Colorado River via the Verde and Salt Rivers.

The wide range of elevations occurring in the area creates a vertically zoned vegetation distribution. C.H. Merriam (1890) worked out his classic "life zone" study on this mountain. Merriam based his zones on vegetation associations which are currently regarded as: Arctic-Alpine (above 12,000 feet, 3,658 meters), Hudsonian (11,000 to 12,000 feet, 3,353 to 3,658 meters), Canadian (9,000 to 11,000 feet, 2,743 to 3,353 meters), Transition (7,000 to 9,000 feet, 2,134 to 2,743 meters), Upper Sonoran (4,000 to 7,000 feet, 1,219 to 2,134 meters), Lower Sonoran (below 4,000 feet, 1,219 meters). Vegetation found specifically on the San Francisco Peaks includes:

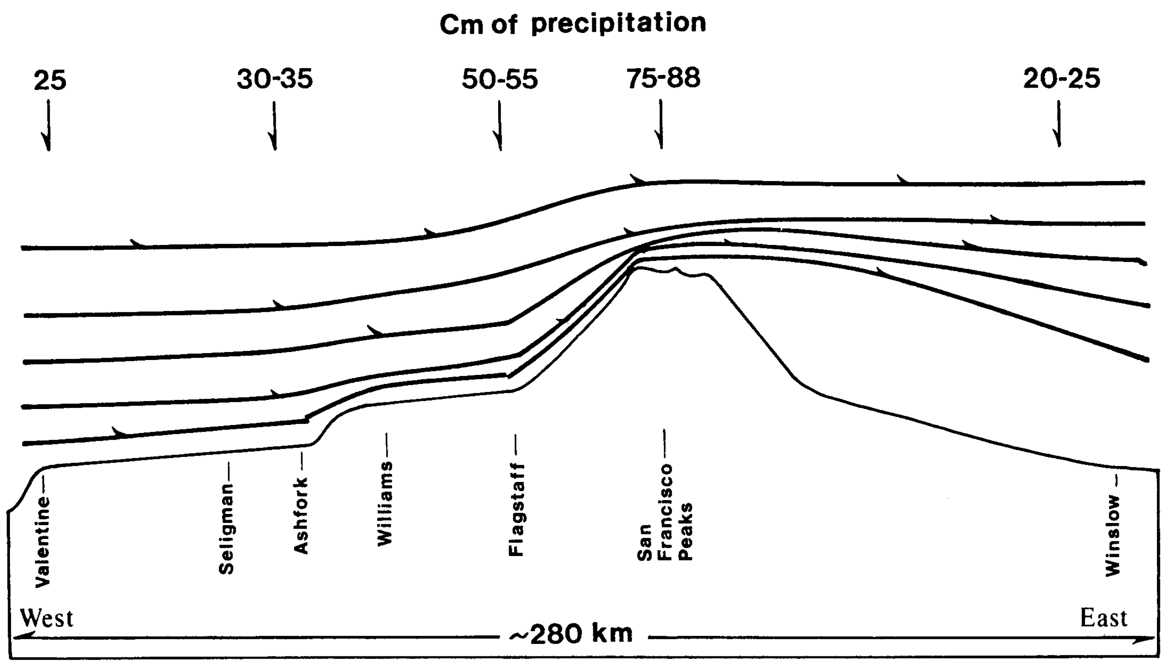


Figure 2. Precipitation, air flow, and topography across Northern Arizona (after Pewe and Updike, 1976).

tundra and alpine vegetation (above 11,500 feet, 3,505 meters), bristlecone pine, Engelmann spruce and corkbark fir (between 10,000 and 11,500 feet,3,408 to 3,505 meters), aspen and Douglas fir (between 8,500 and 10,000 feet, 2,590 to 3,408 meters), ponderosa pine, oak, and juniper(below 8,500 feet, 2,590 meters).

A variety of fauna is found on the mountain including: elk, mule deer, porcupine, coyote, kestrel, grayheaded juncos, Steller's jay, mountain chickadee, nighthawk, water pipit, and dwarf shrew (Aitchison, 1977).

The general climate can be described as a semi-arid highland with two distinct precipitation periods. Winter precipitation results from the passage of cyclonic storm systems, and usually falls as snow. Summer precipitation results from the northward flow of moisture laden air from the Sea of Cortez, or moist easterly waves from the Gulf of Mexico (Sorenson, 1974). When this moist air is lifted by thermal, orographic or frontal processes, intense thunderstorm activity can be produced. Measurements of precipitation falling on the higher portions of the mountain produced abnormally large deviations (Colton, 1958) indicating great microscale precipitation variation. Figure 2 represents the mean precipitation distribution across Northern Arizona.

## Purpose and Scope

Historically, man has had little to do with the San Francisco Peaks in winter and only since the nineteen-thirties has any significant winter usage come about. Since that time, an Alpine ski facility has been in operation on the west slope of the mountain. Other uses, such as logging, grazing, water development, tourism (e.g. use of the defunct Weatherford Road), or astronomy (e.g. operation of Lowell's old Doyle Peak station) were restricted to summer-like conditions.

Within the last few years however, expanded use of the winter backcountry has occurred. This writer believes such use is resulting from the coincident timing of two factors: 1) the rise in popularity of Nordic skiing in the United States and 2) the opening of the Flagstaff City Watershed to daytime recreation use. For the first time in history, the chance for man-avalanche encounters on the Peaks has become significant. Such encounters have, in fact, already occurred.

It is the purpose of this study to lay the foundation for avalanche research on the San Francisco Peaks. A survey approach has been applied in an effort to gain as much basic knowledge of all facets of the topic as is practical within a limited time. The study area was defined to be that portion of the Peaks above 8,000 feet (2,438 meters). The study period was defined as the last 51 years (1930 through 1980).

## Methods

Research of a survey-type problem incorporates many methods:

1) Avalanche Terrain

   A) Field inspection
   B) Air photo mapping
   C) Overflights
   D) Vegetation analysis

2) Snow Climate

   A) National Oceanic and Atmospheric Administration records
   B) Arizona Snow Survey records
   C) Snowpack observations from high elevation (11,250 feet, 3,429 meters) study plots
   D) Data from the San Juan Avalanche Project

3) Dendrochronologic Analysis

   A) Disc sampling of downed trees
   B) Increment core sampling of living trees
   C) Computer analysis of data

4) Recent Events

   A) Ski reconnaissance
   B) Overflights

More detailed methodology will be presented in the appropriate chapter.

## Previous Work

Prior to 1973, virtually no work dealing with snow avalanches had been carried out on the San Francisco Peaks. In 1973, a newspaper article (Arizona Daily Sun, 1973) reported on a spectacular avalanche which had overrun the bounds of the Dunnam Canyon path during the winter of 1972-1973. In the same article, James Beard (former Flagstaff Water Superintendent) presented his views on avalanche frequency on the Peaks. "Avalanches are not common in the area but they do take place once every two or three years". Beard also speculated on the cause of the large event in

Dunnam Canyon, "... new snow came in on top of the already glazed snow in the area and weight became too great". Following the event a weak spate of interest in avalanche study occurred.

Bill Breed (1977) sampled some of the trees knocked down by the 1973 Dunnam Canyon event. Breed determined an age for the trees (and a return time for the event) of over 100 years. Duncklee (ca. 1974) made some educated guesses relating to overall avalanche activity on the Peaks in an unpublished paper on man-land re1ationships. No other work has followed, and only those few pages exist in the literature.

In the San Juan Mountains of Colorado a very extensive avalanche study was undertaken during the nineteen-seventies by the Institute of Arctic and Alpine Research (abbreviated INSTAAR) of the University of Colorado. This study originated through interest in the effects of cloud seeding on avalanche activity. Funding was provided by the Bureau of Reclamation. During the time the project was active, a large amount of research was done, mainly along U.S. Highway 550 between Durango and Ouray, Colorado (Armstrong and Armstrong, 1978).

# Chapter 2

# AVALANCHE TERRAIN

## Methods

Visits to the study area indicated avalanche activity had occurred at several localities, especially at those above 10,000 feet (3,408 meters) elevation. Initial efforts were directed at cataloging the physical characteristic of the most obvious avalanche paths. As the number of cataloged paths increased (66 paths have been named), the value of an overall mapping project became apparent.

The 7½ minute series U.S. Geological Survey map of the Humphreys Peak quadrangle was selected as the base map for the project. Aerial photography from four separate missions was made available on a loan basis from the Flagstaff District of the Coconino National Forest. The missions were; DIN (1949, 1:15,840), EGE (1959, 1:15,840), ERZ (1969, 1:15,840), and 613040 (1978, 1:24,000). Unfortunately, complete coverage of the study area was not available from a single mission, but complete coverage was obtained by combining all four missions. Figure 3 shows the coverage obtained from each mission. The 1:15,840 photography provided adequate resolution and good detail for the work at hand, while the 1:24,000 photography provided excellent resolution and adequate detail. Photography at the 1:15,840 scale with the resolution of the newer small scale photography would have been ideal.

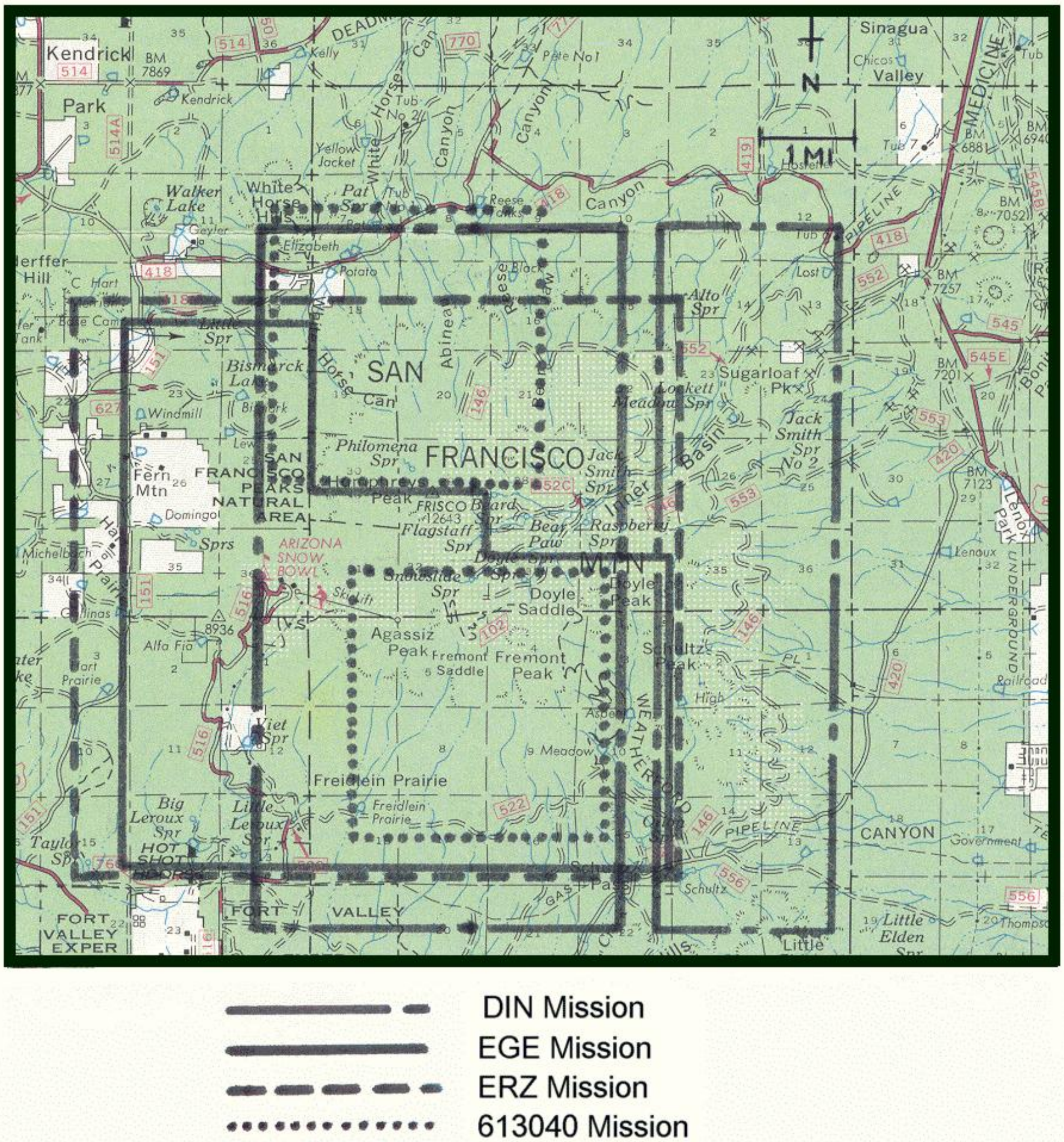


Figure 3. Location index of aerial photography used in mapping.

A Bausch and Lomb ZT4-H Zoom Transfer Scope was used to plot the desired photographic details onto the base map. This instrument superimposes a rectified, ratioed, and stretched image of the photography onto the base map. The operator views the superimposed image through a binocular system and varies the amount of light from each image source to check the match. The final fit of the photography to the map is accomplished as follows:

1) Image rotation to approximate orientation.
2) Zoom to approximate scale.
3) Stretch to match shape.
4) Rotate image to better orientation.
5) Zoom to better scale.
6) Stretch to better shape match.
7) Translate to re-register.
8) Repeat the above steps until fit is acceptable.

A 2x map lens was used to match photo and map scales. Control was maintained by continually matching topographically unique points (such as summits, ridge intersections, and canyon confluences) from photo to map. An effort was made to minimize parallax error by using only the central portion of the photo. As mapping progressed, the images were continually aligned with topographic controls adjacent to the immediate plotting area.

Paths which were known to avalanche from field checks, and paths which presented photographic evidence indicating they could avalanche, were given solid outlines on the base map. Areas of questionable avalanche activity were given dashed outlines. In most cases, the lower portions of the path (runout zones) were mapped from vegetative criteria while the upper portions (starting zones) were mapped from geomorphic criteria.

Once the paths were outlined, the general slope angle for three avalanche related gradient/vegetation zones were mapped as follows:

1) Slopes 25 degrees or steeper without timber.

   This terrain type conservatively contains all the major starting zones, and is almost completely occupied by them.

2) Slopes 25 degrees or steeper with timber.

   This terrain type contains occasional starting zones (usually of smaller paths) and the tracks of the larger paths.

3) Slopes 15 to 20 degrees usually with timber.

   This terrain type defined the lower limit of slide activity, and usually contains the lower track and runout zones of most large paths.

The boundaries of the gradient/vegetation zones were mapped using the following formula:

$$HI = (CI / TAN\Theta^{o}) * (1/24{,}000) * 12 \qquad (1)$$

Where $\Theta$ is the desired limiting angle in degrees, $CI$ is the contour interval in feet, and $HI$ is the horizontal distance in inches between each contour necessary to achieve $\Theta$. By setting a pair of dividers to $HI$, points of equal $\Theta$ were plotted and connected.

An attempt was made to assess plotting errors introduced by parallax, line width, and operator error (Figure 4). Three photos of one path were selected.

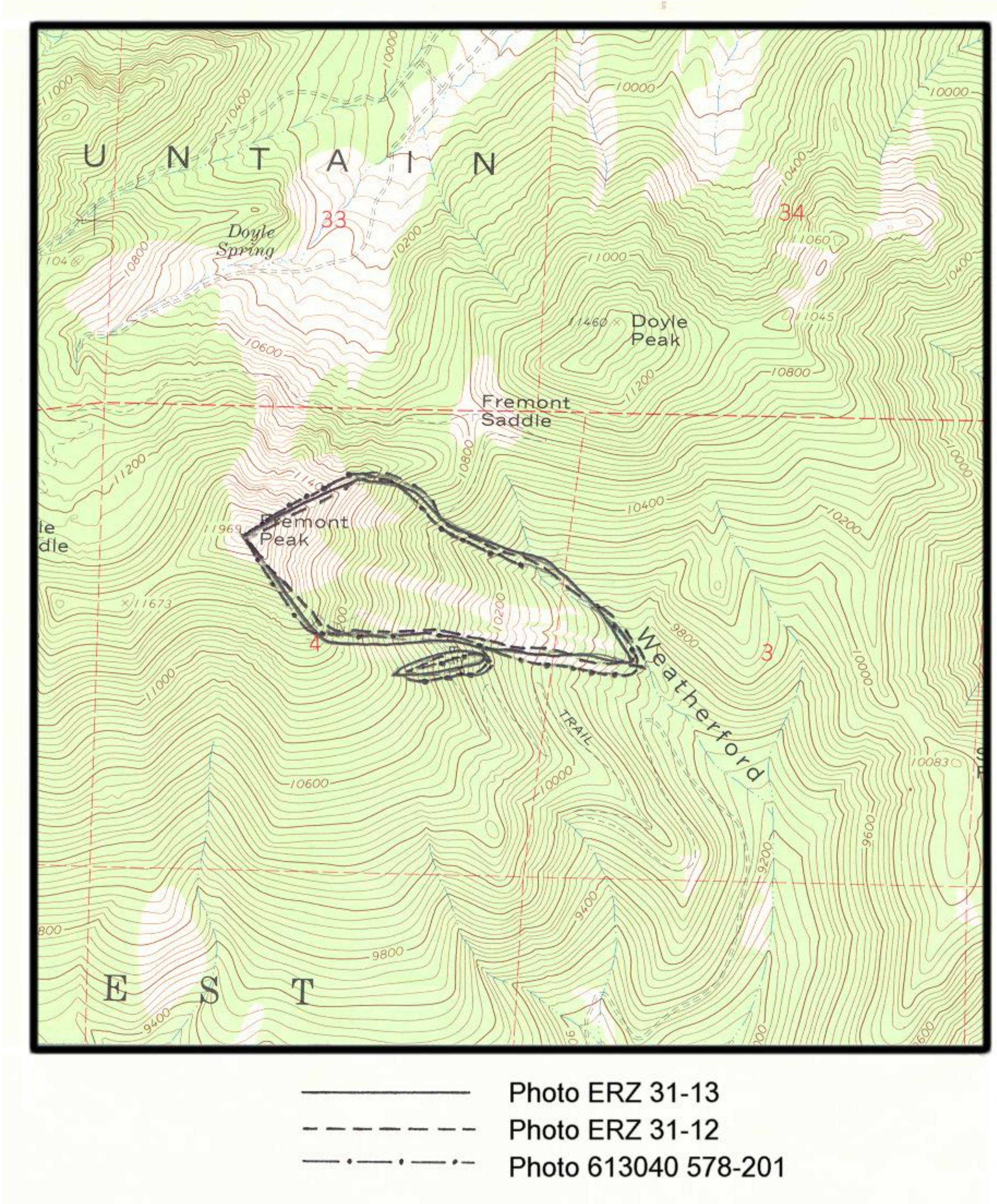


Figure 4. Plotting error.

One photo had the path near the principle point at 1:15,840 scale, another had the path near the edge of the print at 1:15,840 scale, and the last photo had the path near the principle point at 1:24,000 scale. Each photo was optically matched and plotted. The resulting three figures were then plotted on the same base map. Using the primary contour lines of the base map as sample transects, the maximum plot variance was measured, converted to feet of ground distance, and treated statistically to estimate error. The resulting error was found to be 122 feet +/-17 feet with a 95 percent confidence level. This procedure assumes the worst possible plotting situation.

During the years 1977 through 1981 summer and winter field trips to the study area were conducted. A number of these trips were used to check the accuracy of the air photo mapping. During these trips, it became apparent that several areas displayed signs of large and/or repeated avalanche activity. These areas include:

1) The Abineau Canyon group.
2) Beard Canyon.
3) Dunnam Canyon.
4) Snowslide Spring Canyon.
5) The North Fremont Peak group.
6) The East Fremont Peak group.
7) The Reese Peak group.
8) Allison Clay Path.

Several paths from these areas were used for other portions of this study. Since these paths were singled out for various reasons, more detailed mapping followed. Photographic enlargements of the base map were used for this mapping.

## General Characteristics

### Geomorphic Considerations

Mellor (1969), Perla and Martinelli (1976), and others have published average slope angle limits for avalanche activity (Figure 5). Generally speaking, snow does not accumulate in large amounts on slopes steeper than 60 degrees, but rather sluffs off continuously during deposition. Snow deposited on slopes shallower than 15 degrees rarely slides because the bulk compressive component overcomes the shear component even in the weakest of snowpacks. It is on slopes between 25 degrees (Mellor, 1968) or 30 degrees (Perla and Martinelli, 1976) and 60 degrees that most large avalanches start; and the largest events appear to originate in the lower half of that range (Perla and Martinelli, 1976).

Although avalanche events may be active only a few seconds out of any given number of years, they tend to occur repeatedly in the same area (see Chapter 4) following topographically low channels termed paths. Paths generally originate on steep slopes in areas of abnormally high snow deposition (usually on leeward slopes). More specifically, the avalanche path can be divided into three zones, sometimes geomorphically separable from each other and sometimes not (Figure 6). The area where the slides originate is referred to as the starting zone and it is usually the steepest portion of the path.

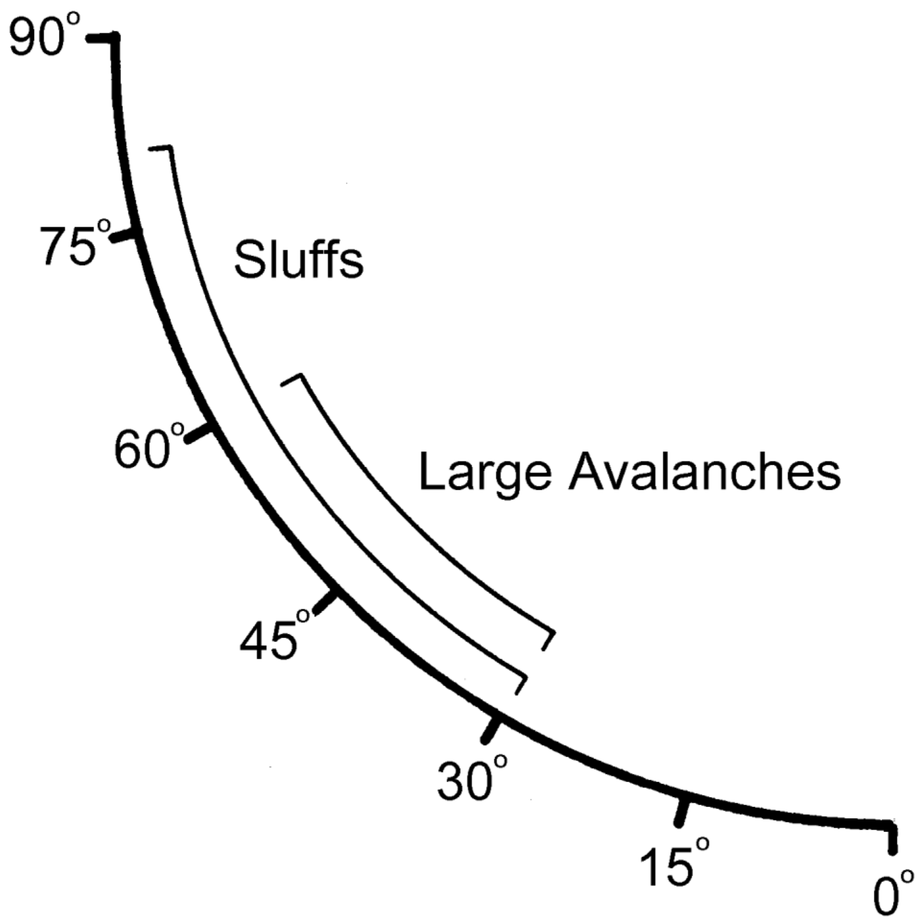


Figure 5. Generalized avalanche starting zone angles.

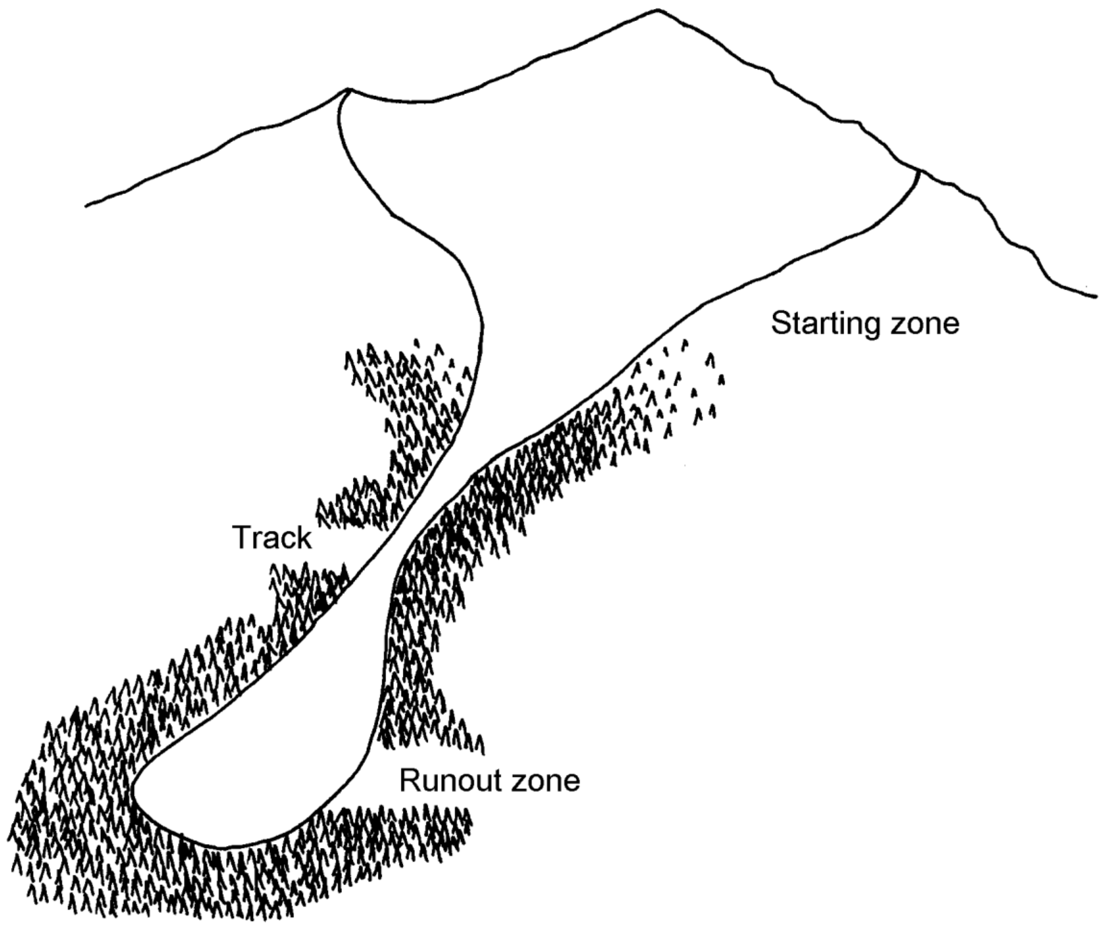


Figure 6. Avalanche path nomenclature.

It is here where stress is maximized and failure most often occurs (Martinelli, 1974). Starting zones of paths on the San Francisco Peaks typically range from 33 degrees to 40 degrees. Most are above timberline and are covered with volcanic blocks and cinders. Starting zones near or below timberline are typically less blocky and occasionally grass covered.

Starting zones may be simple open slopes (e.g. Sneaky Pete, #070), or complex multi-branched basins (e.g. Silverton, #090) (Appendix 3). Most paths on the Peaks have a simple single-basin starting zone, though a few have some form of low topographic divide that breaks the starting zone into two or more partitions.

The track is that portion of the path over which the entire mass of snow runs during its descent. Tracks may be confined to a gully system or unconfined over open slopes, through trees, over benches, or over small hills and other minor terrain features (Martinelli, 1974). Most tracks have angles less than the starting zone above. Typical track angles on the Peaks range from 15 degrees to 35 degrees and track lengths extend up to 5,000 feet (1,524 meters). Tracks on the Peaks are surfaced by a mixture of volcanic rubble, brush, small trees, and grass.

The runout zone is the area of deceleration and deposition at the bottom of the path. The angle is usually shallow and may even grade into an upslope area across a canyon bottom from the rest of the path (Perla and Martinelli, 1976) (e.g. Crossfire, #360).

Runout zone slopes on the Peaks range from about 10 degrees to 20 degrees. They are covered with volcanic rubble, overgrown with brush, small trees or grass, and are littered with vegetation debris.

## Vegetation Consideration

Depending on the geographic locale, avalanches may penetrate below timberline and affect the vegetation in some fashion (Martinelli, 1974). The San Francisco Peaks are an area of relatively high avalanche-forest interaction. The first order effect of avalanching on forests is the obvious clear swath of the path downslope through the timber. Several second order effects may also be present.

High Frequency Channel. This term is applied by this writer to that portion of a path which is swept much more frequently than the large event boundary may suggest (Figure 7). The event frequency of any path depends on several factors, but most paths which have high frequency channels would typically run at least once every season or two. This portion of the path is usually devoid of any significantly sized vegetation.

Trimlines. Trimlines are clearly marked edges in forest, scrub, or other vegetation which are produced by avalanche activity (Burrows and Burrows, 1976). Most trimlines on the Peaks represent the action of very large events of long return periods. Trimlines have been identified in at least the following paths; Allison Clay (#450), Crossfire (#360), North Ridge (#370), Hohokam (#340), Sinagua (#350), Dunnam Canyon (#210), Snowslide (#170), Zipper (#240),

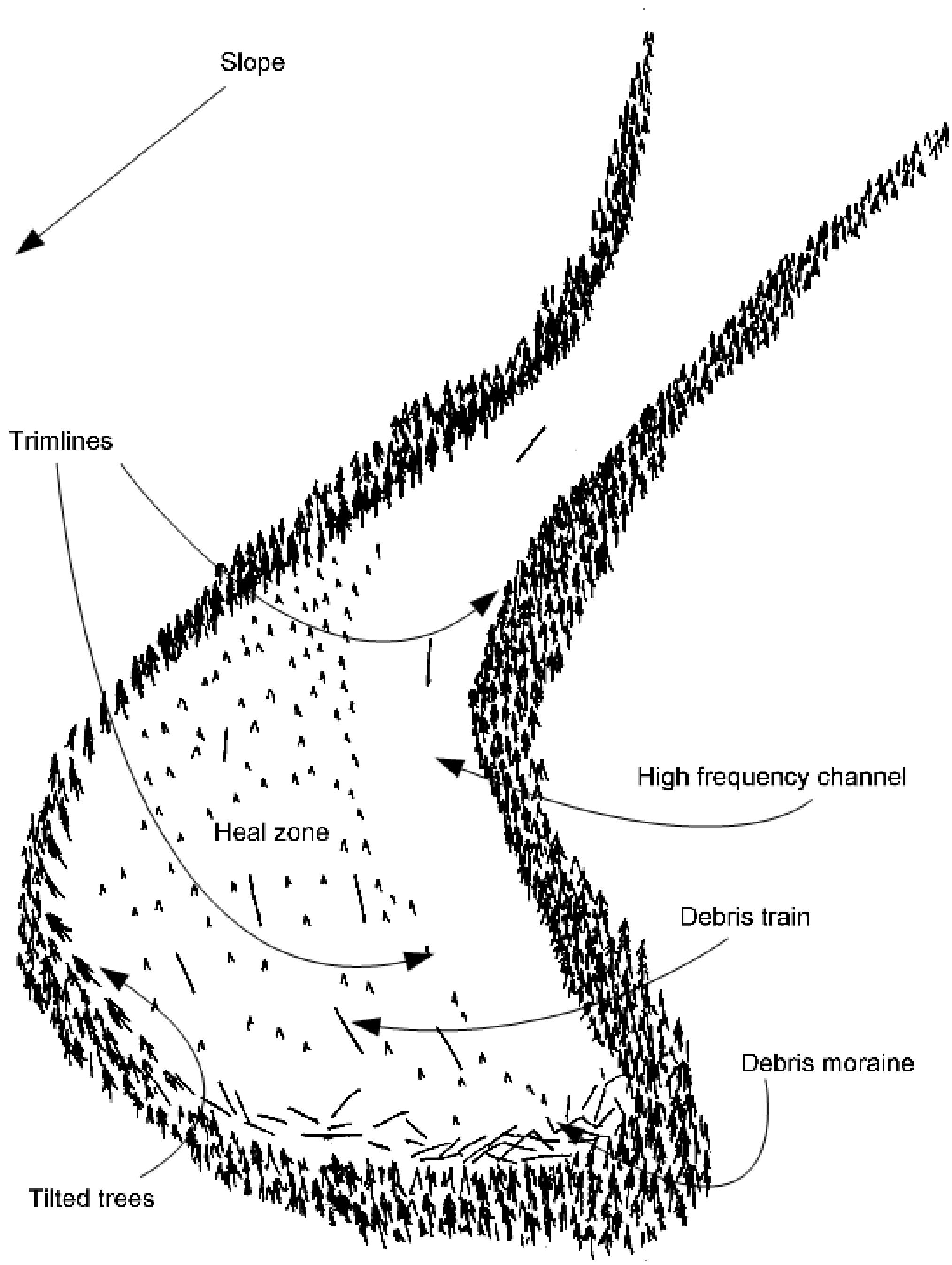


Figure 7. Vegetation modification along avalanche paths.

Pipeline (#420), White Horse (#400), Telemark (#100), and Silverton (#90).

Heal Zone. This term, also applied by the writer, is used to define the area between two adjacent trimlines. The age of the recolonized vegetation in the heal zone should give clues to the date of the clearing event that last maintained the adjacent trimline (see Chapter 4).

Debris Moraines and Debris Trains. These features result from the deposition of displaced vegetation. Moraines result from a pileup of trees carried to the toe of the runout zone in the avalanche. Trains result from the alignment of knocked-down timber by the flow.

Individual Damage. Each tree growing in an area of potential avalanche activity is a station with the ability to record indicators of past events. Damage such as tilting, scarring, and breaking may be used to estimate parameters of such events (See Chapter 4) (Burrows and Burrows, 1976).

## Terrain Characteristics of Six Selected Paths

During the course of this study, certain paths were singled out for various reasons. Six of these paths are described in detail (Figures 8-25) to present a closer view of avalanche terrain on the San Francisco Peaks. It is perhaps not coincidental that these paths are among the largest and most active within the study area. Five of the paths were used in tree ring dating past events.

Telemark (#100)was not used but is included here because it is by far the most active path on the mountain in light of recent observations.

Figure 8.

## AVALANCHE SUMMARY SHEET

**PATH NAME:** Beard Canyon **REFERENCE NO.:** 220

**SPECIFICATIONS:**

**ASPECT:** East **LOADING DIRECTION:** Northwest to Southwest

**TOP ELEV.:** 12,600' 3,840m **BOTTOM ELEV.:** 10,200' 3,170m **FALL:** 2,200' 671m

**PATH LENGTH:** 4,700' 1,433m **NO. OF STARTING ZONES:** 2

| | STARTING ZONE: | TRACK: | RUNOUT ZONE: |
|---|---|---|---|
| SLOPE ANGLE: | $34^{\circ}$ | $31^{\circ}$ | $18^{\circ}$ |
| AREA (ACRES): | 36.0 aerial<br>44.0 surface | | 11.6 aerial<br>12.2 surface |
| LENGTH: | | 3,800'<br>1,158m | |
| WIDTH: | | 350'<br>107m | |

**TERRAIN & VEGETATION:**

**STARTING ZONE:** A shallow bowl with a low divide. Surface consists of volcanic blocks and cinders.

**TRACK:** A funnel shape track which runs over cliffs into a narrow gully. Cover is mostly rock scree with some grass.

**RUNOUT ZONE:** An extension of the track gully. Cover is grass and scree. Two other paths enter the lower track and runout zone.

**EVENT HISTORY:**

**TREE RING:** 1935, 1937, 1942, 1945, 1952, 1957, 1958, 1960, 1962, 1965, 1973, 1976, 1980

**RECENT OBSERVATIONS:** 1978 (none reported), 1979 (2 up to size 3), 1980 (1 size 4)

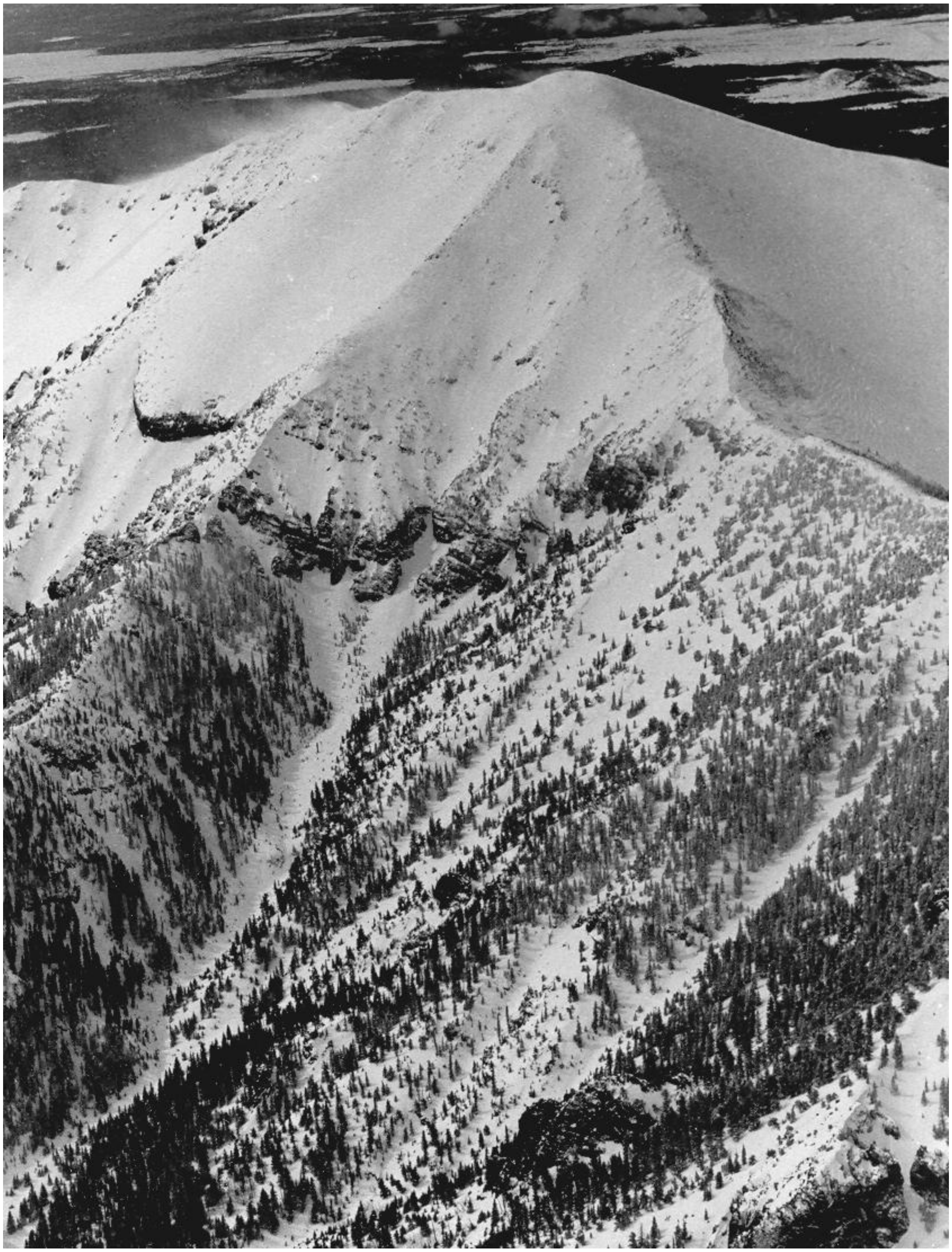

Figure 9. Beard Canyon Path.

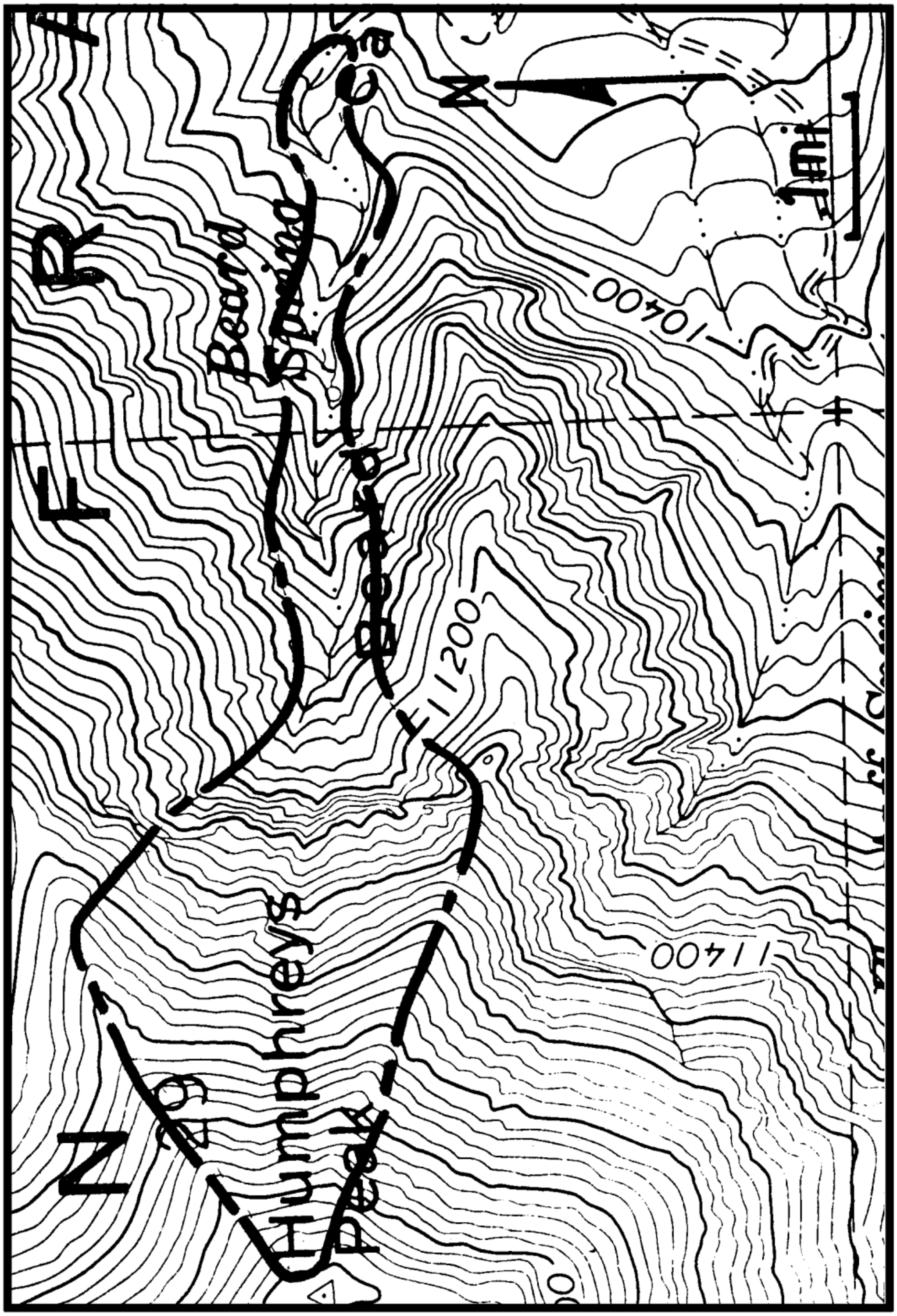


Figure 10.   Map of Beard Canyon Path.

Figure 11.

# AVALANCHE SUMMARY SHEET

**PATH NAME:** Dunnam Canyon **REFERENCE NO.:** 210

**SPECIFICATIONS:**

**ASPECT:** Southeast **LOADING DIRECTION:** West

**TOP ELEV.:** 12,600' 3,840m **BOTTOM ELEV.:** 10,200' 3,109m **FALL:** 2,400' 732m

**PATH LENGTH:** 5,500' 1,676m **NO. OF STARTING ZONES:** 1

| | STARTING ZONE: | TRACK: | RUNOUT ZONE: |
|---|---|---|---|
| SLOPE ANGLE: | 34° | 31° | 10° |
| AREA (ACRES): | 43.5 aerial<br>52.5 surface | | 11.6 aerial<br>11.8 surface |
| LENGTH: | | 3,100'<br>945m | |
| WIDTH: | | 350'<br>107m | |

**TERRAIN & VEGETATION:**

**STARTING ZONE:** A shallow bowl terminated by a cliff. The cover is volcanic blocks and cinders.

**TRACK:** A strong funnel shape bounded by cliffs. Steep upper section with a short transition to the shallow lower section.

**RUNOUT ZONE:** Prior to 1973, the runout was a narrow boulder filled stream gully. The 1973 event at least doubled the area. The increased area was formerly occupied by mature trees.

**EVENT HISTORY:**

**TREE RING:** 1932, 1944, 1949, 1952, 1957, 1960, 1962, 1965, 1966, 1969, 1973, 1976, 1978, 1980

**RECENT OBSERVATIONS:** 1978 (none reported), 1979 (none reported), 1980 (none reported until tree ring field trip showed recent damage)

Figure 12. Dunnam Canyon Path, center of photograph.

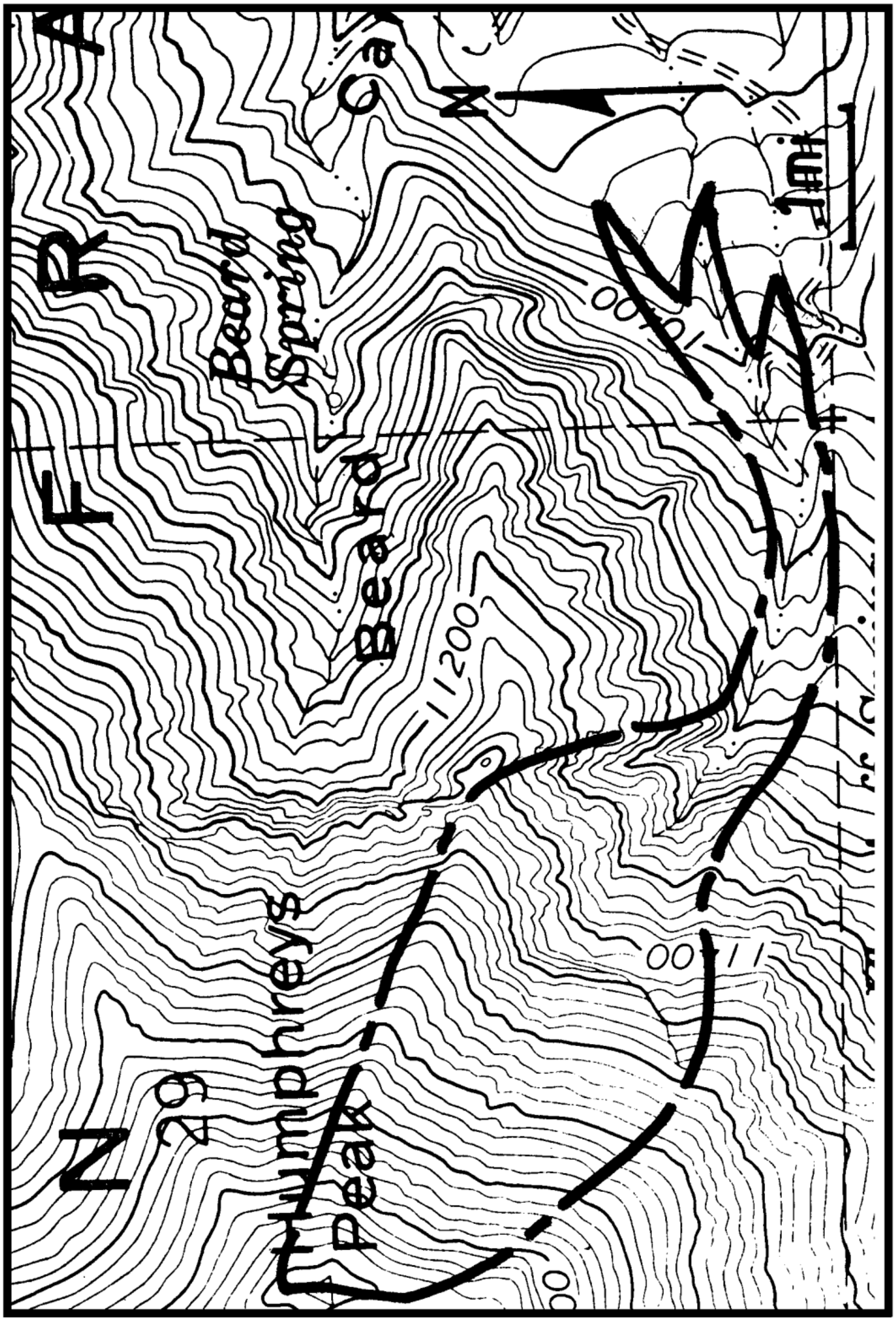


Figure 13. Map of Dunnam Canyon Path.

Figure 14.

# AVALANCHE SUMMARY SHEET

**PATH NAME:** Snowslide Canyon **REFERENCE NO.:** 170

**SPECIFICATIONS:**

**ASPECT:** East **LOADING DIRECTION:** West to South

**TOP ELEV.:** 12,000' 3,675m **BOTTOM ELEV.:** 10,400' 3,170m **FALL:** 1,600' 488m

**PATH LENGTH:** 5,200' 1,585m **NO. OF STARTING ZONES:** 2

| | STARTING ZONE: | TRACK: | RUNOUT ZONE: |
|---|---|---|---|
| SLOPE ANGLE: | 34° | 17° | 14° |
| AREA (ACRES): | 43.5 aerial<br>52.5 surface | | 11.6 aerial<br>12.0 surface |
| LENGTH: | | 3,800'<br>1,158m | |
| WIDTH: | | 150-200'<br>46-61m | |

**TERRAIN & VEGETATION:**

**STARTING ZONE:** A large bowl on the south, gullies on the north. Cover is volcanic blocks and cinders.

**TRACK:** A confined gully with high frequency channel originating from the chutes on the north portion of the starting zone.

**RUNOUT ZONE:** A narrow tongue-like extension of the track covered with grass and small trees along with old debris.

**EVENT HISTORY:**

**TREE RING:** 1932, 1941, 1949, 1952, 1957, 1958, 1960, 1962, 1965, 1966, 1968, 1970, 1973, 1978, 1980

**RECENT OBSERVATIONS:** 1978 (1 size 1), 1979 (1 size ?), 1980 (1 size 3)

Figure 15. Snowslide Spring Canyon Path, center of photograph.

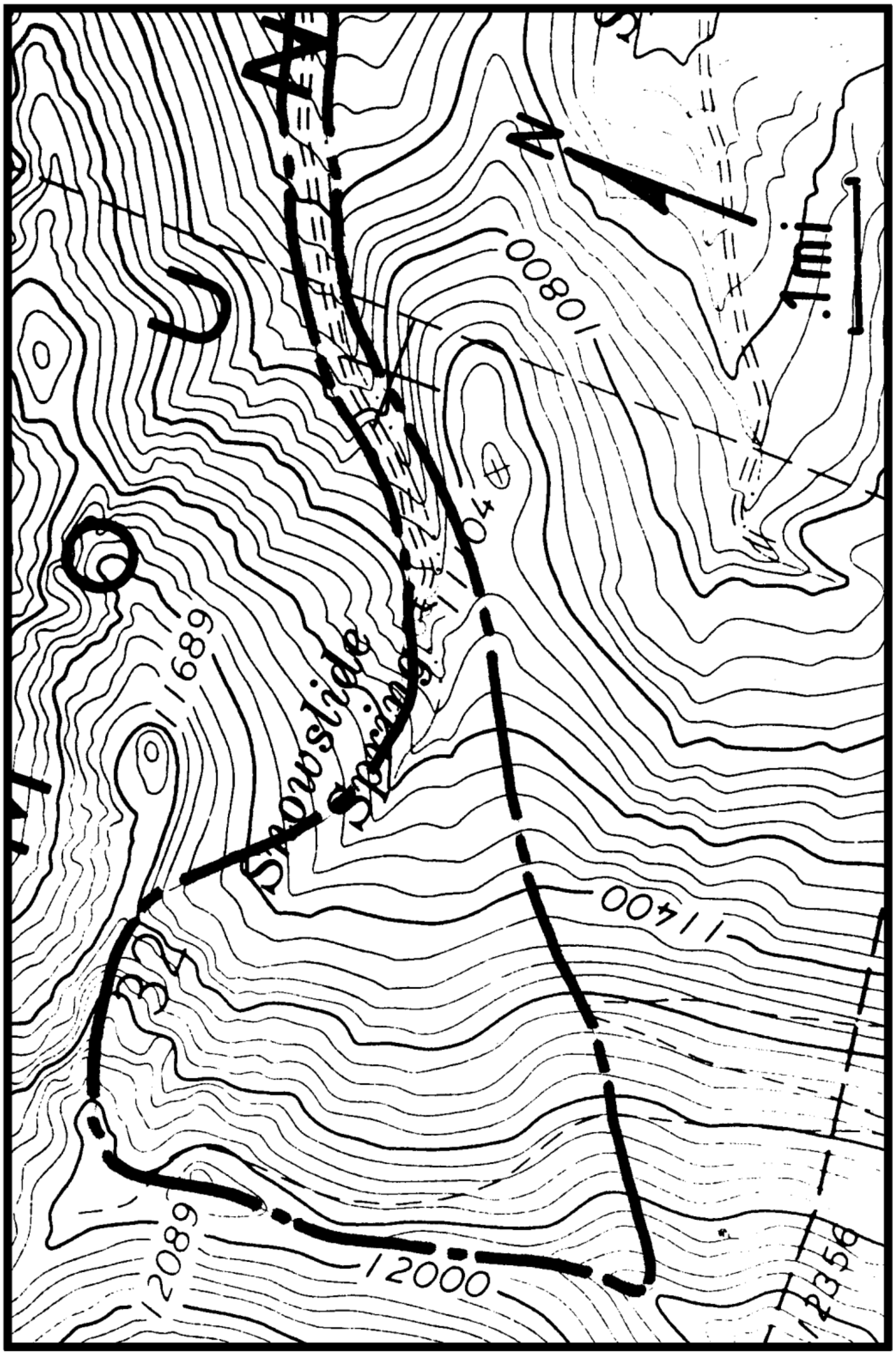


Figure 16. Map of Snowslide Spring Canyon Path.

Figure 17.

# AVALANCHE SUMMARY SHEET

**PATH NAME:** Allison Clay **REFERENCE NO.:** 450

**SPECIFICATIONS:**

**ASPECT:** West **LOADING DIRECTION:** South and East

**TOP ELEV.:** 12,300' 3,749m **BOTTOM ELEV.:** 9,900' 3,018m **FALL:** 2,400' 732m

**PATH LENGTH:** 6,500' 1,981m **NO. OF STARTING ZONES:** 1

| | STARTING ZONE: | TRACK: | RUNOUT ZONE: |
|---|---|---|---|
| **SLOPE ANGLE:** | 34° | 27° | 12° |
| **AREA (ACRES):** | 50.0 aerial<br>60.0 surface | | 9.0 aerial<br>9.2 surface |
| **LENGTH:** | | 4,900'<br>1,494m | |
| **WIDTH:** | | 400'<br>122m | |

**TERRAIN & VEGETATION:**

**STARTING ZONE:** Blocks and cinders in a large bowl.

**TRACK:** Blocks and cinders with partial grass cover in the bottom of a wide gully.

**RUNOUT ZONE:** Blocks and cinders with partial grass cover.

**EVENT HISTORY:**

**TREE RING:** 1932, 1944, 1949, 1952, 1956, 1960, 1965, 1966, 1968, 1973, 1980

**RECENT OBSERVATIONS:** 1978 (1 size 2), 1979 (none reported), 1980 (none reported until tree ring field trip showed damage)

Figure 18. Allison Clay Path, center of photograph.

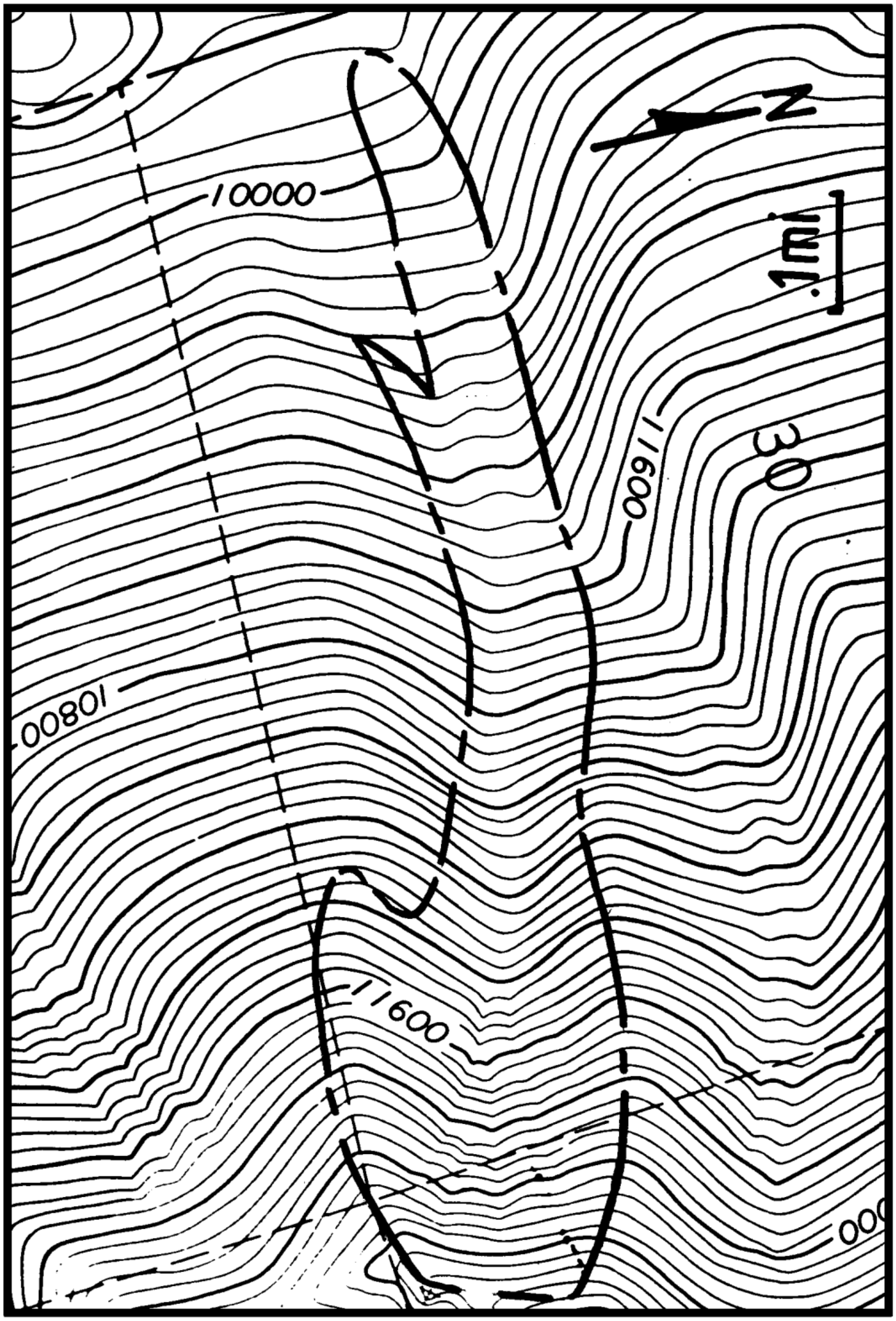


Figure 19. Map of Allison Clay Path.

Figure 20.

# AVALANCHE SUMMARY SHEET

**PATH NAME:** Crossfire **REFERENCE NO.:** 360

**SPECIFICATIONS:**

**ASPECT:** Northeast **LOADING DIRECTION:** Southwest to West

**TOP ELEV.:** 12,000' 3,658m **BOTTOM ELEV.:** 10,300' 3,139m **FALL:** 1,700' 518m

**PATH LENGTH:** 3,800' 1,158m **NO. OF STARTING ZONES:** 2

| | STARTING ZONE: | TRACK: | RUNOUT ZONE: |
|---|---|---|---|
| **SLOPE ANGLE:** | $34^{\circ}$ | $28^{\circ}$ | $16^{\circ}$ |
| **AREA (ACRES):** | 13.0 aerial<br>16.0 surface | | 9.0 aerial<br>9.4 surface |
| **LENGTH:** | | 2,600'<br>792m | |
| **WIDTH:** | | 200-300'<br>61-91m | |

**TERRAIN & VEGETATION:**

**STARTING ZONE:** Two elongate gullies. Cover is volcanic blocks and cinders.

**TRACK:** The Track converges from each starting zone, crosses and diverges toward the runout. Cover is blocks, scree and grass.

**RUNOUT ZONE:** The runout meets Abineau and rebounds down-channel into it. Cover is scree, grass and occasional trees.

**EVENT HISTORY:**

**TREE RING:** 1932, 1936, 1945, 1952, 1958, 1966, 1968, 1973, 1980

**RECENT OBSERVATIONS:** 1978 (none reported), 1979 (1 size 4), 1980 none reported until tree ring field trip showed damage)

Figure 21. Crossfire Path, full length path on the right.

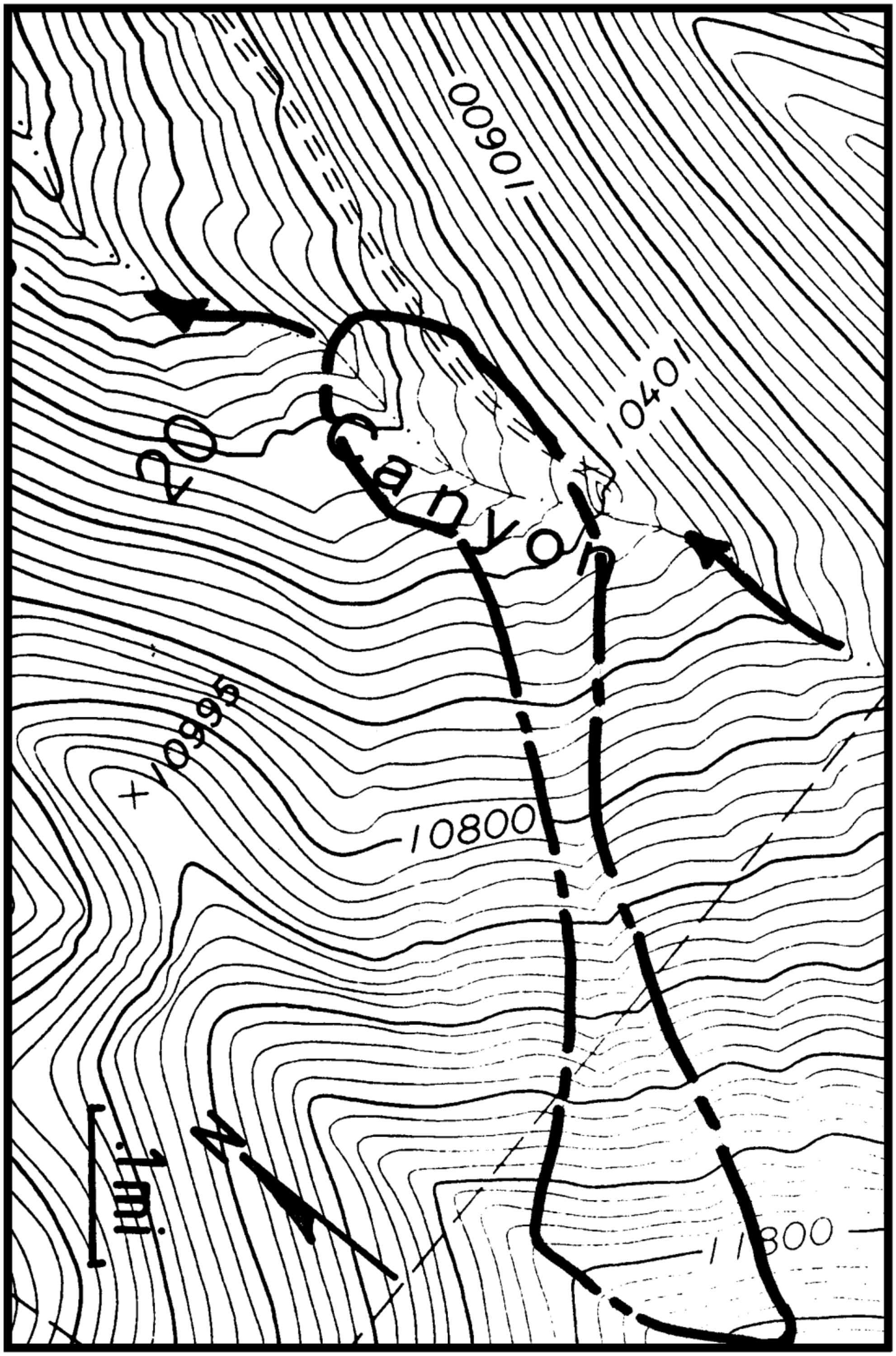


Figure 22.   Map of Crossfire Path.

Figure 23.

## AVALANCHE SUMMARY SHEET

**PATH NAME:** Telemark **REFERENCE NO.:** 100

**SPECIFICATIONS:**

**ASPECT:** North **LOADING DIRECTION:** Southwest to South

**TOP ELEV.:** 11,900' 3,627m **BOTTOM ELEV.:** 10,200' 3,109m **FALL:** 1,700' 518m

**PATH LENGTH:** 3,800' 1,158m **NO. OF STARTING ZONES:** 2

| | STARTING ZONE: | TRACK: | RUNOUT ZONE: |
|---|---|---|---|
| SLOPE ANGLE: | $36^{\circ}$-$40^{\circ}$ | $27^{\circ}$ | $5^{\circ}$-$10^{\circ}$ |
| AREA (ACRES): | 14,5 aerial<br>17.5 surface | | 22.0 aerial<br>22.3 surface |
| LENGTH: | | 2,700'<br>823m | |
| WIDTH: | | 350-400'<br>107-122m | |

**TERRAIN & VEGETATION:**

**STARTING ZONE:** Wide gully covered with volcanic blocks and cinders. Usually loads over northwest shoulder.

**TRACK:** Wide gully covered with volcanic blocks and cinders.

**RUNOUT ZONE:** Broad fan extending to small mound near Doyle Spring. Cover consists of blocks and scree with spotty grass and bushes.

**EVENT HISTORY:**

**TREE RING:** Not dated.

**RECENT OBSERVATIONS:** 1978 (4 up to size 4), 1979 (6 up to size 4), 1980 (3 up to size 4)

Figure 24. Telemark Path, center of photograph.

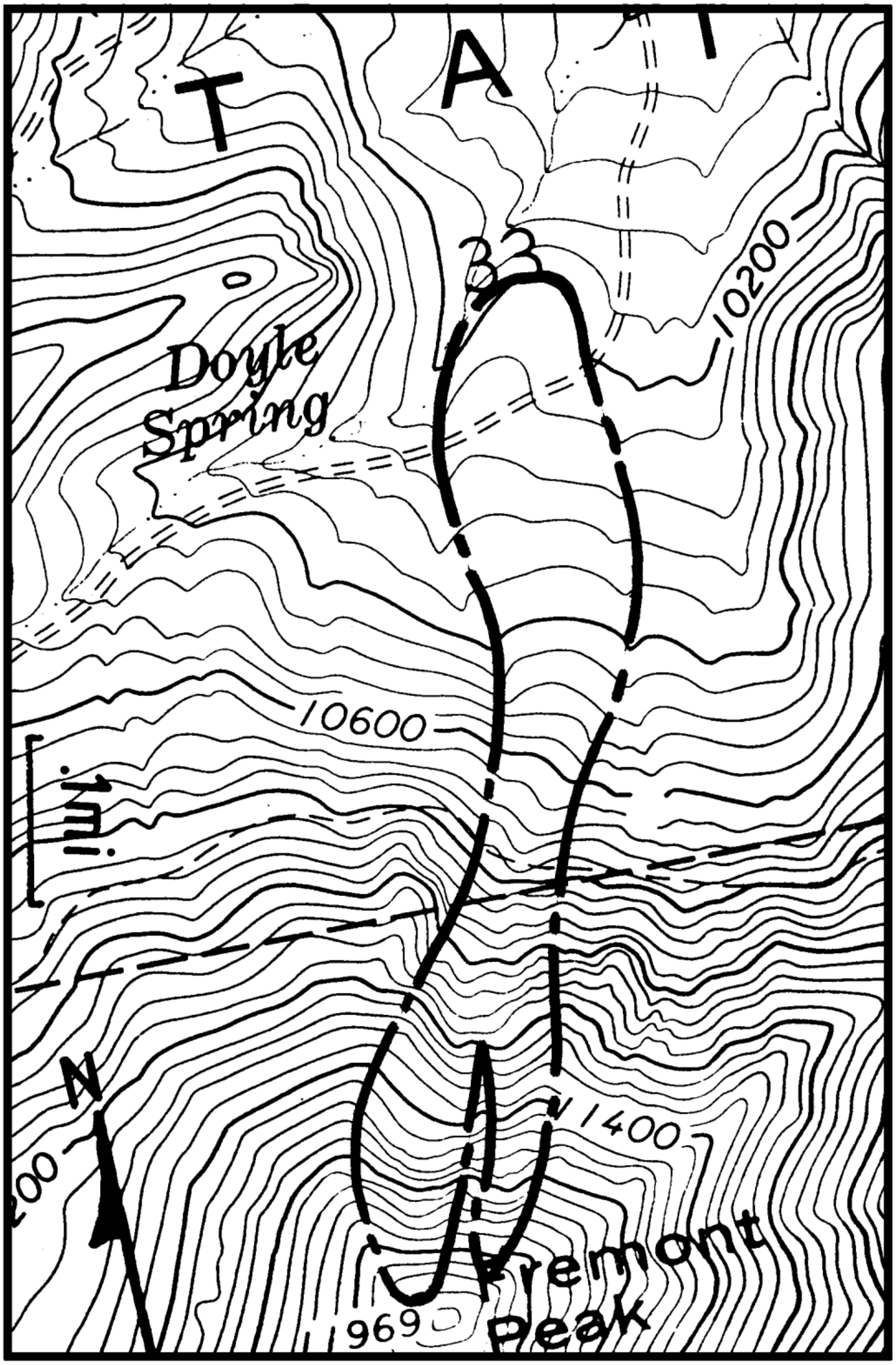


Figure 25. Map of Telemark Path.

# Chapter 3

# THE ARIZONA SNOW CLIMATE

## Methods

Weather and snowpack analysis comprise a major portion of avalanche studies. Reasonable understanding of the avalanche process within a given area requires a database acquired from many years of weather and snowpack observations. Very little data exist for the San Francisco Peaks. Over the last four years the San Francisco Mountain Avalanche Project has gathered avalanche related weather and snowpack data on a somewhat sporadic basis. Weather data have been collected from several sources; Winslow WSO (upper air), Flagstaff WSO, N.A.U. Weather Station, Arizona Snow Bowl, and two private stations (Mountainaire and Brannigan Park). In 1981 a remote weather station was installed on the mountain. Snowpack data were obtained from Arizona Snow Survey records and from snowpits dug at high elevation study plots. Standard snowpit analysis is done at the "alpha" plot located on a level site at 11,250'. Three "beta" plots, located on slopes, are sampled occasionally. Much reference has been made to the work done in the San Juan Mountains of southwest Colorado by the Institute of Arctic and Alpine Research (INSTAAR). Questions relating to snowpack evolution on the Peaks are often tested against, and compared to, the San Juan Project findings. Due to the sporadic and limited nature of the database, only the most general ideas are presented here. It is hoped that in the future, work in this area will be expanded.

# Weather

## General Circulation Considerations

Uneven distribution of solar radiation over the surface of the earth is the basic driving force of weather processes affecting avalanche conditions. Air masses formed within differing thermal regimes clash in the mid-latitudes along a zone referred to as the polar front. These air masses do not mix readily, hence their boundaries remain distinct. Due to the fluid nature of air, these boundaries are continually shifting to achieve equilibrium. Heat flux from the equator to the poles establishes perturbations in the polar front which, when modified by the rotation of the earth, form a series of wave-like ridges and troughs termed "Rossby" or long waves. These long waves are relatively persistent features, or at least are resistant to any rapid change. Generally these waves migrate eastward, though they may occasionally retrograde. Associated with the long waves are high speed winds in the upper levels (9,000-11,000 meters or 30,000-40,000 feet), referred to as the jet stream. The long wave pattern, with its attendant jet stream, profoundly affects the winter weather of Arizona. Long waves direct cold air south, warm air north, and pump maritime moisture inland (Figure 26).

The physical relationship of the long wave pattern to the earth's surface dictates the gross winter weather for the mid-latitudes. Areas under the influence of a long wave crest (termed a ridge) will be in a zone of atmospheric subsidence (high pressure) with ensuing dry, warm weather.

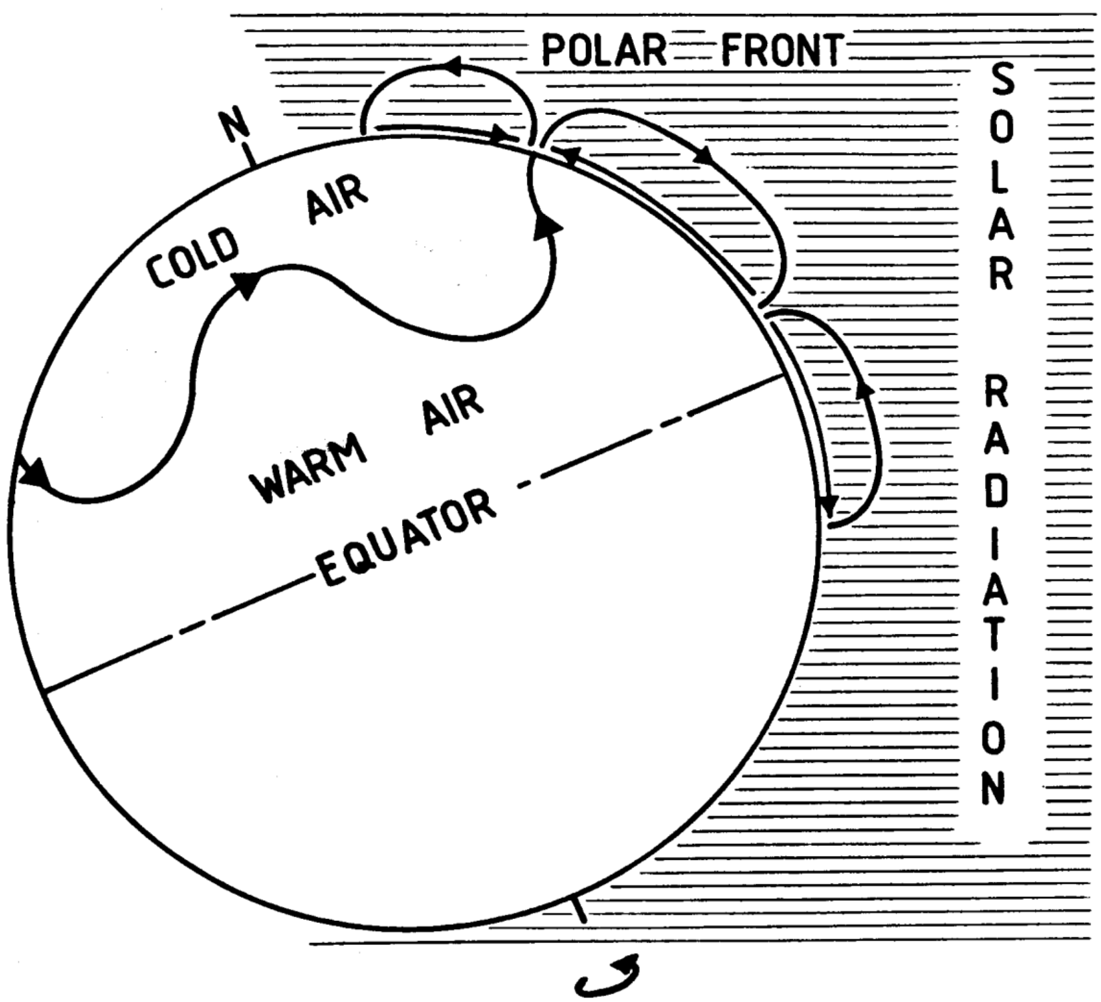


Figure 26. A schematic representation of the wave-like nature of the polar front (shown at winter solstice).

Areas under the inf1uence of a long wave trough will be in a zone of convergence (low pressure) and will experience stormy or unsettled weather. Smaller disturbances called short waves move along on the Rossby waves and form the cyclonic storms that pass through Arizona during the course of a winter.

Synoptic Scale Considerations

The seasonal shift and resident position of the semi-permanent long wave ridge over the eastern Pacific Ocean controls the prevailing winds (Figures 27-28), the potential for snowfall, and subsequent avalanche activity (Sellers and Hill, 1974). If this high pressure ridge maintains its position over the western states, the prevailing upper level flow diverts short wave storms away from Arizona. The few storms that do affect the state then occur as upper air cutoff lows (Figure 31). Some of these storms are also influenced by the sub-tropical jet stream. As winter begins, the semi-permanent high pressure ridge usually weakens and shifts to a position just west of the Pacific coast. The prevailing upper air flow is thus favorably positioned to steer cyclonic storms down the west coast and direct them inland over Southern California (Figure 29). Occasionally, the jet stream will split into two channels, producing what is referred to as a "blocking pattern", where storms may be directed along either channel. Storms entering Arizona during blocking conditions present additional forecasting difficulties (Figure 32).

Long wave patterns are obscured by frictional effects at the surface, but are quite evident at the 500 millibar level (Figure 29)

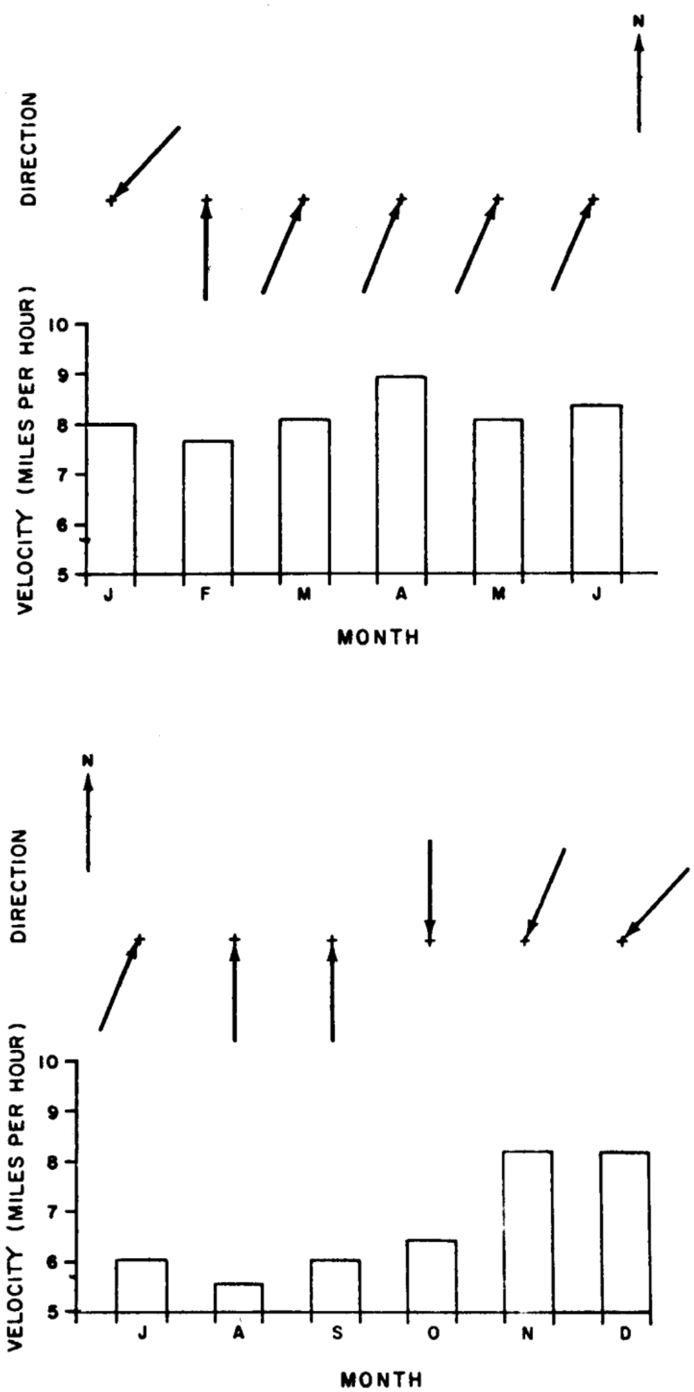


Figure 27. Mean wind direction and velocity, Flagstaff Arizona (2 and 8 years of record respectively). (from Bestcha, 1976).

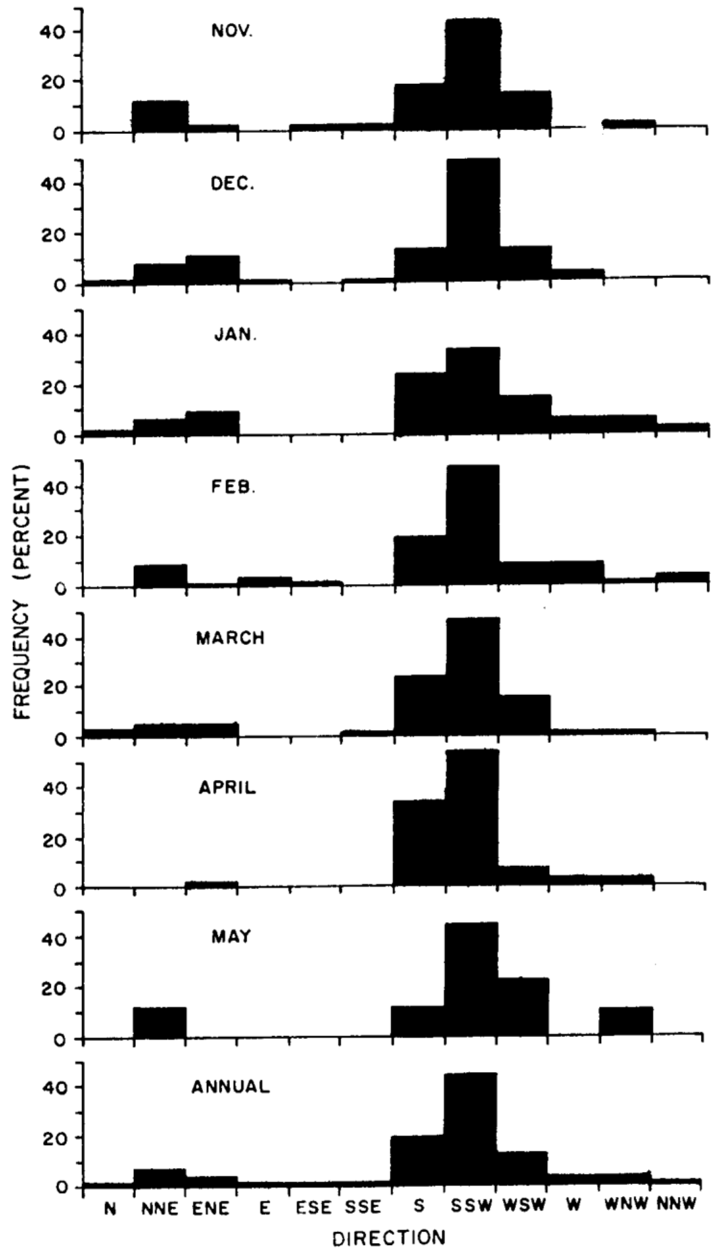


Figure 28. Prevailing winds during snowfall periods, Flagstaff, Arizona (10 years of record). (from Beschta, 1976).

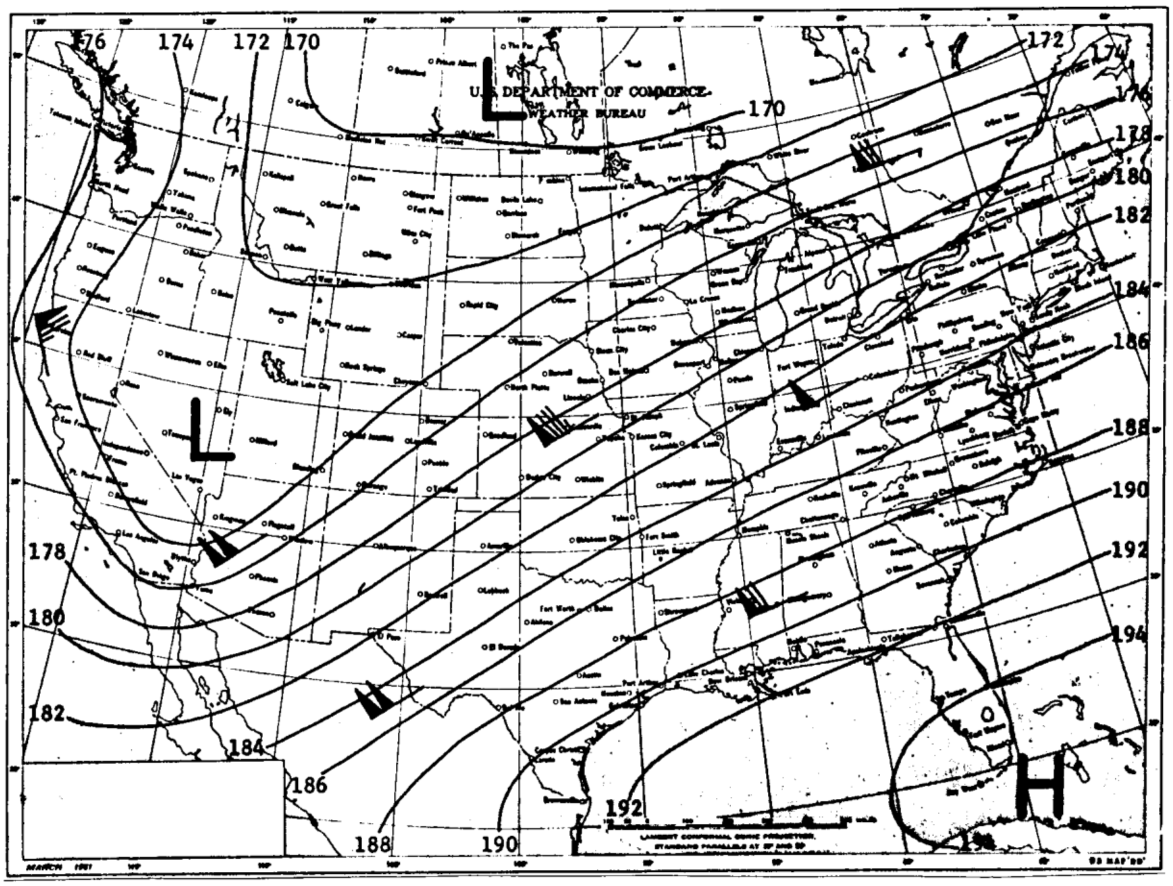


Figure 29. Idealized 500 millibar pattern associated with the heaviest winter snowfall in Arizona according to Sellers and Hill (1974).

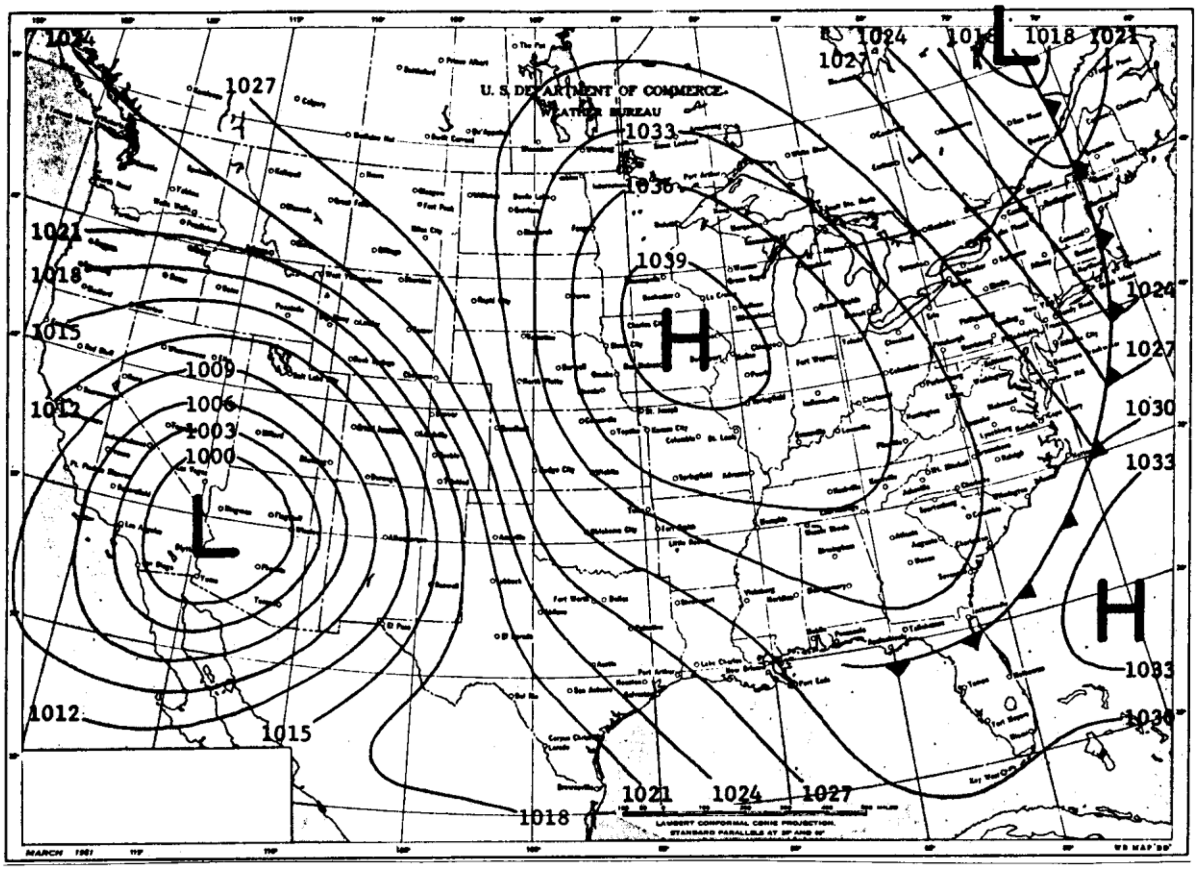


Figure 30. Idealized surface pattern associated with the heaviest winter precipitation in Arizona according to Sellers and Hill (1974).

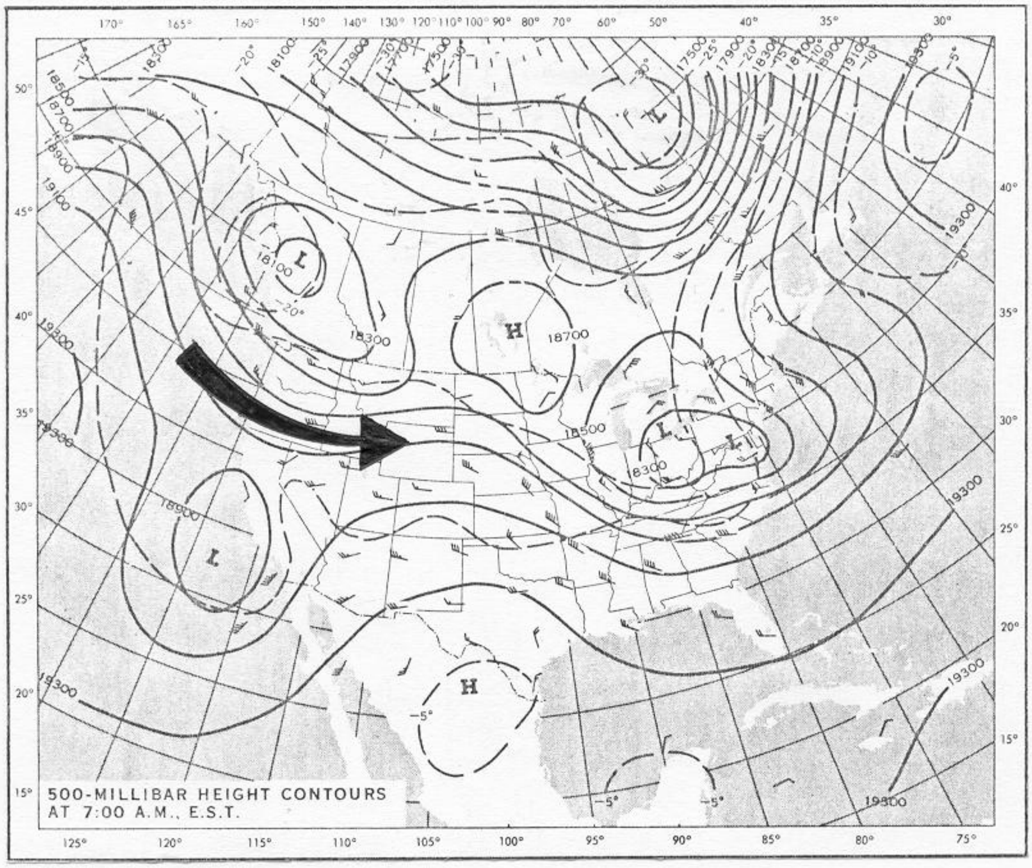


Figure 31. A 500 millibar representation of a cutoff low which is south of the main polar jet stream (from Hidore, 1976).

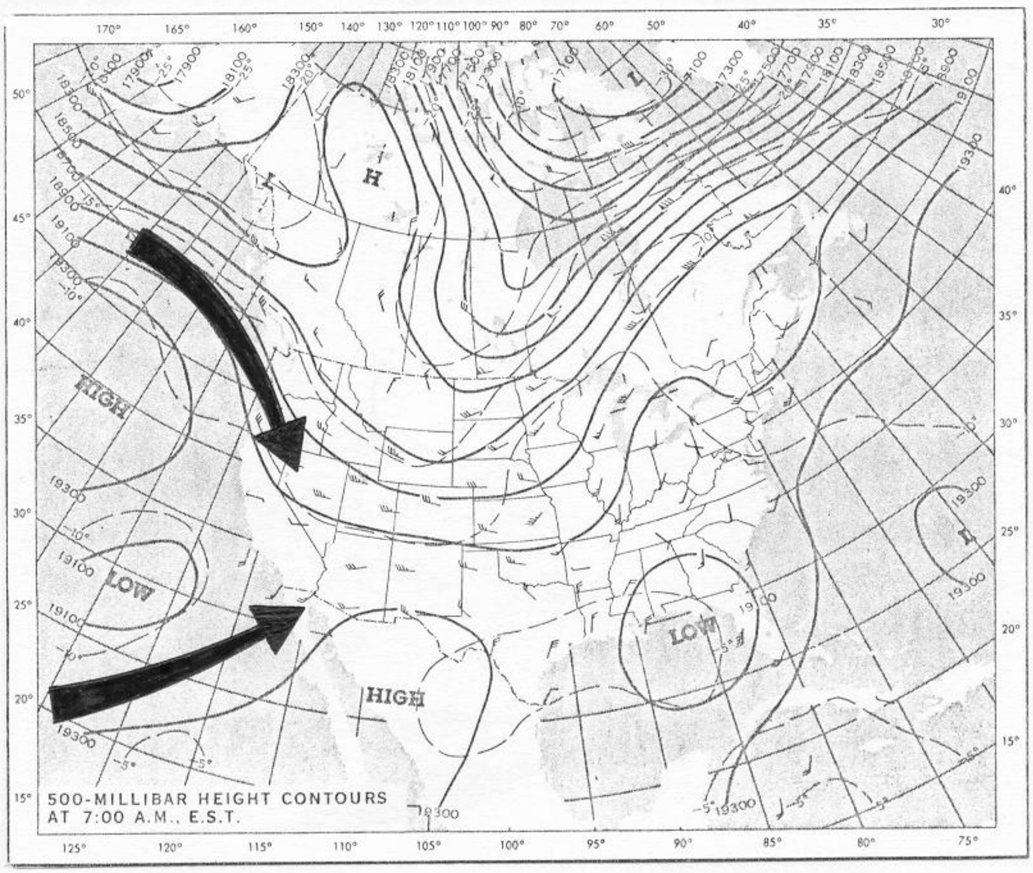


Figure 32. A 500 millibar representation of a blocking pattern (Rex blocks and Omega blocks etc.). (from Hidore, 1976).

or roughly 5,500 meters (18,000 feet) above sea level. The 500 millibar pressure surface is a standard meteorological level commonly used as an indicator of overall upper air conditions. For avalanche work the 700 millibar (approximately 3,000 meters or 10,000 feet) level is also quite useful as it displays some surface interaction, while retaining the long wave characteristics. The 700 millibar level is usually found near the elevation of most avalanche starting zones in the United States (Perla and Martinelli, 1976). In addition, data from the 650 millibar level (approximately 3,500 meters or 12,000 feet) is used for studies specifically on the San Francisco Peaks.

Depending on the long wave pattern prevailing at the time, short wave impulses are steered into Northern Arizona along one of three statistically favorable tracks (Sorenson, 1974) (Figure 33).

1) Type A, or northern track, storms move onshore over the Pacific Northwest or Northern California and approach Arizona through the Great Basin.

2) Type B, or western track, storms move south offshore of the Pacific coast, come onshore over Southern California and track east into Arizona. Occasionally these storms stagnate over the Colorado River valley.

3) Type C, or southern track, storms move inland from the south or west over San Diego and track east through Southern Arizona.

A fourth track has been added by this writer, which is a variant of the Type A, northern track, and is referred to as the “Type A prime” or far northern track. Type A' storms may drop only a little precipitation in Arizona, however; even minor snowfall, under the influence of high winds, must be considered in terms of avalanche activity. Type A' storms are usually more common early or late in the winter season, as the polar front shifts latitude.

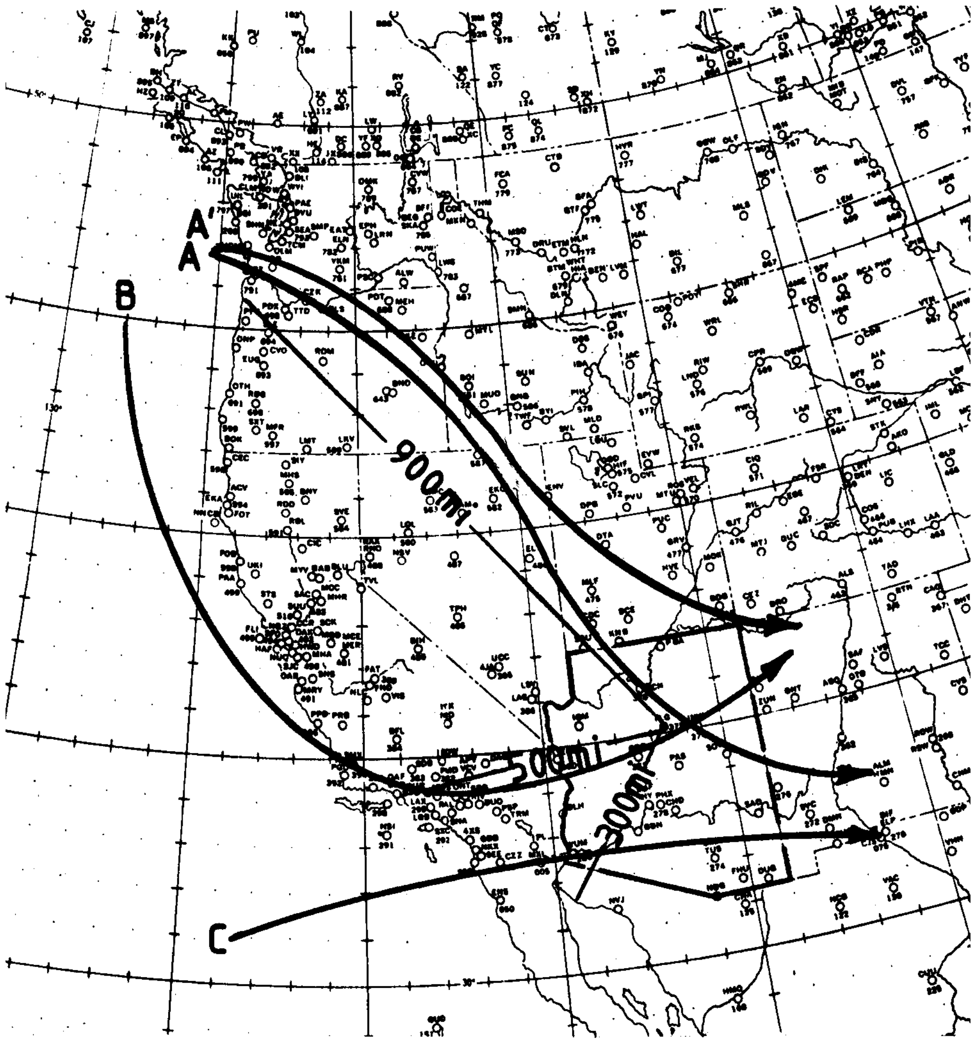


Figure 33. Primary storm tracks affecting Arizona.

Sorenson (1974) estimated the percentages of heavy winter storms (those leaving over 20 inches of snow) affecting Flagstaff via each of the storm tracks:

1) Type A - 10 percent
2) Type B - 80 percent
3) Type C - 10 percent

It should be noted that Type A storms comprise over 10 percent of the total number of winter storms (including those leaving less than 20 inches of snow) but, due to their inland track, they lose considerable moisture by the time they reach Arizona. Since storm type has a significant effect on avalanche conditions, each track will be examined in terms of its influence on the San Francisco Peaks.

## Meso-scale Considerations

Type A storms. Figure 34 illustrates a typical Type A storm which passed over the Peaks around 00 Zulu (5:00 PM MST) December 7, 1978. The notable features of such Type A storms are; strong cold air advection (Table 1), high winds, and generally light snowfall (even though the snow level may be low). It is easy to underestimate the consequences of Type A storms on avalanching due to their modest precipitation. For example, the dry snow may be concentrated by high winds in favorably oriented avalanche starting zones, leading to slab (cohesive layer) avalanche conditions (Perla and Martinelli, 1976). Type A' storms produce even less snowfall than Type A storms but may produce similar effects (e.g. localized slab conditions).

Type B storms. Observations from 1977 into 1981 indicate that Type B storms produced most of the large avalanche events during that

**Table 1**

**A Comparison of 500 mb Temperature and Wind Over Winslow, AZ.**

**During the Passage of Three Storms**

| Storm Type | Time/Date | Temperature | Wind |
|---|---|---|---|
| Type A | 00Z 5 Dec. 78 | -13°C | NNW |
| | 12Z 5 Dec. 78 | -14°C | W |
| | 00Z 6 Dec. 78 | -16°C | WSW |
| | 12Z 6 Dec. 78 | -26°C | SW |
| | 00Z 7 Dec. 78 | -34°C | WSW |
| | 12Z 7 Dec. 78 | -37°C | WSW |
| | 00Z 8 Dec. 78 | -35°C | W |
| | 12Z 8 Dec. 78 | -36°C | NW |
| | 00Z 9 Dec. 78 | -20°C | N |
| | 12Z 9 Dec. 78 | -21°C | NW |
| Type B | 00Z 21 Apr. 80 | -14°C | SSW |
| | 12Z 21 Apr. 80 | -14°C | S |
| | 00Z 22 Apr. 80 | -14°C | SW |
| | 12Z 22 Apr. 80 | -17°C | SW |
| | 00Z 23 Apr. 80 | -20°C | S |
| | 12Z 23 Apr. 80 | -25°C | SSW |
| | 00Z 24 Apr. 80 | -26°C | S |
| | 12Z 24 Apr. 80 | -25°C | N |
| | 00Z 25 Apr. 80 | -17°C | N |
| | 12Z 25 Apr. 80 | -17°C | NNW |
| Type C | 12Z 8 Mar. 79 | -15°C | NW |
| | 00Z 9 Mar. 79 | -16°C | NW |
| | 12Z 9 Mar. 79 | -17°C | NW |
| | 00Z 10 Mar. 79 | -18°C | NNW |
| | 12Z 11 Mar. 79 | -18°C | SE |
| | 00Z 12 Mar. 79 | -19°C | E |

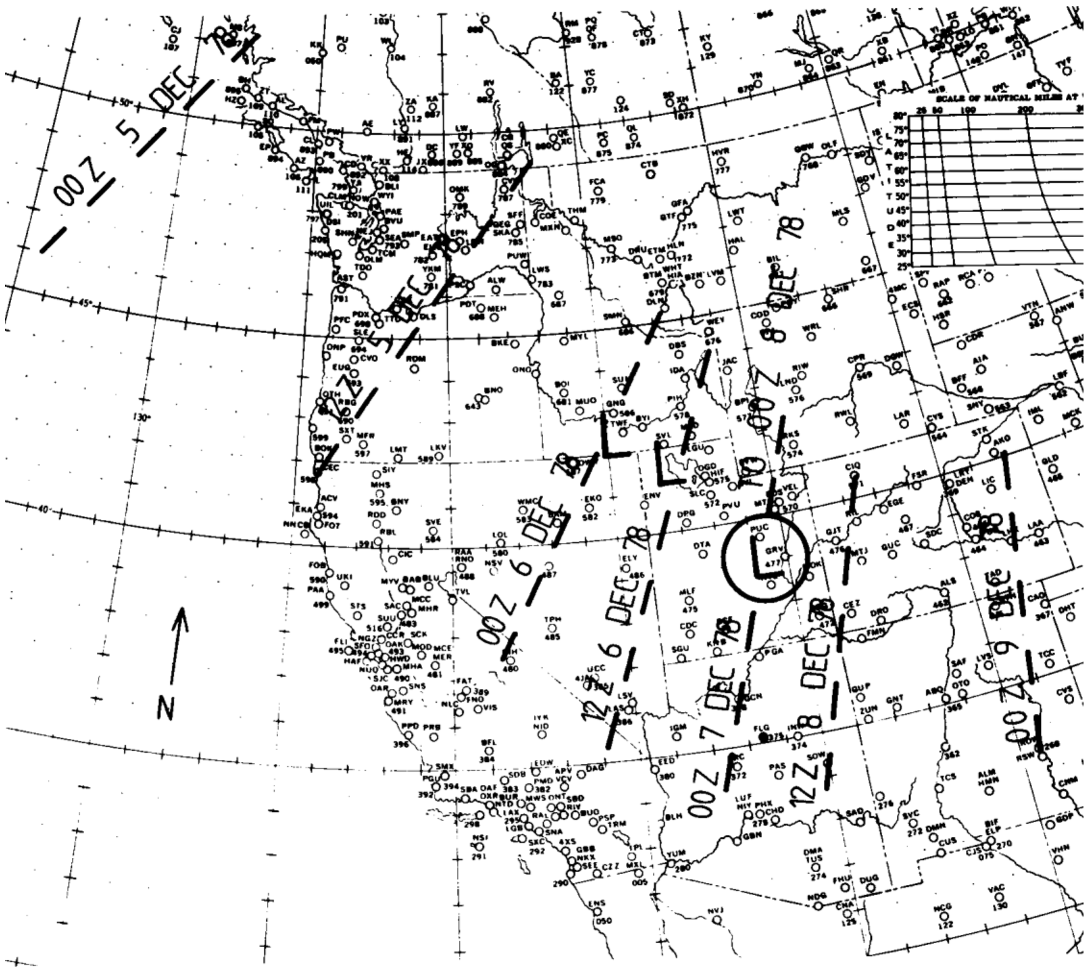


Figure 34. A typical Type A storm system track. (Clipped from The original thesis figure to fit portrait format).

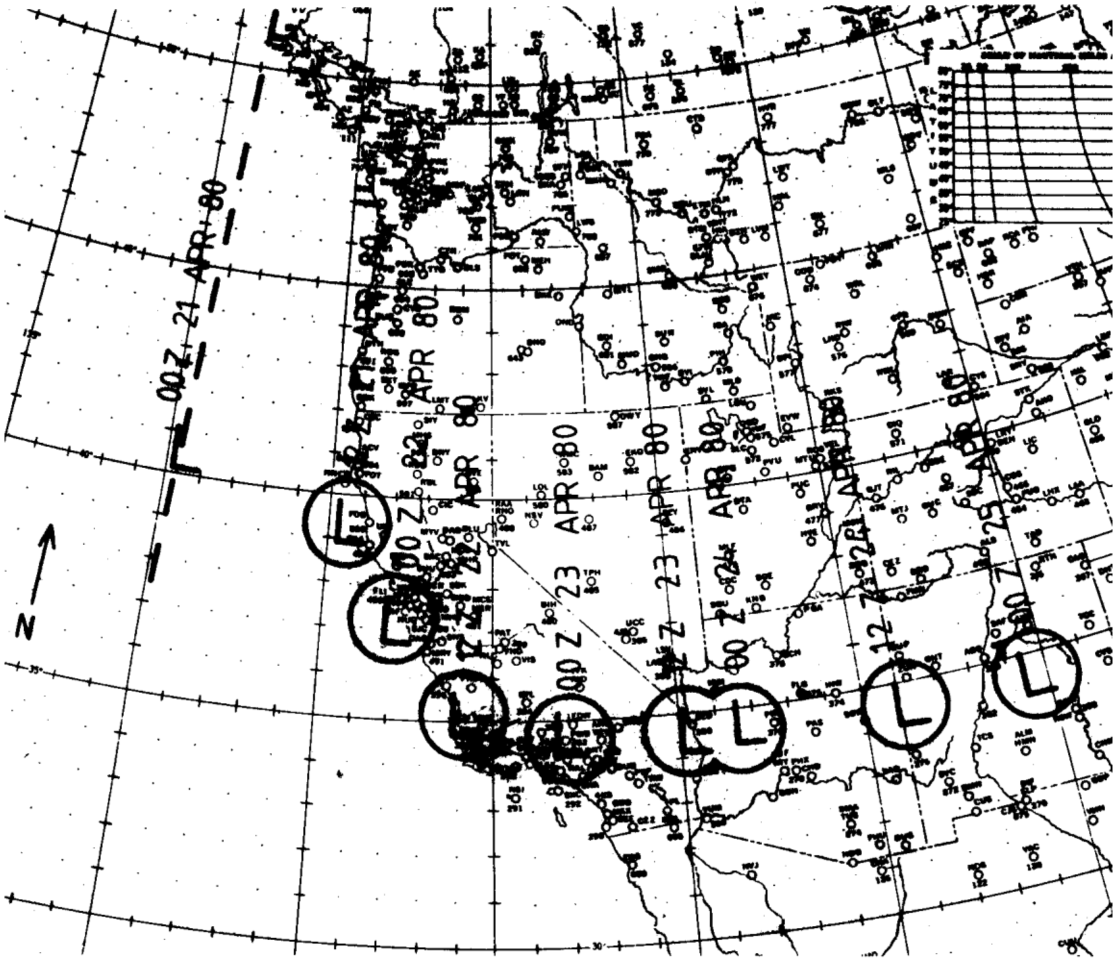

Figure 35. A typical Type B storm system track. (Clipped from the original thesis figure to fit portrait format).

period. Figure 35 traces the path of a typical Type B storm which passed over the Peaks around OO Zulu (5:00 PM MST) April 24, 1980. Storms such as this are characterized by cool to cold air advection (Table 1) over a moisture source relatively close to Arizona. This flow can produce large amounts of cold snow with snow levels typically around 1,220 to 1,830 meters (4,000 to 6,000 feet). Stagnation often occurs over the Colorado River. The storm system illustrated in Figure 36 displays an important variation in tracking, often associated with Type B systems from 12 Zulu (5:00 AM MST) January 15, 1979 to 12 Zulu January 16, 1979 where the eastward progression of the system was replaced with a southward motion referred to as "digging". The extent to which a system digs is a function of the relation between the position of the jet stream core and the position of the low pressure center. The additional time spent over the ocean allows such systems to gather strength and greatly increase the potential for large snowfall.

The position of the moisture mass, with respect to the cold air advected during a storm, has great influence on avalanche conditions. If cooling is coincident with maximum snowfall a so called "standard" temperature pattern is produced. If warming is coincident with maximum snowfall a so called "inverted" temperature pattern is produced (Perla and Martinelli, 1976). Inverted temperature trends imply poor bonding at the old snow surface and increasingly dense new snow deposition. Figure 37 illustrates an inverted storm that passed from the 7$^{th}$ to the 14$^{th}$ of January, 1980 and was associated with large avalanche events on the San Francisco Peaks.

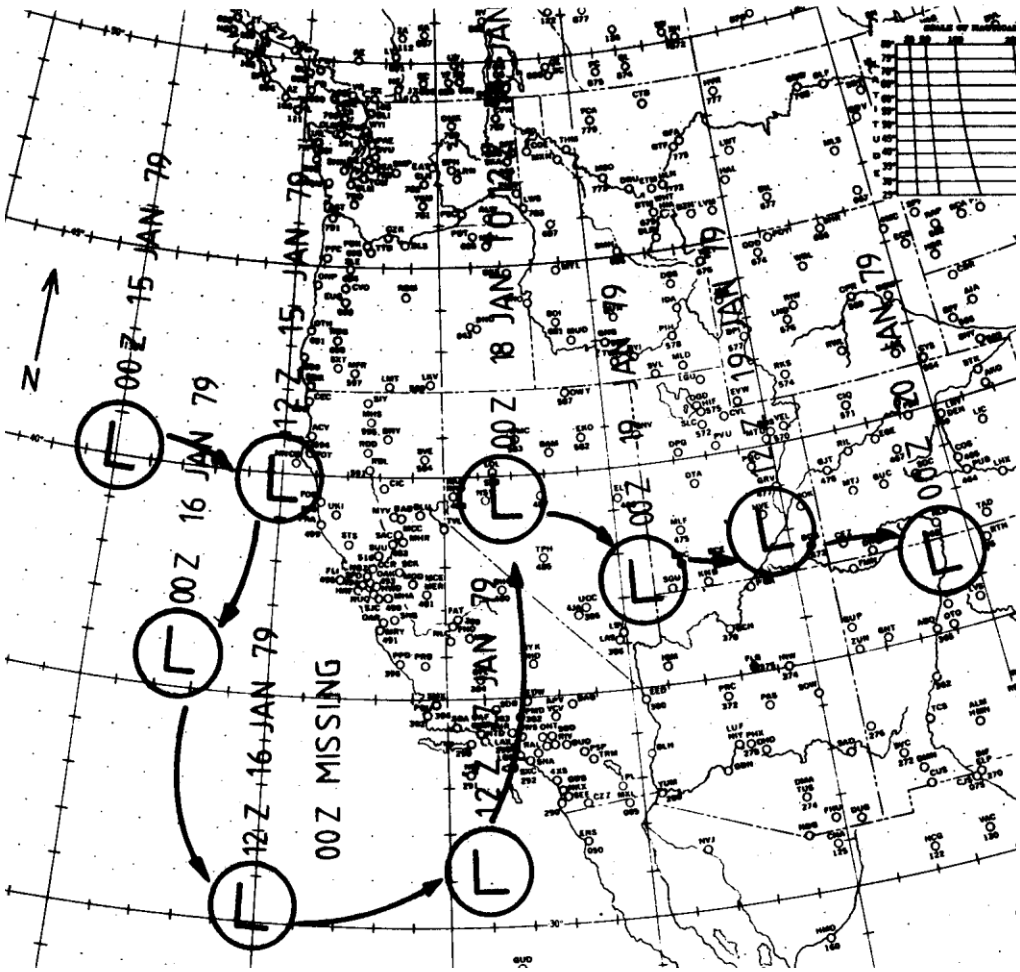


Figure 36. A Type B storm system track with associated digging. (Clipped from the original thesis figure to fit portrait format).

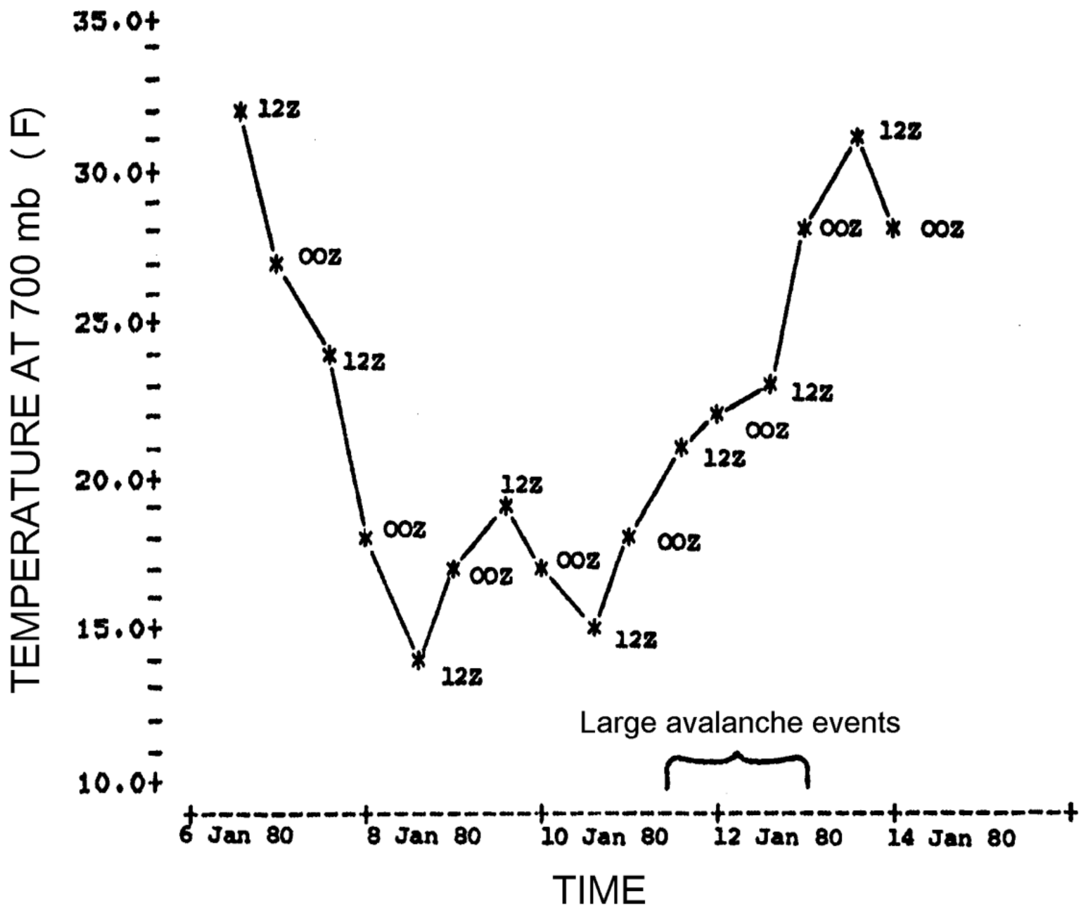


Figure 37. A normal temperature trend followed by an inverted temperature trend with associated avalanche events.

In terms of avalanche events, Type B systems are of great importance in Arizona. Large amounts of snow may be deposited especially if the system digs and subsequently stagnates over the Colorado River (Figure 30 and 35). The resulting heavy snowfall, deposited on a typically weak early season snowpack (as will be discussed) produces large avalanche events of the climax or direct action type. In addition, if the storm is inverted, the poorly bonded load is added more rapidly near the end of the storm, resulting in the involvement of maximum amounts of snow in the event. The large events of January 13, 1980 were of this nature. If winds average over 15 MPH (Perla and Martinelli, 1976) during or shortly after the storm loading of leeward slopes becomes significant. Due to the southwest flow prevalent during storms (Figure 28) the north and east slopes of the San Francisco Peaks are the most heavily loaded aspects.

Type C storms. These southerly storms are warm (table 1) and produce wet heavy snow with 1,830 to 2,440 meter (6,000 to 8,000 foot) snow levels indicative of tropical influence. The early storms of the 1977-1978 winter season were of the Type C variety. Figure 38 traces the progress of a Type C system through Arizona around 12 Zulu (5:00 AM MST) March 11, 1979. As indicated in Table 1, the 500 millibar temperature from the Winslow radiosonde release for this storm was about 7° C warmer than the Type B example and 18° C warmer than the Type A example. The dense snow of such Type C systems can put heavy loads on the snowpack triggering climax or direct action events. Given the return to normal winter temperatures following the passage of the

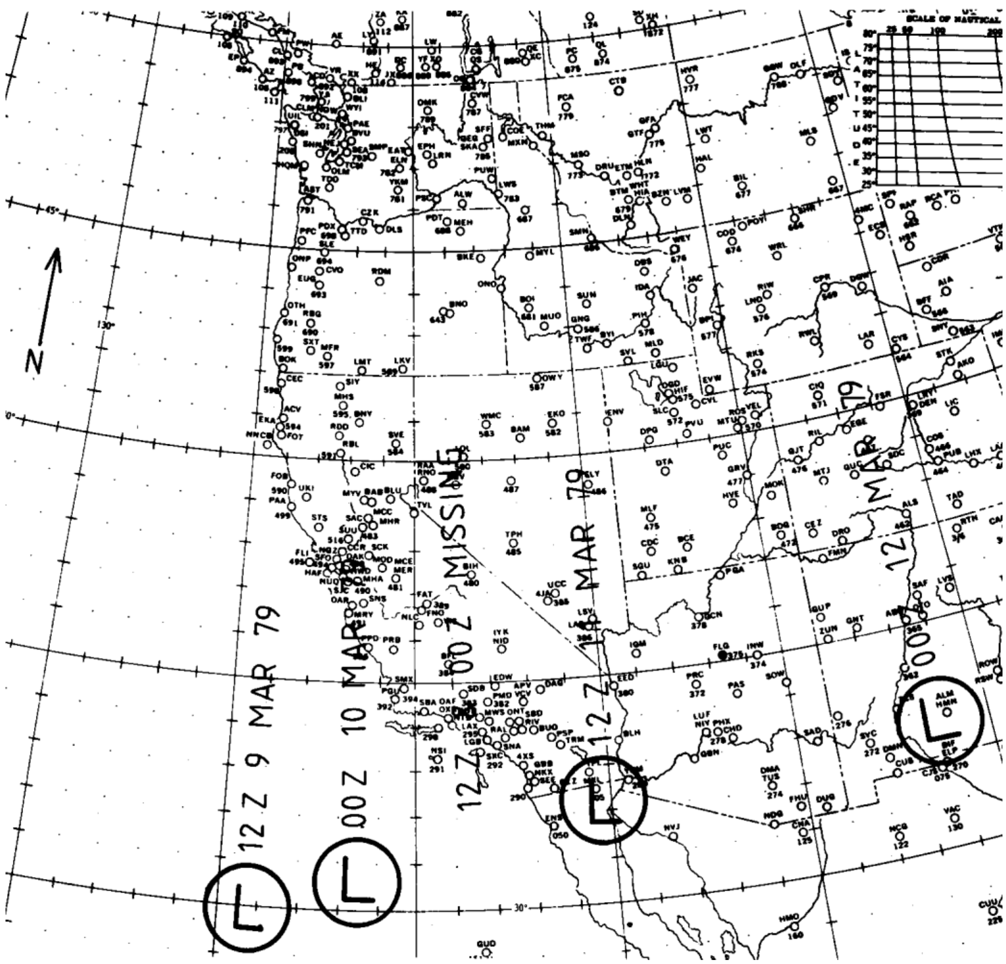


Figure 38. A typical Type C storm system track. (Clipped from The original thesis figure to fit portrait format).

system, the snow from such storms usually bonds rapidly producing high density values in certain layers (up to 400 $Kg/M^3$).

Maritime-continental effects. Maritime-continental effects play two roles. First is the moderating effect of large bodies of water on climates nearby (coastal climates). This is due to the heat storage capacity of water. Second is the modification of a storm system as it moves over land. Table 2 illustrates the degree of moderation caused by the Pacific Ocean on the western states. The table lists the mean January temperatures for several mountain stations along a west to east line from Huntington Lake, California to Alamosa, Colorado. All stations are within 180 meters (600 feet) elevation of each other.

Any given location is, of course, fixed in geographic space and hence fixed with respect to maritime-continental influence. A somewhat notable characteristic of Arizona's geographic location is found in the high variability in overland distance to the Pacific Ocean depending on the storm track azimuth (Figure 33). This in turn allows for variability in the effective maritime-continental nature of storms acting on the San Francisco Peaks, depending on which track is operative during a given disturbance.

Orographic effects. Orographic lifting over the Mogollon Rim and the San Francisco Peaks effectively increases the amount of precipitation received from most storm systems. In addition to the long overland track on the Type A systems discussed earlier, these storms are “wrung out” by orographic lifting over the Cascades and some of the

**Table 2**

**Temperature and Precipitation Values Showing**

**Continental/Maritime Effects**

| LOCATION | Huntington Lake, California | Fort Valley, Arizona | Durango, Colorado | Alamosa, Colorado |
|---|---|---|---|---|
| Elevation | 7,020' | 7,200' | 6,800' | 7,500' |
| $\bar{X}$ Jan Temp. | 30.2 F | 25.2 F | 25.3 F | 11.4 F |
| $\bar{X}$ Jan Ppt. | 5.23" | 2.18" | 1.16" | 0.26" |
| Mi. Inland | 150 mi. | 350 mi. | 500 mi. | 650 mi |

larger Basin and Range mountains, well before the San Francisco Peaks can act on them. In contrast, Type B and especially Type C storms have very few topographic barriers in their path before being lifted over the "Rim" in Arizona.

Micro-scale Considerations

As a storm system evolves, the moisture and temperature stratification within the system will determine the amount of, physical state of, and subsequent modifications to the precipitation. Rates of crystal growth, preferred axes of growth, melting, riming, and wind action all affect the character of the snow particle before it reaches the ground (LaChapelle, 1969) (Figure 39).

Art Pundt, who has spent considerable time studying the relation of new snow types to avalanche activity, has found a peculiar type of rimed particle (usually formed around a spatial or stellar pattern core) that appears to be common in this area. These particles are widely distributed and fall during short periods within a storm. They result, perhaps, from some form of intense lifting. These particles, form thin, relatively cold, layers in the accumulating snowpack, which are almost always identifiable in a snowpit as a zone of weakness (low cohesion, low shear strength) (Pundt, 1981).

Once on or near the ground, the snow particle may be transported by winds interacting with topography, producing a meso-micro scale redistribution of large quantities of snow. Windward slopes are scoured while leeward slopes are loaded. Figures 40 through 43 show some of the more common redistribution patterns. On the San Francisco Peaks

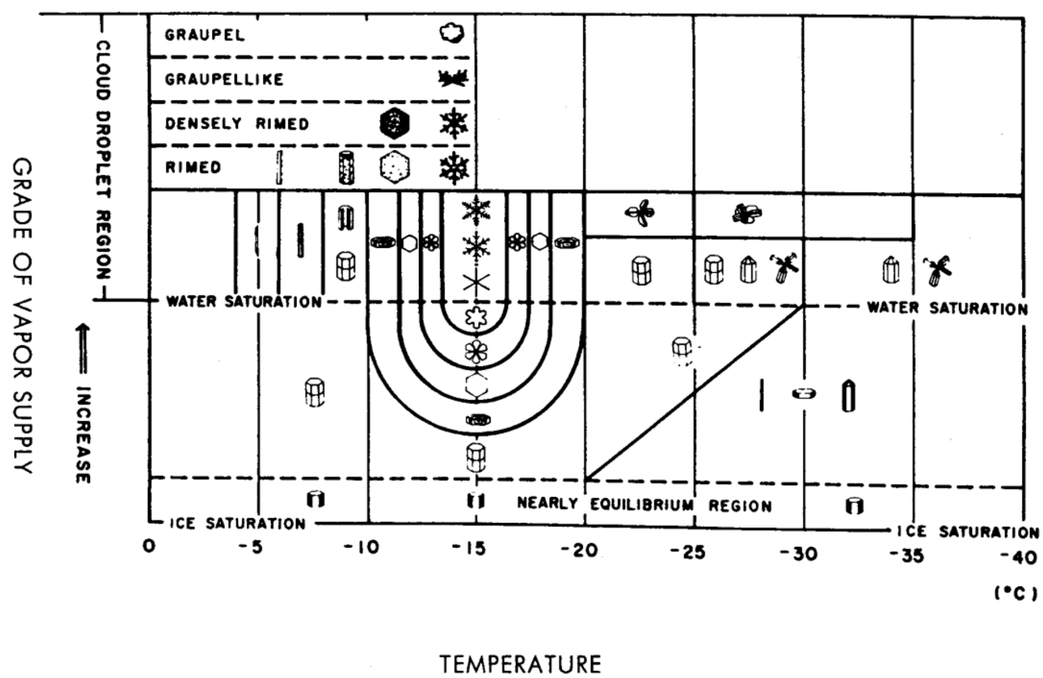


Figure 39. Saturation versus temperature effects on snow crystallization (from LaChapelle, 1969).

Figure 40. Loading of the Snowslide Springs Canyon Path starting zone occurs as a result of wind transport over the skyline ridges.

Figure 41. Loading of the Crossfire Path starting zone occurs as a result of long-ridge winds. Note the extremely wind altered avalanche debris in the runout zone.

Figure 42. Loading of the Telemark Path starting zone occurs as a result of winds crossing the northwest shoulder of Fremont Peak. A sizeable snow pillow forms in this area very quickly.

Figure 43. Flat-faced cornices are common on the San Francisco Peaks.

most loading occurs on north and east slopes within the Inner Basin. Some avalanche paths possess an overall west or south aspect but receive heavy loads in an obscure portion of the starting zone from the prevailing southwest flow. Allison Clay (path #450) and Sneaky Pete (path #070) are two examples.

## Snowpack

### Snow Climates

The winter progression of cyclonic storms delivers snow to the mountains of Arizona in varying quantity and quality. During the inter-storm periods, other environmental factors alter the snow as it lies on the ground. The resulting snowpack is thus composed of non-homogeneous stratigraphic layers differing in thickness, temperature, density, hardness, grain size, grain type, cohesion and adhesion. The factors, which affect the snowpack at a given locality, appear to be recurrent from season to season producing a snow climate. Although no study has yet attempted to define and map all possible snow climates, the designations in Figure 44 will serve for illustrative purposes.

### Radiation considerations

Radiation is not only operative on a planetary scale, but also operates to some degree on all scales right down to the domain of the individual snow grain as it evolves within the snowpack, the sub-micro scale, so to speak. Ed LaChapelle (in Ives, Harrison and Armstrong,

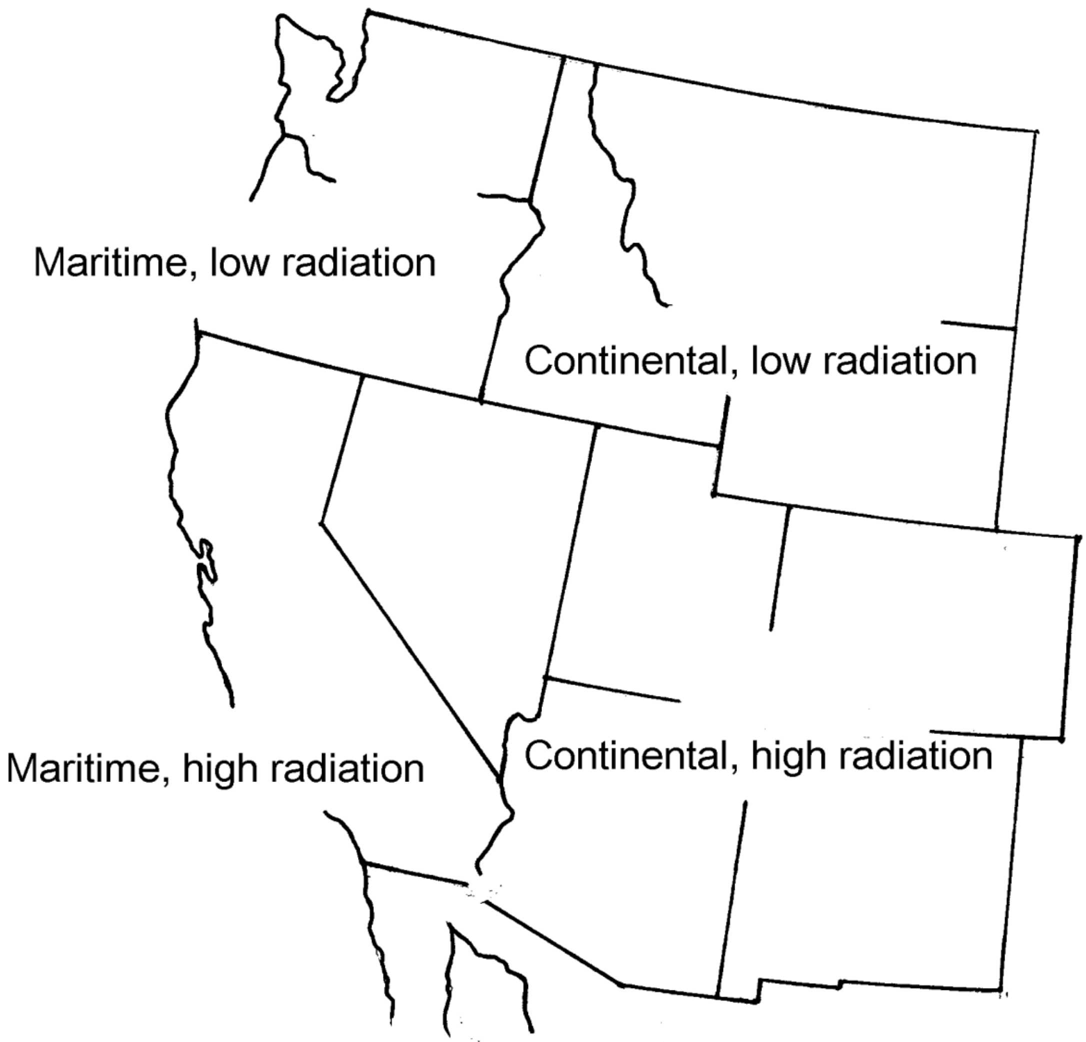


Figure 44. Basic factors affecting snow climates.

1973) first described the "radiation snow climate" from studies done in the San Juan Mountains of Southwestern Colorado {latitude 37°54′ north). LaChapelle wrote:

> "The combination of high altitude, low latitude, and predominately continental climate produces what we now define as a radiation snow climate."

The consequence of such a climate on avalanche activity was not well known prior to the INSTAAR studies (Armstrong and Ives, 1976). LaChapelle continues:

> "... They (the San Juan Mountains) exhibit climatic extremes not found in the more northerly latitudes where most practical and scientific knowledge of snow avalanche formation has been accumulated."

The San Francisco Peaks (latitude 35° 20' north) occupy one of the most radiation intense snow climates in the united States, having an average of 12 clear days in January compared to only 2-9 clear days for most other mountain areas in the Western states (Ruffner and Blair, 1977). As a consequence, the relatively thin Arizona snowpack receives large amounts of direct solar radiation on south facing slopes. Due to the low latitude very little shading of such slopes occurs. North slopes, under clear skies, experience radiation loss during most of the day. Both aspects lose radiation during clear nights. On the south slopes, such rapid and intense radiation fluctuations almost always produce inter-storm sun crusts of some thickness. These crusts often have thin temperature gradient (abbreviated TG) skins caused by some form of clear sky radiation loss related process (e.g. radiation recrystallization) (Perla and Martinel1i, 1976). These thin crusts are

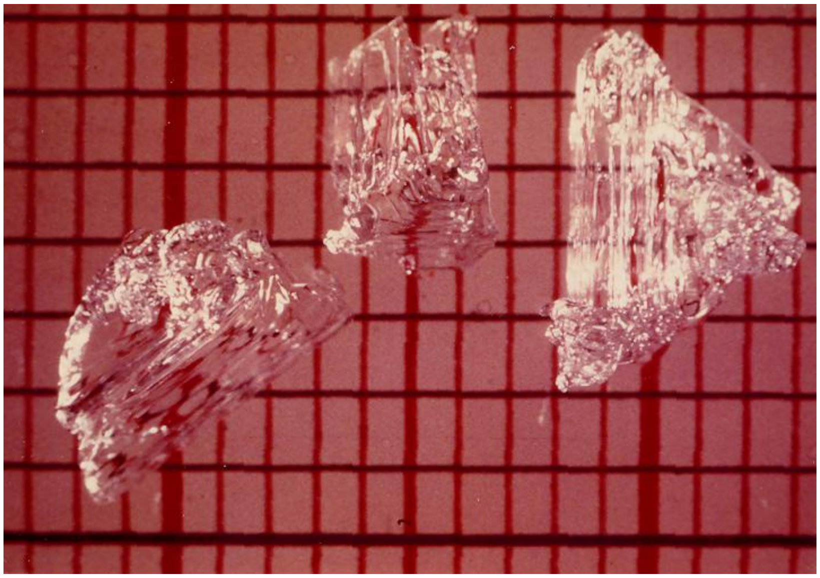

Figure 45. Temperature gradient (TG) snow is formed by intergranular mass diffusion of water vapor resulting in angular, stepped, poorly bonded grains (1 mm grid).

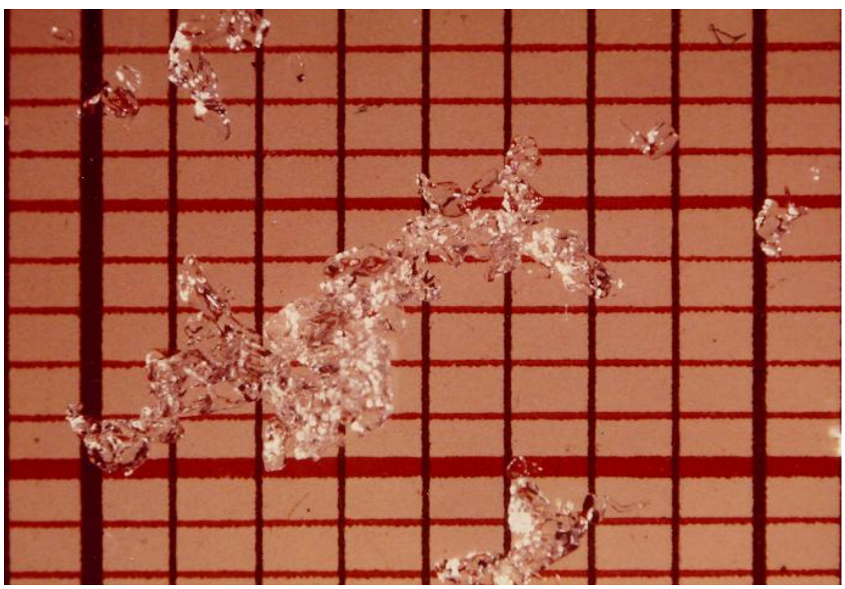

Figure 46. Equitemperature (ET) snow is formed by intragranular mass diffusion of water vapor which accumulates and freezes (sintering) at narrow necks connecting the grains into a continuous, strong ice skeleton (1 mm grid).

typically interspersed with thin layers of cohesionless snow undergoing more deeply-seated temperature gradient metamorphism (Figure 45). Hasty pits dug on south facing slopes reveal low mechanical strength within the layers and several skiers have reported unstable snowpack conditions on south slopes although natural releases are rare here. Strong wind redistribution appears to unload potential starting zones in prevailing (southwest) conditions to the point where natural releases rarely happen. Nonetheless, terrain and vegetation features indicate some natural activity does occur.

By comparison, north facing slopes are mostly shaded especially at starting zone angles. Under the influence of predominantly clear skies extensive and continuous radiation loss is the rule. Pits dug into north facing slopes show strong, deep seated temperature gradient snow, especially within the bottom meter (i.e. depth hoar). Crusts, some of substantial thickness (several cm.), are commonly interbedded within this early sequence. This basal TG/crust sequence is the product of light snowfalls from early season storms (usually Type A or A'). Strong radiation cooling follows the storm and establishes a steep temperature gradient within the thin snowpack. The daytime temperatures gradually return to fall normals during the long inter-storm periods. Weeks, or even months, of clear weather can separate these early storms allowing crust formation without direct solar input. Observations on the Peaks indicate that these crusts reduce vapor flow, but do not block the reestablishment of the TG process in subsequent layers. Indeed, the strongest TG metamorphism appears in the topmost layers (e.g. Figure 48) during the formation of this early season sequence.

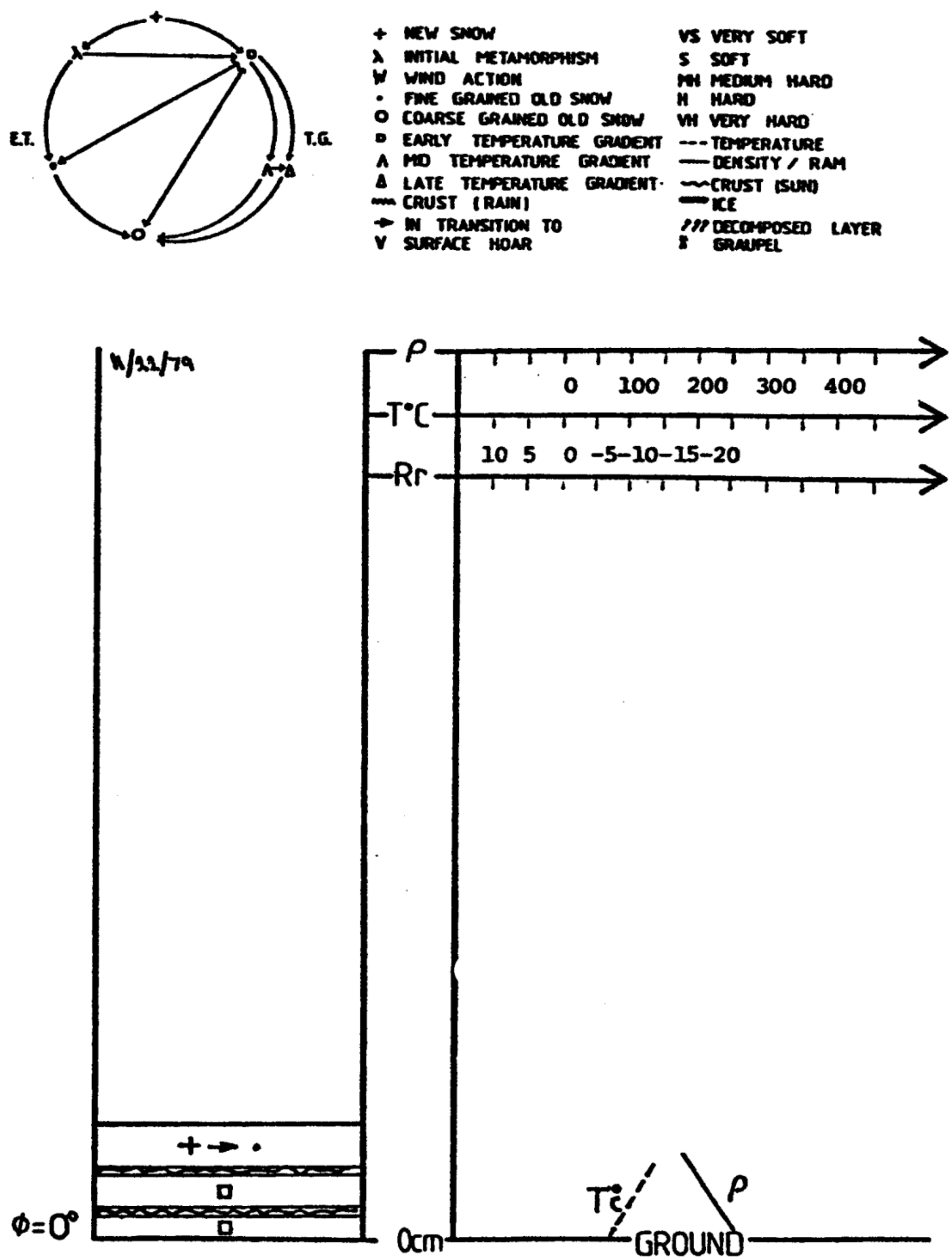


Figure 47. Snowpit profile on November 22, 1979.

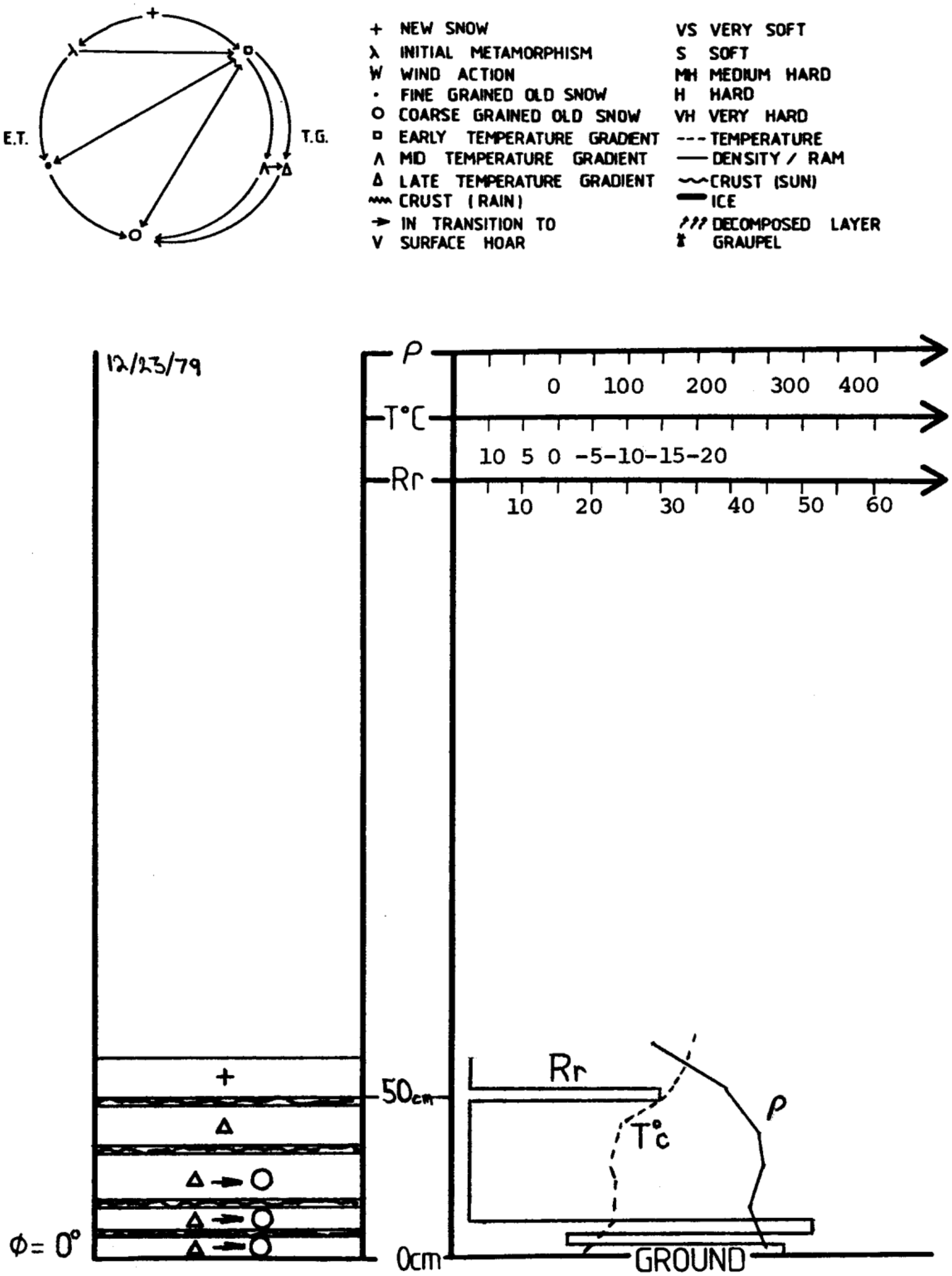


Figure 48. Snowpit profile on December 23, 1979.

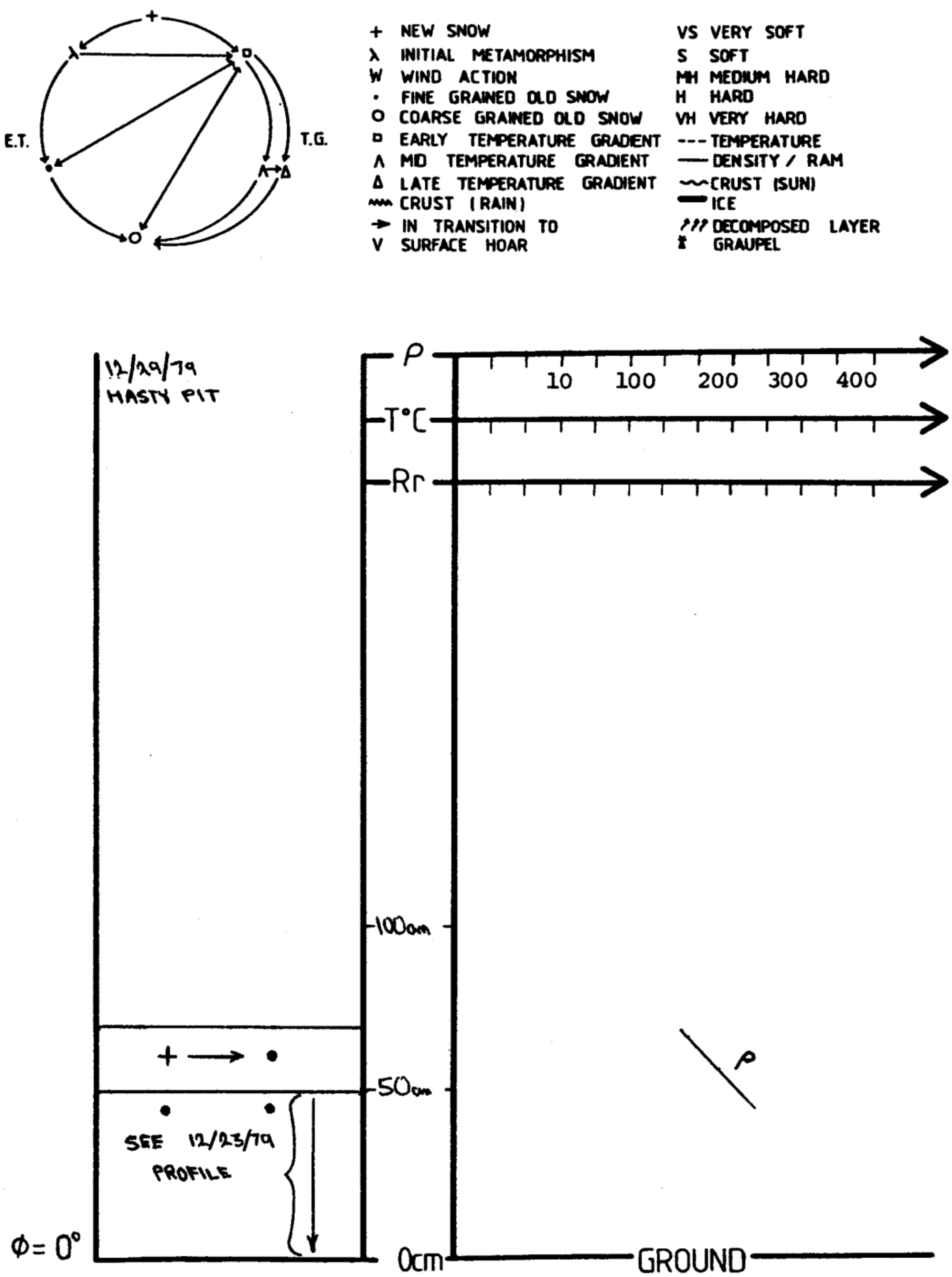


Figure 49. Snowpit profile on December 29, 1979.

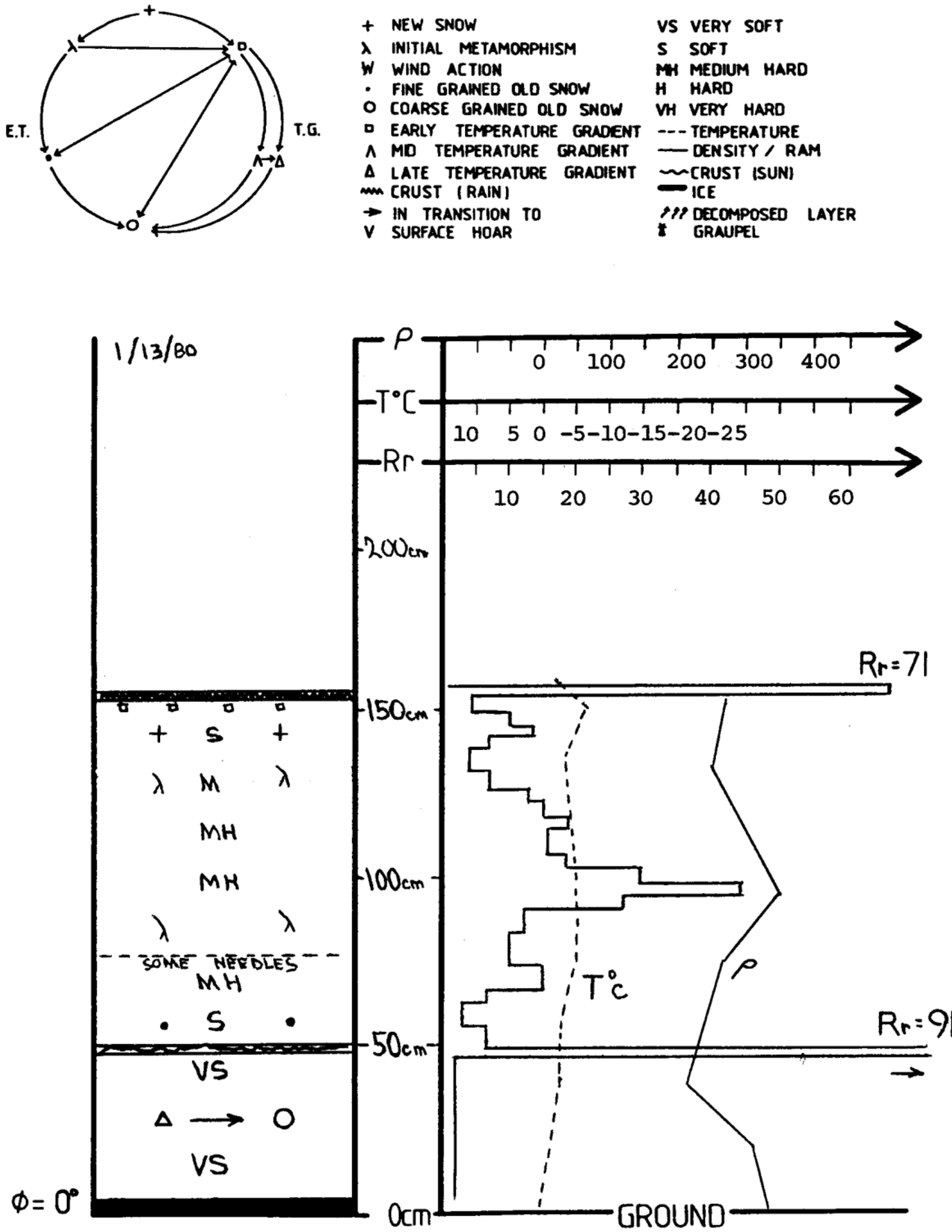


Figure 50. Snowpit profile on January 13, 1980. Large avalanche events were observed which ran on the basal temperature gradient snow.

Given seasonally normal conditions, this TG/crust sequence will be deep enough to cover terrain features, but remain shallow long enough to allow advance TG crystal evolution (i.e. depth hoar) with associated reduction in intergranular cohesion (Figures 47-50). Several large climax events have been observed to run on such basal sequences (Figure 50).

As winter progresses, the snowpack begins to build up rapidly (Figure 51). This heavy accumulation of snow tends to weaken the temperature gradient to the point where little, if any, TG metamorphism can be identified in the thicker layers with low magnification (10-20x) (Figure 50). Temperature gradient processes, active in this thick snowpack, now work on the snow/air interface or ice lenses (Figure 50) to produce occasional surface hoar lenses. Such layers of surface hoar may be preserved by rapid burial and become very hard to detect by any method except shear type tests.

Recrystallized grains (TG snow) are very slow to change their character once the steep gradient is removed. Angular grains have been found within isothermal (0°C) spring snowpacks, many weeks after the temperature gradient process had ceased.

North slope instability has also been observed to be induced by layers of cold, cohesionless new snow, very early equitemperature (abbreviated ET) snow (Figure 46), or layers of graupel (or other rimed particles). One note of interest is the lack of natural releases on deeply buried graupel layers even though they remain cohesionless. This is in contrast to frequent events involving graupel close to the surface of the snowpack.

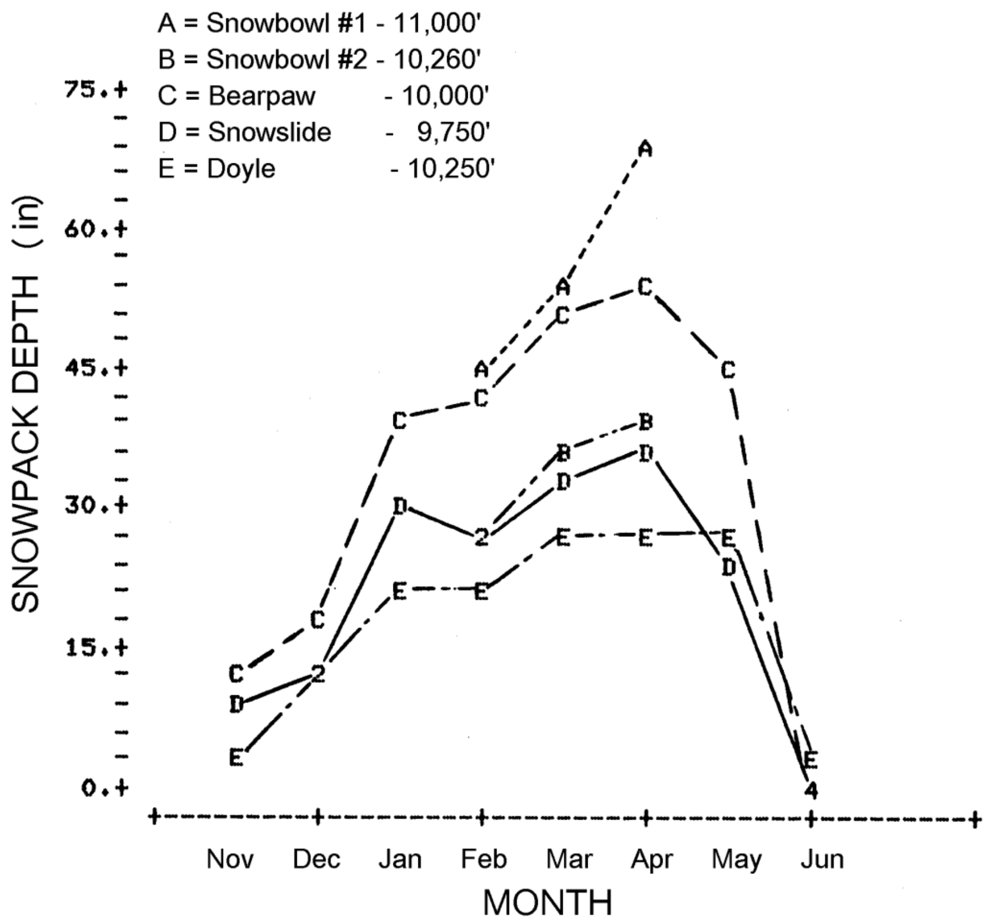


Figure 51. Snow accumulation for five sites on the San Francisco Peaks.

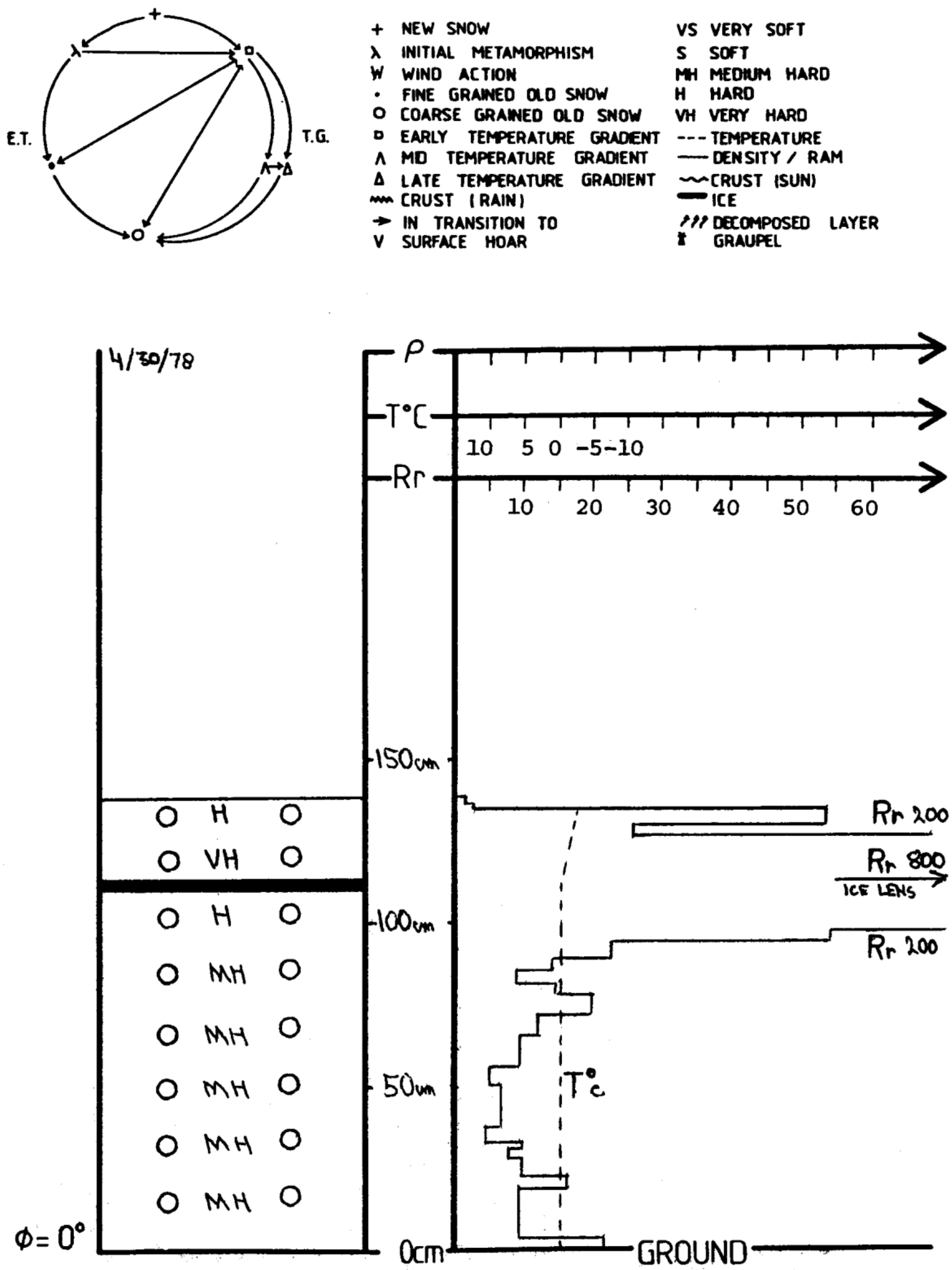


Figure 52. Snowpit profile on March 30, 1978. A typical spring snowpack.

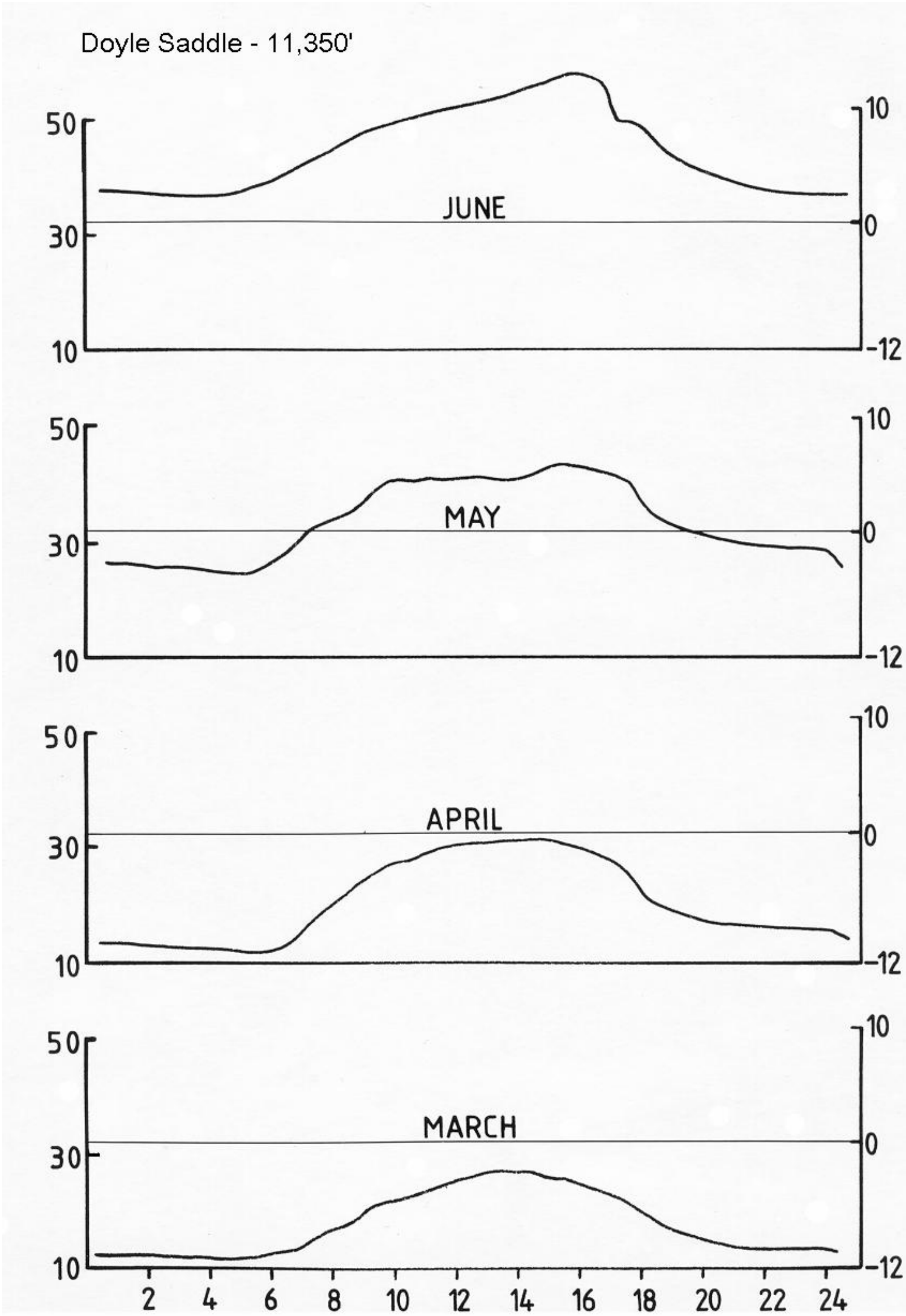


Figure 53. Air temperature progression with the onset of spring 1975 at Doyle Saddle. The Y axis is degrees (F and C) and the X axis is hour of the day (Society of Physics Students, 1975).

As spring approaches, warmer temperatures return (Figure 53). Increasing amounts of free water are found within the snowpack until the entire mass comes to 0°C. This condition is referred to as isothermal. Melt-freeze metamorphism (abbreviated MF) becomes the dominant metamorphic process during this change (Perla and Martinelli, 1976). Large amounts of free water break down the ice skeleton of the snowpack into a low cohesion "mush". This mush is most pronounced on the surface and along ice lenses deep in the snowpack. Extreme instability can be induced by rain, adding free water to an already wet snowpack. The events of May 31, 1979 represent this kind of overload. These wet avalanches are referred to as the spring avalanche cycle and appear to start when the mean temperature in the starting zone reaches O°C for at least two days (Armstrong and Ives, 1976) (Figures 52-53).

Maritime-continental Considerations

Northern storms (type A) leave small amounts of cold, dry snow; a distinctly continental characteristic. Type B systems leave large amounts of cool snow producing the highest avalanche activity yet observed. This is a product of interaction between continental and maritime influences. Type C systems, with high freezing levels (up to 3,350 meters or 11,000 feet during one January storm in 1980), drop heavy, damp snow characteristic of the more maritime Sierra Nevada range.

# Chapter 4

# DENDROCHRONOLOGIC DATING OF AVALANCHE EVENTS

## Principles

The application of tree ring analysis in dating recent geologic events is not new. Lawrence (1950), followed by Siqafoos and Hendricks (1961), used such methods in glacial studies. More recently, Potter (1969), followed by Burrows and Burrows (1976), applied similar techniques specifically to avalanche event dating. Most current methods are based on information from damaged trees which survive the events. Such damage is usually represented in the ring growth pattern. The major problems with such techniques relate to the separation of avalanche damage from non-avalanche damage. For example, several episodes of fire in the Inner Basin during the late 1800s are reported by Colton (1930) and Duncklee (ca. 1974). Damage to trees from such fires could be mistaken for avalanche damage. With this in mind, it is best to sample a <u>suite</u> of damage types from known areas of avalanche occurrence and compare the results to those obtained from an adjacent non-avalanche area.

The writer termed any damage readable from the ring pattern an event “indicator". It was realized that some indicators were capable of greater accuracy than others. “Direct” indicators can, theoretically, be dated to the actual year of the event. “Conditionally” direct indicators may, but do not necessarily, date the exact year of the event.

Conditionally direct indicators do not necessarily respond immediately and, thus, suggest a trend back in time toward the exact year of the event. "Indirect" indicators can only approximate the year of the event. Table 3 categorizes specific damage types.

| Direct | Conditionally Direct | Indirect |
|---|---|---|
| Scars<br>Reaction wood<br>Terminal year | Change in ring width<br>Epicormic growth | Colonization age<br>Absolute age<br>Decay rate |

Table 3. Types of Avalanche Event Indicators

It is important to understand the nature of these indicators and their relation to both avalanche and non-avalanche events.

### Scars

Scars are wounds on trees resulting from damage to the cambium.

Dating assumptions. The year of the scarring action can be determined directly from the ring pattern by using standard ring counting procedures. Avalanche related scars are usually located low on the trunk (within the first few meters) and on the uphill side (Burrows and Burrows, 1976) (Figure 54).

Problems. Rockfall, lightning, animals, sun scald, and fire all can produce scars. Most non-avalanche scars can be detected by slope and height relations, by lack of agreement within a statistically significant number of samples, or by the inclusion of carbon residue in the case of fire scars (Burrows and Burrows, 1976).

Figure 54. A main trunk showing several scarring events, one of which corresponds to the absolute age of the epicormic branch (left) taken from higher up the same tree.

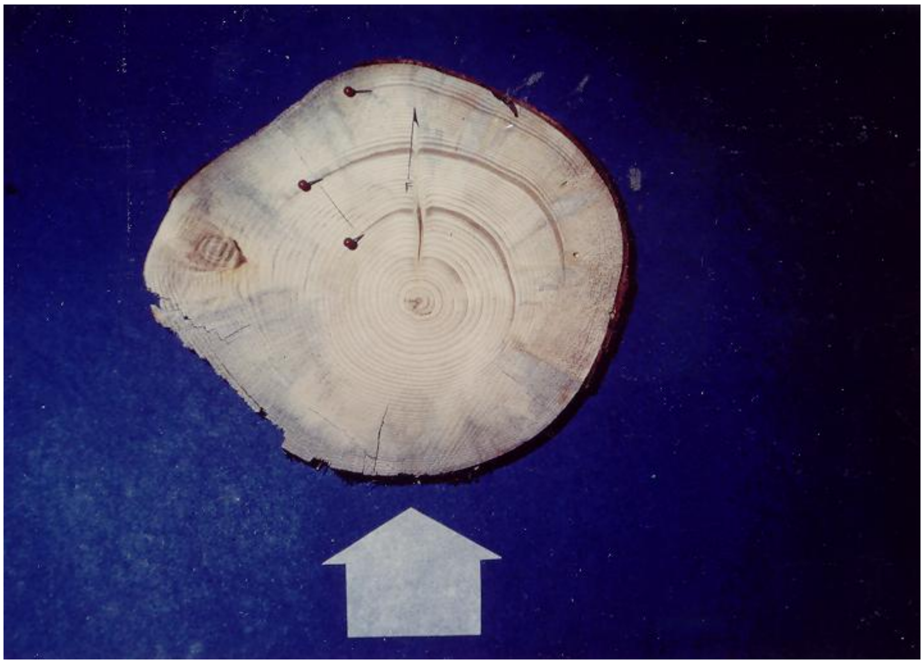

Figure 55. Thin reaction wood (rotholz) on a tree located at a sensitive site with respect to avalanches.

Reaction Wood

Trees with strong apical dominance attempt to maintain vertical growth with respect to gravity. The corrective mechanism for maintaining vertical growth occurs in the xylem. In Gymnosperms, a modification of the trachied cells on the downslope side of the tree (with respect to gravity) produces compression wood. Compression wood forms eccentric growth rings which exert preferential force within the downslope side of the trunk. This force slowly returns the apical leader to a vertical position. The specialized xylem cells are much darker than the normal earlywood and are called "rotholz" or "redwood" (Wardrop et. al., 1965).

Dating assumptions. Avalanche induced tilting results in the formation of reaction wood especially on the downslope (with respect to topography) side of the tree. Reaction wood seen in spruce sampled on the Peaks is easi1y identified and the year of the tilting event can be found by standard ring counting procedures (Burrows and Burrows, 1976) (Figures 55 and 59). Reaction wood appears to be the most sensitive and widely distributed indicator in the study area.

Problems. Windthrow, soil creep and snow creep can induce tilting with subsequent reaction wood production. Massive windthrow usually displays less terrain control than avalanche throw. In addition, windsnap (in the upper portion of the tree) and lack of scars can be used to distinguish wind damage. Soil and snow creep are harder to deal with. Close inspection of adjacent timber should reveal the degree to which creep affects the overall locality. In addition, control transects should be used to compare avalanche versus non-avalanche

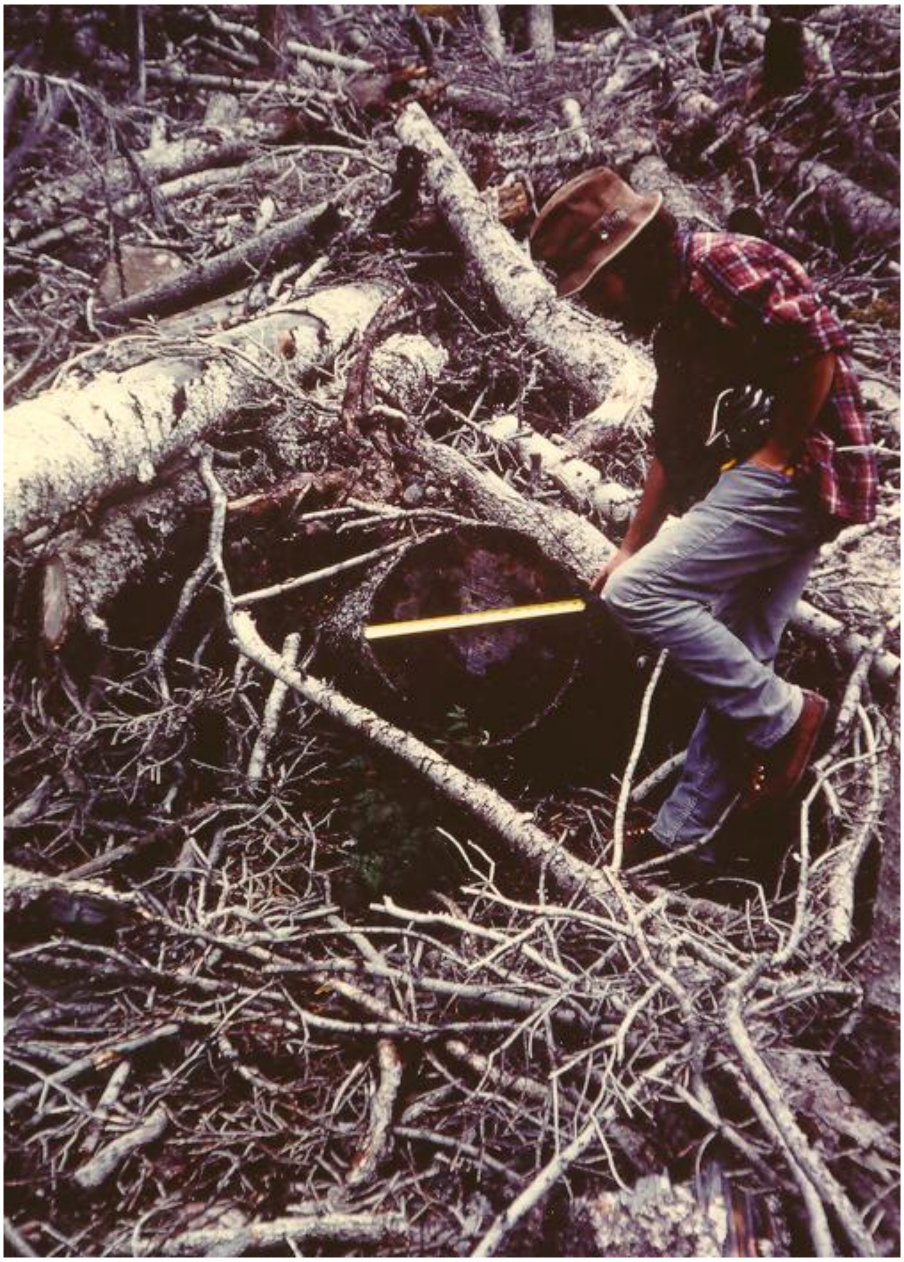

Figure 56. Several trees knocked down by the 1973 Dunnam Canyon avalanche were over 200 years old.

Figure 57. An epicormic branch in Allison Clay Path which dates to 1932.

reaction wood quantities.

Such comparison sampling done as part of this study indicates about 10 times more reaction wood can be expected from trees growing in distinctly avalanche prone sites. Branches may not be used for reaction wood dating as they produce compression wood continuously in response to gravity. It is especially desirable to have corroboration from other indicators when working with an event dated primarily by reaction wood.

## Terminal Year

In theory, the most accurate dating method would be the determination of the terminal growth year for a large sample of downed trees in the runout zone. For example, most all of the 200 samples used in this study come from 1980 avalanche knock-downs.

Dating assumptions. The terminal growth year (i.e. the last year the living tree added a ring) would be the event year minus one.

Problems. In practice, the determination of the terminal year is not so simple. Comparison chronologies may not be available or may not cross date reliably. The writer is currently working on a cross dating method based both on ring width and damage positions within the ring pattern. Wind or fire-killed trees may be infused along with the avalanche-kills and care should be taken to distinguish them if possible.

## Changes in Ring Width

Relative ring width is usually controlled by environmental conditions of the area in which a particular tree is growing.

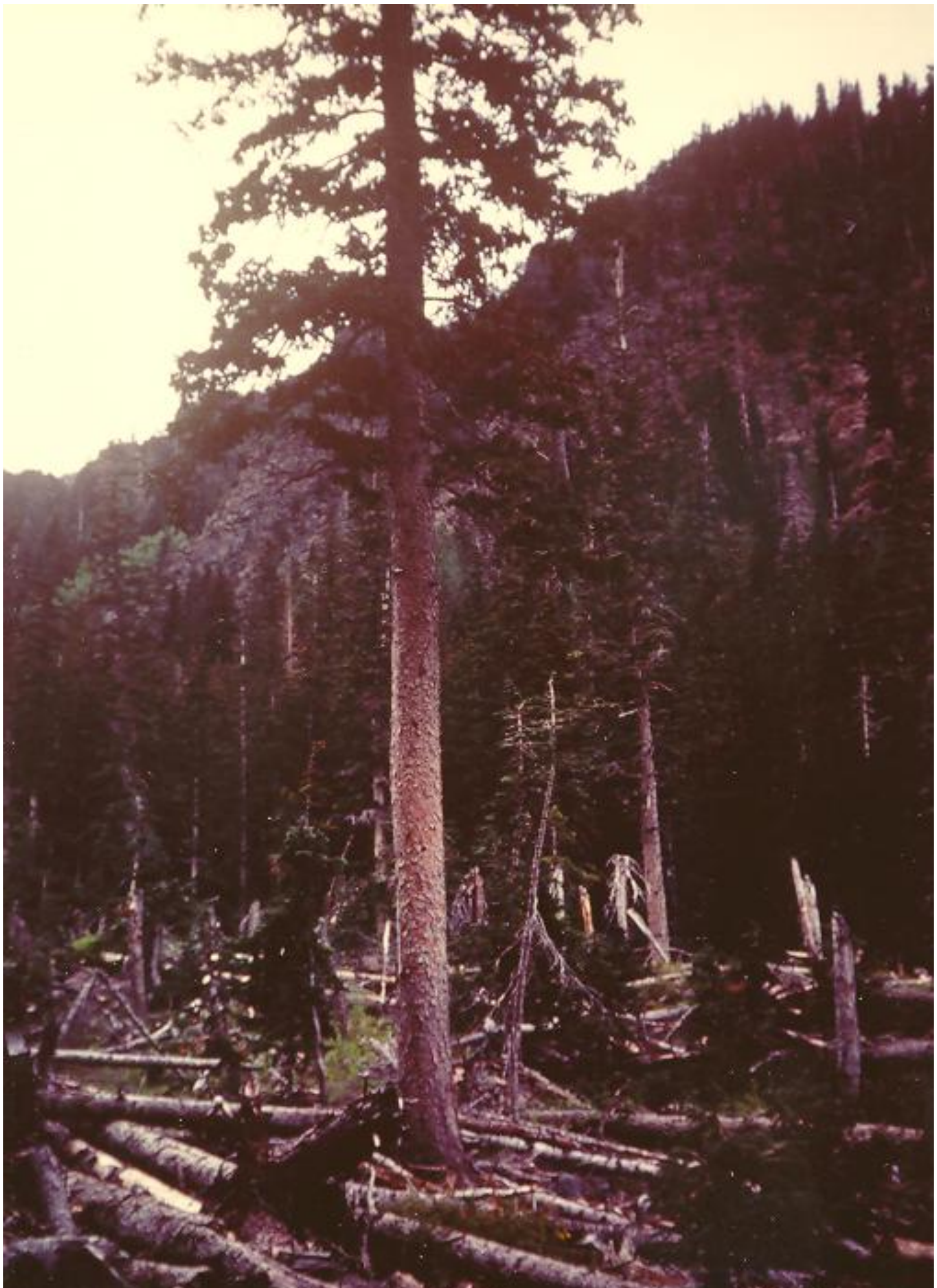

Figure 58. Specimen number DN-012 taken from this tree in Dunnam Canyon shows marked ring width expansion due to removal of competition in 1973.

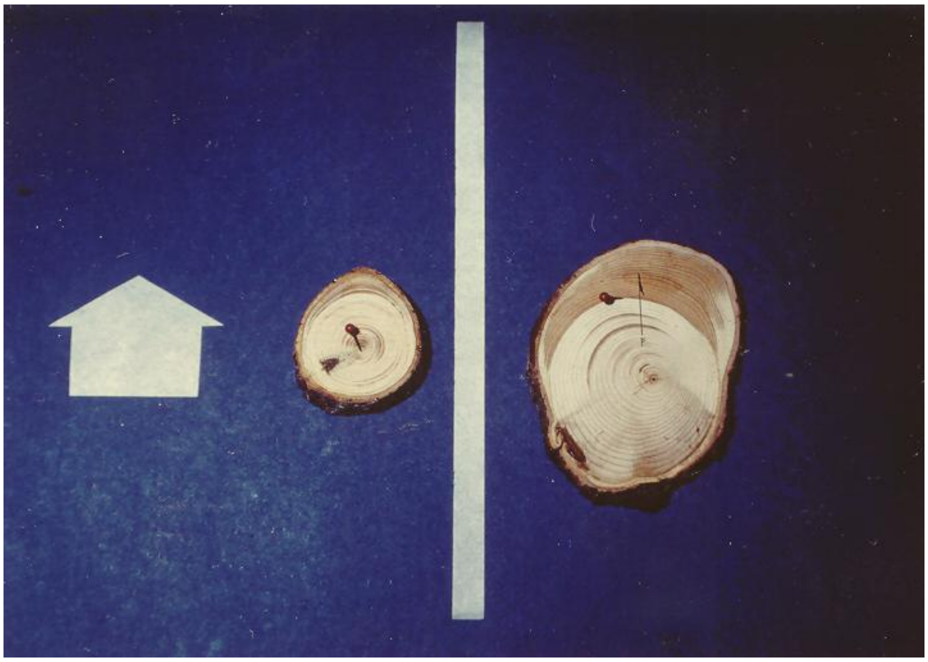

Figure 59. A hypothetical trimline showing re-colonized trees to the left of the line. Note the reaction wood on the specimen to the right of the trimline.

Figure 60. A view down track in Dunnam Canyon.

This change in ring width has been the cornerstone of dendrochronolgy and dendroclimatology. Environmental change may occasionally result in a limited area from avalanche activity (Potter, 1969).

Dating assumptions. Radical ring width changes found only on specimens in, or immediately adjacent to, avalanche paths may indicate avalanche activity. Trees growing at, or very near, trimlines may show ring width expansion due to removal of competition (Figure 58), or ring width suppression due to damage (Potter, 1969).

Problems. Other factors may have produced ring with changes. Other indicators should be sought for corroboration.

## Epicormic Growth

Suppressed buds may be released following the removal of a branch or stem. Growth from these buds will replace the lost member.

Dating assumptions. The absolute age of an epicormic branch will date the year of growth following the breakoff (Burrows and Burrows, 1976).

Problems. Epicormic release does not always occur immediately after the breakoff, although several such branches dated exactly the type event (Dunnam Canyon, 1973) used in this study. Epicormic branch dates are conditionally direct and should be given latitude to drift back in time to a position of agreement with other indicators (Appendix 1). Windsnap may mimic avalanche damage but generally avalanche breakage occurs close to the ground (Figure 54 and 57).

Absolute Age

Absolute age should not be confused with terminal year. Absolute age is the number of years a tree has lived. Absolute age is useful in determining minimum return periods of avalanche events (especially unusually large events) (Burrows and Burrows, 1976).

Dating assumptions. The age of a statistically significant number of downed trees will indicate the minimum return period for an event reaching that area (Figures 56 and 60).

Problems. Many trees may escape or survive several events only to be destroyed by a direct hit from a relatively small event. Many small shattered trees may survive the worst of events as well. This type of indicator is best applied to large events which overrun the high frequency channel (e.g. Dunnam Canyon, 1973).

Colonization Age

This indicator is much like absolute age, but relies on living trees which have colonized an avalanche clearing to give a date to the causal event.

Dating assumptions. Areas cleared by avalanche will begin to heal by the establishment of pioneer species whose absolute age will date the event (Figure 59).

Problems. Colonization age is an indirect indicator because usually not all trees are removed during an event. Small, resilient trees may survive. Even in areas where complete clearing has taken place, dates are still inexact due to varying germination times (Burrows and Burrows, 1976).

## Decay Rate

A rather inexact method, the use of wood decay rates has been tested in at least one study (Burrows and Burrows, 1976). This indicator was used in this study to select trees for sectioning. Green needles present on downed trees were taken to indicate a previous winter kill (i.e. winter 1980).

Dating assumptions. Fallen trees exist in various states of decay proportional to the length of time elapsed since the terminal year (Figure 56).

Problems. Poor accuracy and precision severely limit the use of this principle.

# Methods

## The Sampling Scheme

The selection of a representative, yet practical, sampling scheme was complicated by several factors:

1) The population of interest (i.e. avalanche events over the last 51 years) was non-extant.

2) The extent of the sample population (i.e. a sensor population) of avalanche damaged trees was not known.

3) Ethical and governmental restrictions existed on the sample population.

   a) No living trees could be sectioned.

   b) Increment boring of living trees was allowed.

4) For a downed tree to be usable, its terminal growth year had to be ascertainable. In practical terms, this meant the tree had to be dead yet still possess green needles.

These difficulties were resolved by the adoption of a loosely structured systematic sampling scheme in which transects were run vertically along trimlines or horizontally around contours. At intervals of approximately 200 to 400 feet (60 to 120 meters) a sampling area of about 50 feet (15 meters) in diameter was selected. Trees displaying avalanche damage within the assigned area were sampled. This method allowed for the scarcity of useable specimens while keeping the systematic "net" dense enough to "catch" major avalanche events. Trimlines were used as vertical guides because they represent lines of greatest avalanche-forest interaction. Occasionally, horizontal transects were run to investigate multiple trimlines, successional stages and other cross-path variations.

Paths considered for inclusion in the study were reviewed in terms of:

1) Significant size of the path.
2) Sufficient avalanche/forest interaction.
3) Path aspect (some similar, some diverse).

Field reconnaissance indicated the following five paths best fit the requirements (Figures 61-62):

1) Beard Canyon (#220).
2) Dunnam Canyon (#210).
3) Snowslide Canyon (#170).
4) Allison Clay Path (#450).
5) Crossfire Path (#360).

Two control transects were also selected:

1) Flying Dutchman Ridge.
2) Reese Peak Ridge.

The control transects were sampled in the same manner as the actual active avalanche paths. It was felt the control transects would provide a basis for differentiating random damage levels from damage incurred by avalanche activity.

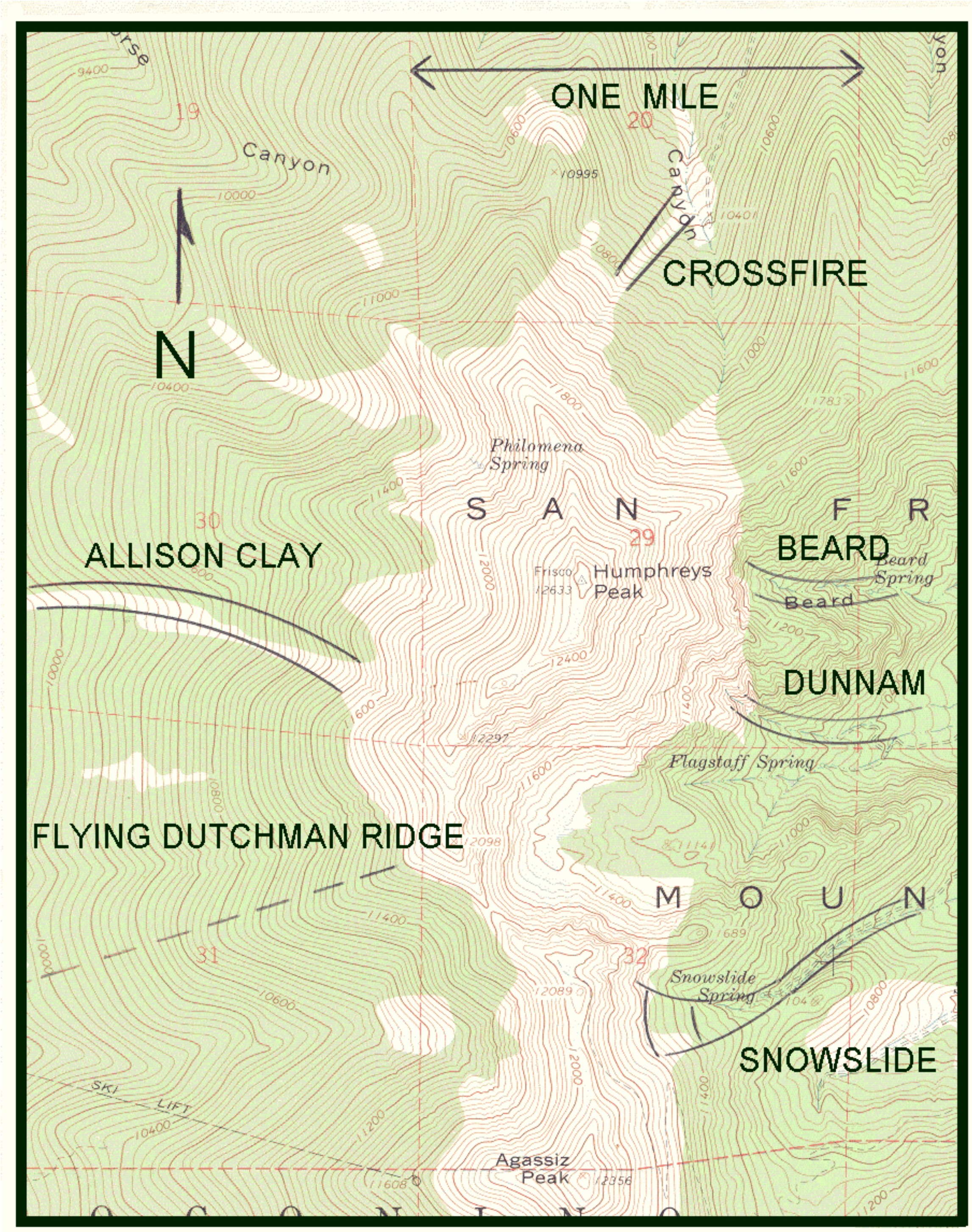


Figure 61. Sample (solid line) and control (dashed line) transects, western portion.

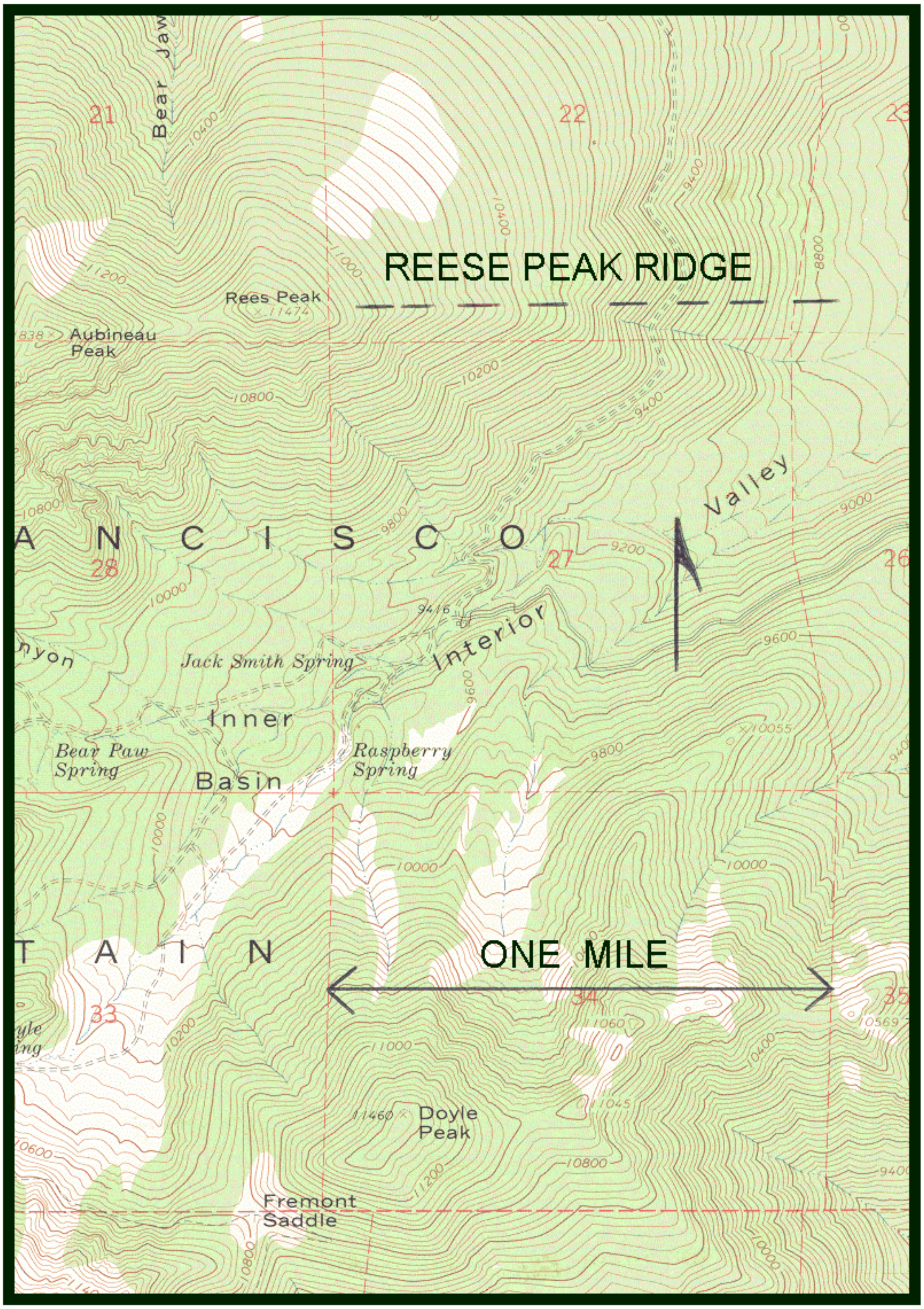


Figure 62. Sample (solid line) and control (dashed line) transects, eastern portion.

A major event of known age (the February, 1973 Dunnam Canyon avalanche) was assigned as the "type event" for the study (Arizona Daily Sun, 1973). All methods, assumptions and problems were compared to this event for confirmation or resolution.

Once the sampling route for a particular path was determined, the actual sampling was done. Location control was maintained with the aid of a U.S. Geological Survey 7½ minute topographic map and a Thommen altimeter. Trees meeting the criteria for cross-sectioning were cut with a Poulan Micro XXV chain saw or a bow saw. Living trees were cored with a Finnish FK increment borer (5mm x 40cm). Each tree was treated as a single site and multiple specimens from the same tree were assigned the same sample number with a unique letter suffix. In the laboratory, each cross-section disc was thinned to approximately 1 cm and belt sanded to a fine finish on one side. Each core was glued in a mount or clamped in a special block for sanding or shaving.

Rather than establish an independent master chronology, several key sample discs were shown to Jeff Dean at the Laboratory of Tree Ring Research and he visually confirmed that the samples could be cross dated to the Flagstaff area master chronology (Dean, 1980).

## Extraction and Reduction of Data

Each of the 227 specimens was examined for event indicators and a date was assigned to each indicator found. Counts were done either under naked eye or under low (10x - 30x) magnification. Most ring counts were straightforward but a few were of questionable accuracy. Missing rings, false rings, and confused patterns can cause count problems (Stokes and Smiley, 1968).

All counts were assigned an estimate of count error. This value was typically 0 but ranged to +/- 5 years. Less than 3% of the indicators ranged over +/- 2years. An average error value was estimated at +/- 1 year. Once all counts were logged, a plotting scheme was devised by the writer to summarize the data. These figures are referred to as "damage versus time plots" (Appendix 1). Their use allows rapid comparison between:

1) Year of Damage.
2) Type of Damage.
3) Range of count error.

A damage versus time plot was compiled for each path and for the combined control transects. Two data files were built from these plots to perform statistical operations on a Sigma VI computer. The files were built as follows:

1) Raw quantitative data (Figures 63-68)

   The percentage of the total samples from a given path showing damage on a per year basis.

2) Adjusted nominalized data (Figures 70-74)

   All counts were allowed to drift to a best fit within the range allowed by estimated count error. All values were reduced by the 10 percent maximum expected random damage as determined from the control transects.

The raw quantitative data are presented as the most accurate representation of the field situation. The adjusted nominalized data are presented as the most reliable representation of true avalanche activity.

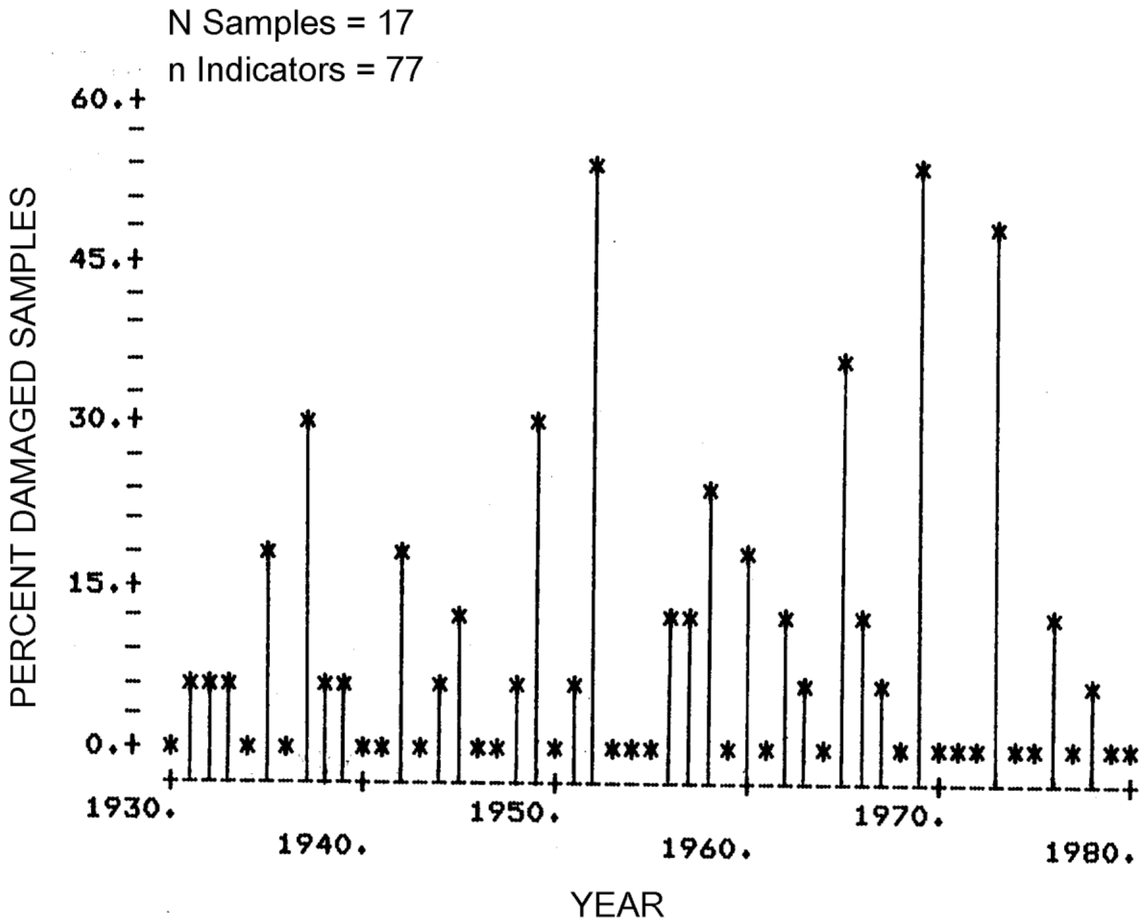


Figure 63. Raw tree tring data for Beard Canyon Path.

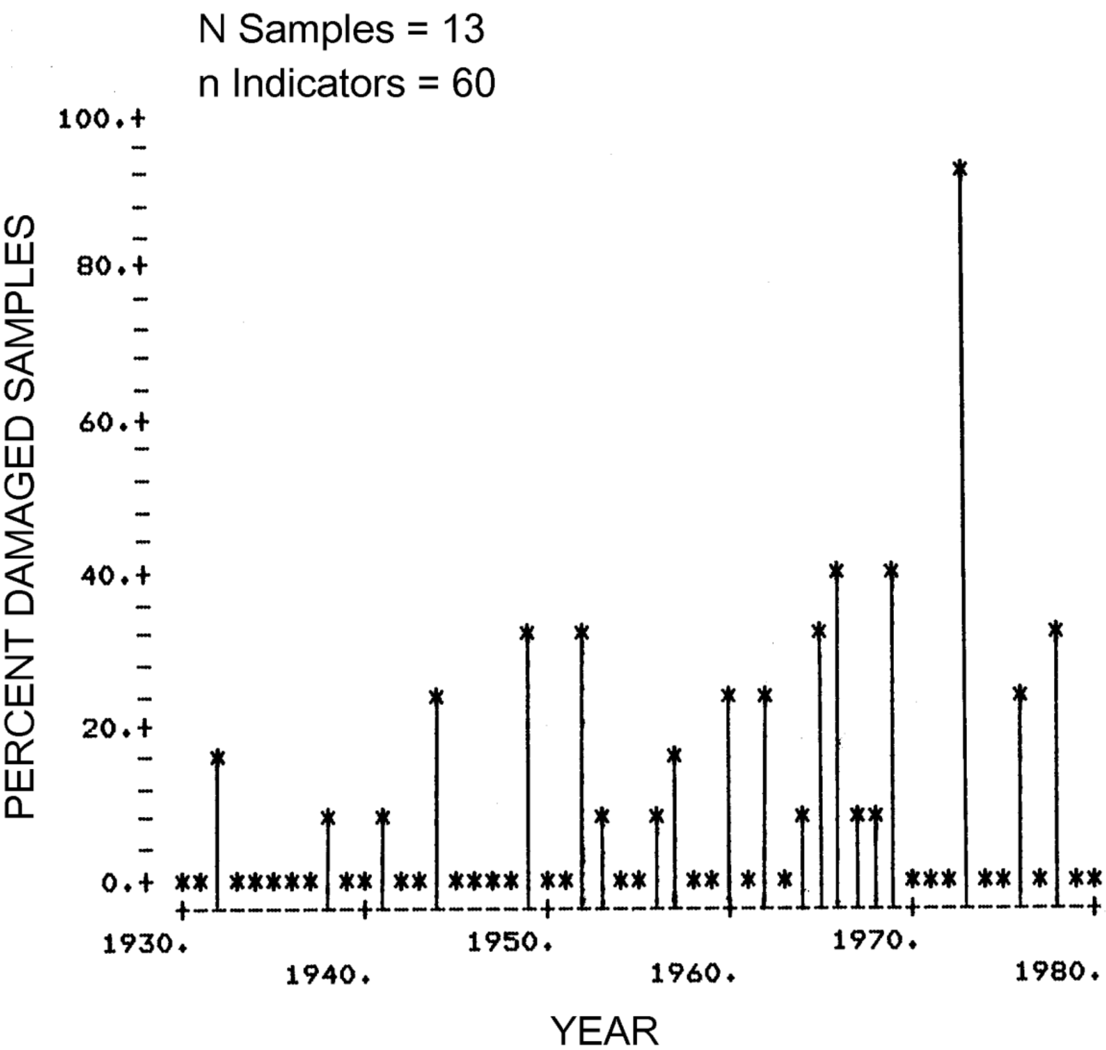


Figure 64. Raw tree ring data for Dunnam Canyon Path.

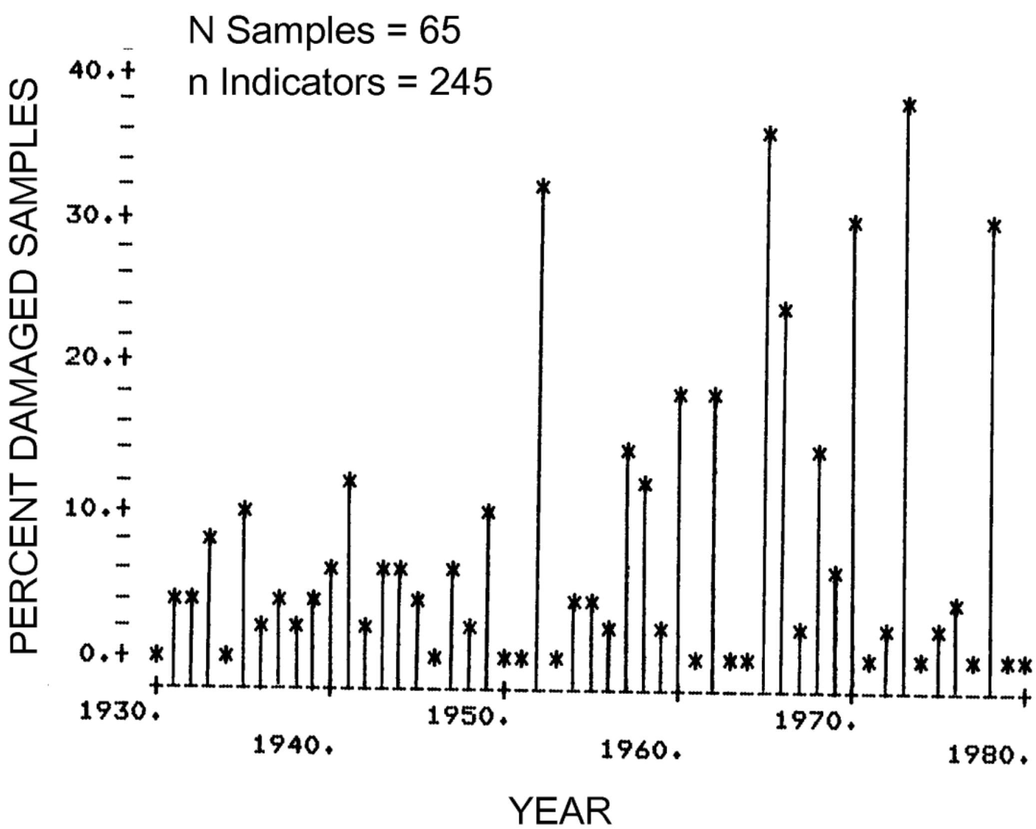


Figure 65. Raw tree ring data for Snowslide Spring Canyon Path.

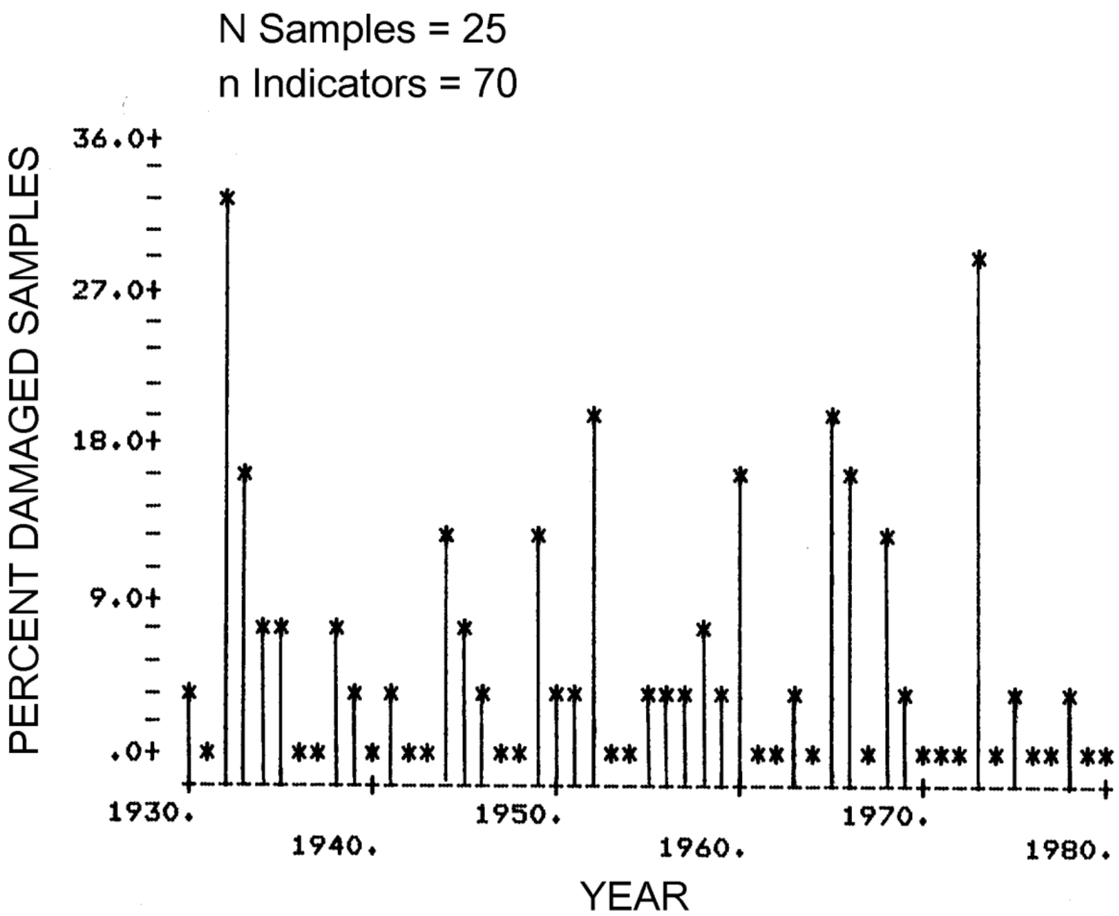


Figure 66. Raw tree ring data for Allison Clay Path.

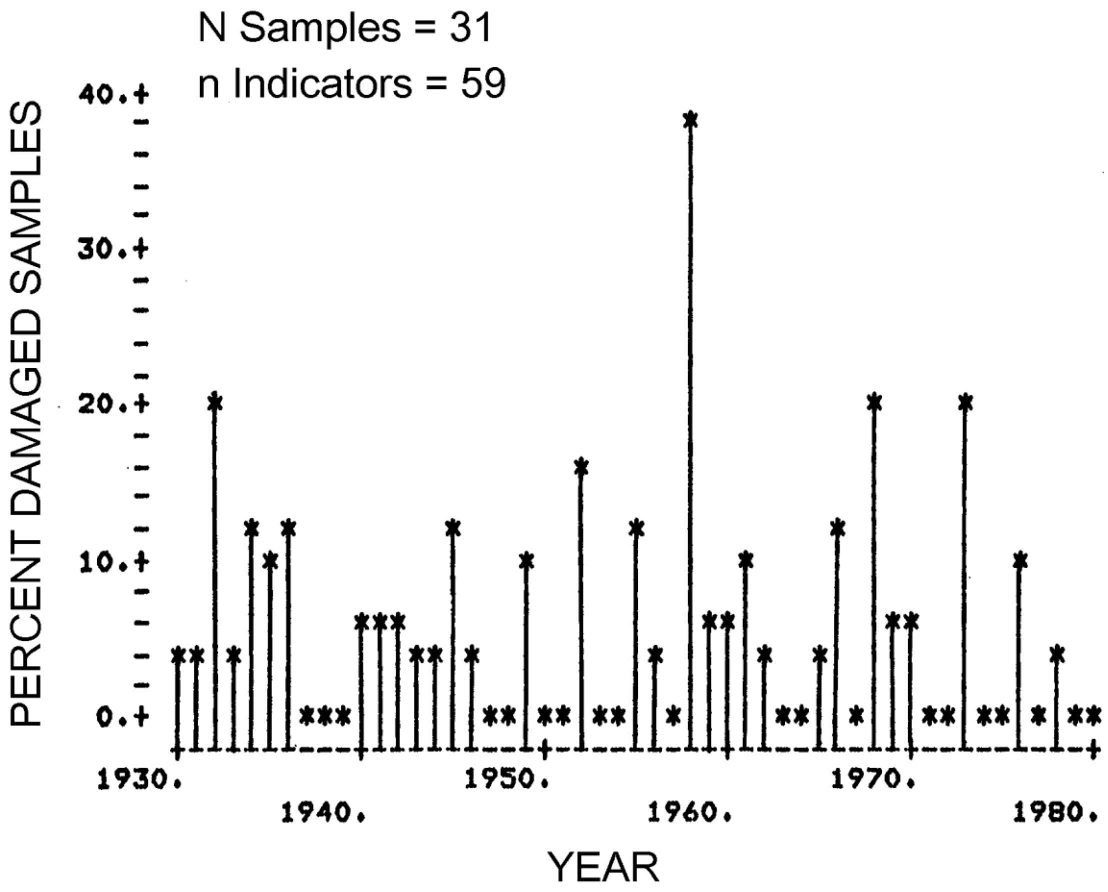


Figure 67. Raw tree ring data for Crossfire Path.

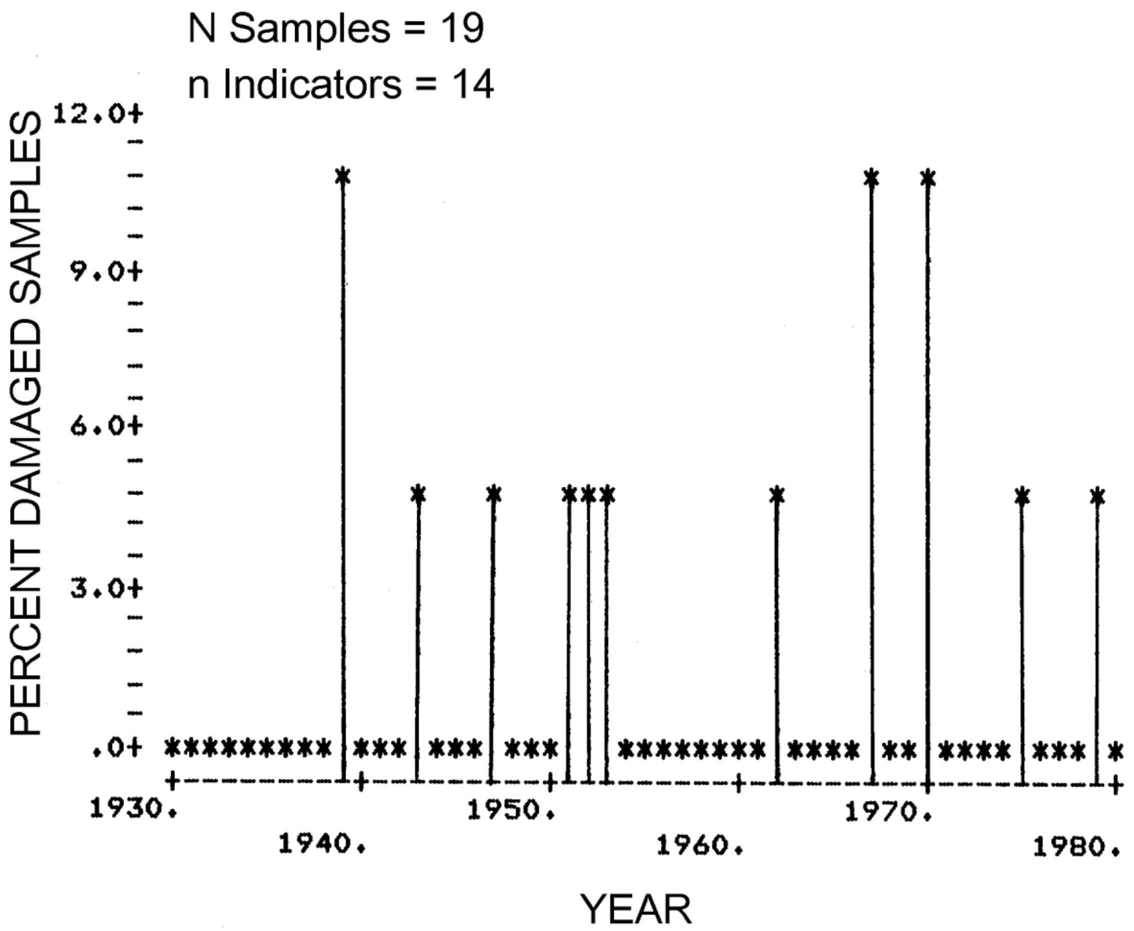


Figure 68. Raw tree ring data for the control transects.

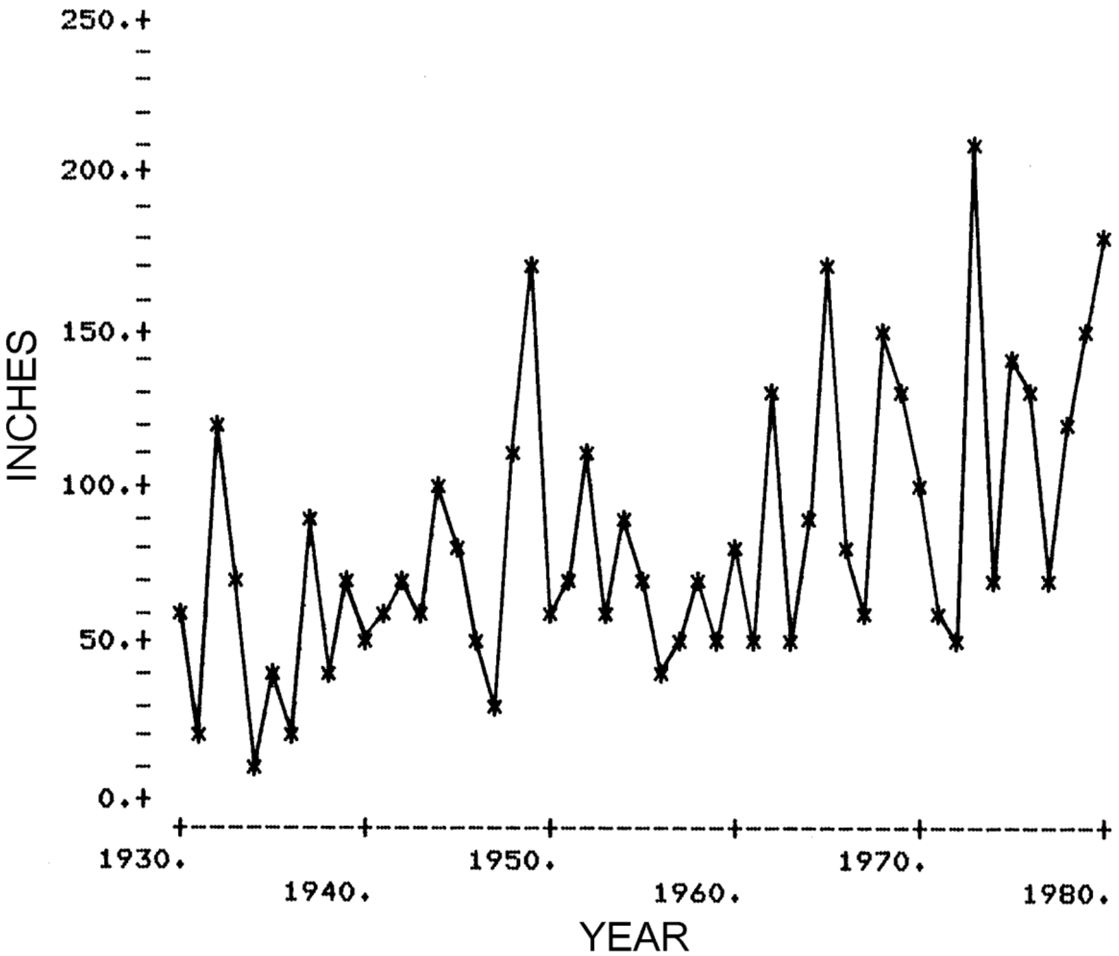


Figure 69. Flagstaff snowfall from 1930 to 1980.

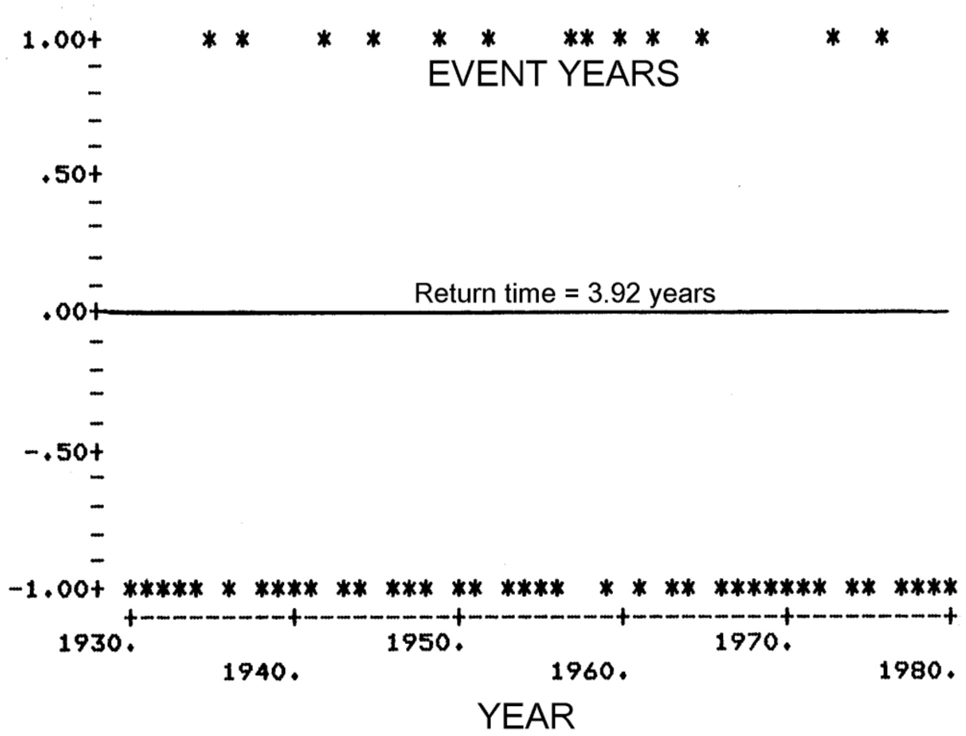


Figure 70. Adjusted and nominalized tree ring data for Beard Canyon Path.

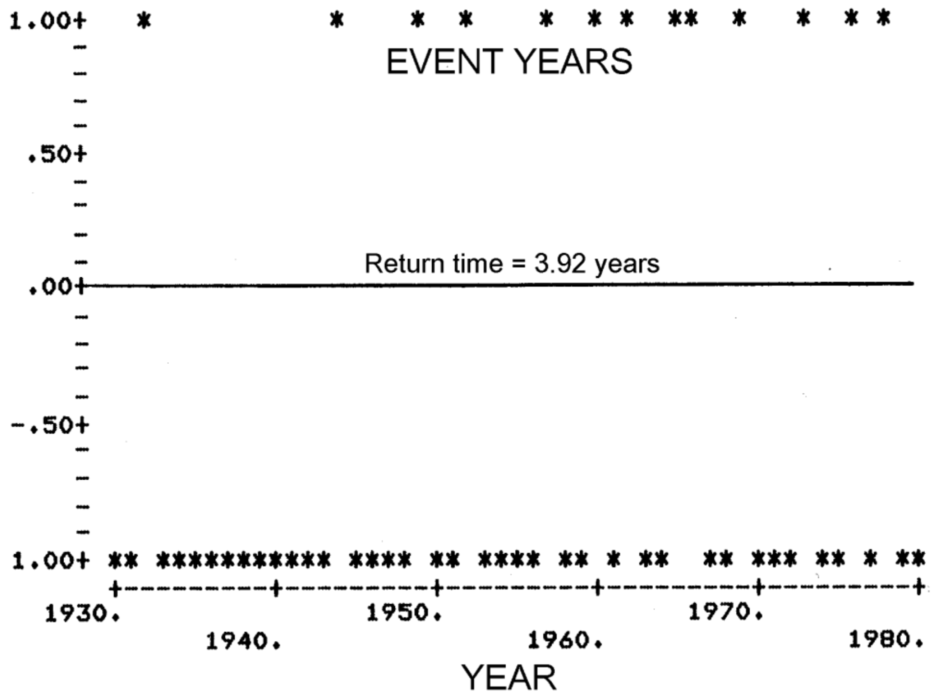


Figure 71. Adjusted and nominalized tree ring data for Dunnam Canyon Path.

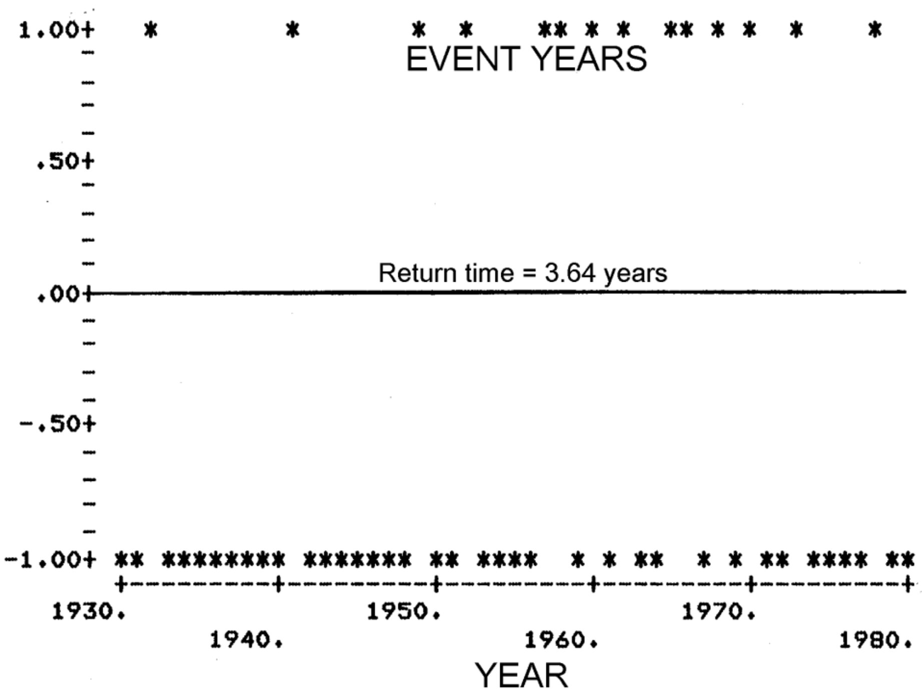


Figure 72. Adjusted and nominalized tree ring data for Snowslide Canyon Path.

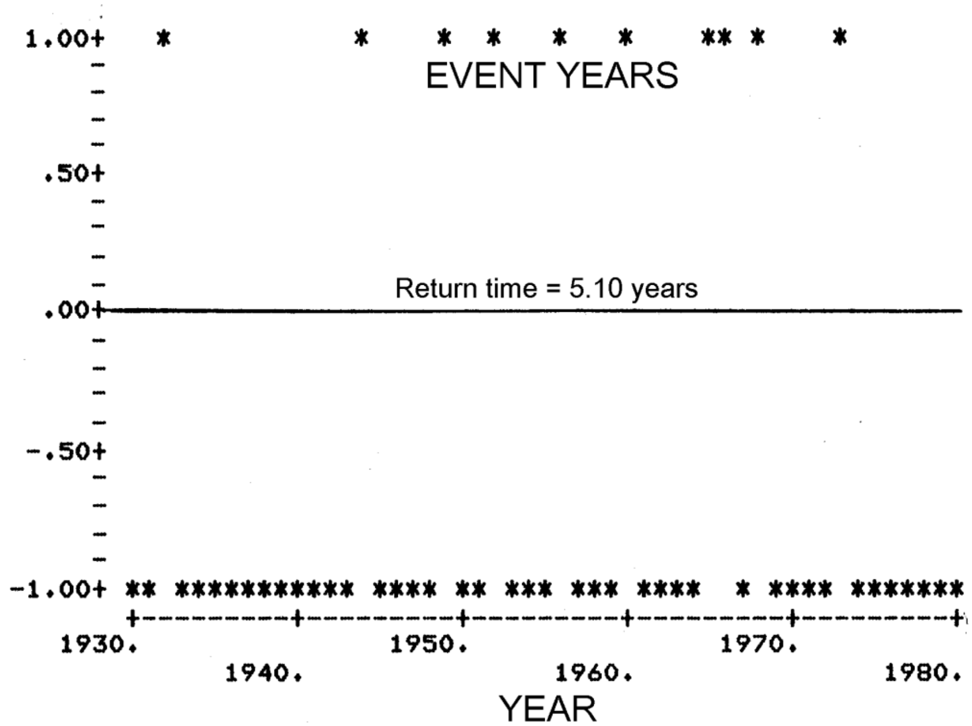


Figure 73. Adjusted and nominalized tree ring data for Allison Clay Path.

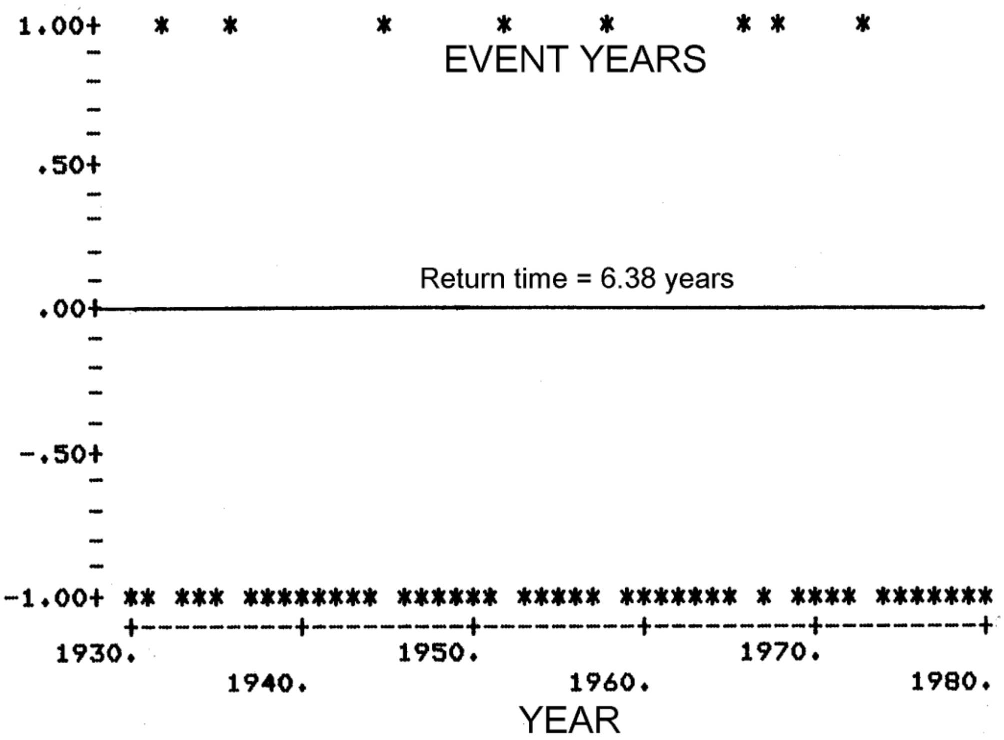


Figure 74. Adjusted and nominalized tree ring data for Crossfire Path.

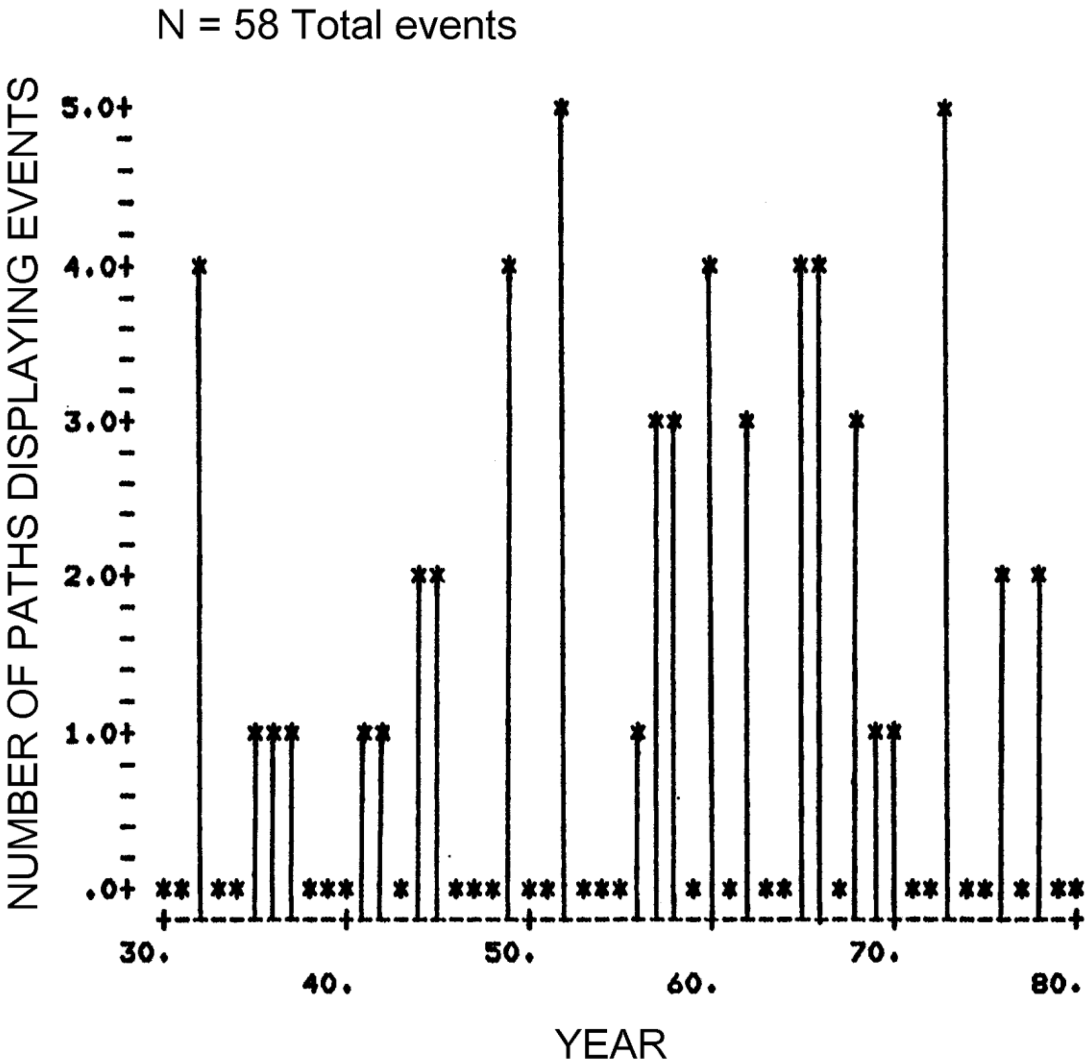


Figure 75. Tree damaging avalanche events as a function of time.

## Statistical Analyses

Following a basic outline for analyzing time series in Davis (1973), the two sets of data were applied under the following assumptions:

1) The population is most likely not normal.
2) The quantitative data are assumed to be indicative of event magnitude.
3) No assumption of event magnitude is implied in the nominal data set.

A variety of statistical methods (mainly non-parametric) were applied as follows:

| Characteristics | Methods | Data |
|---|---|---|
| Trends | Regression<br>Runs Test | Raw quantitative<br>Adjusted nominal |
| Cycles | Autocorrelation<br>Poisson<br>Runs test | Raw quantitative<br>Adjusted nominal<br>Adjusted nominal |
| Similarities | Spearman's Rho<br>K-S statistic<br>Cross-association<br>Coefficient of Similarity | Raw quantitative<br>Raw quantitative<br>Adjusted nominal<br>Adjusted nominal |

Table 4. Statistical methods.

### Trend Analyses Methods

Regression. Visual inspection of the data did not suggest any linear trend over the fifty year study period (see Figures 63-67). To confirm this notion the raw quantitative data was regressed against time in years.

Linear trends, if present, should produce the following regression characteristics:

1) Low deviation about the regression line.

2) A high $R^2$ value (coefficient of determination).

3) A high mean square value indicating most of the fit comes from a real agreement between the data points.

Regression was run via Minitab II on the Sigma VI computer.

Runs Test. The presence of a non-random influence in the data set (e.g. trends or cycles) can be brought out of the nominal data by use of the non-parametric runs test. This test counts the number of times a distribution passes a specified value and compares this value to that expected for a similar random distribution. This test was carried out at the 95% confidence level.

## Cyclic Analysis Methods

Autocorrelation. Autocorrelation is a statistical process numerically equivalent to sliding a time series past an image of itself and noting the match of values (Yi) in the form of the coefficient of autocorrelation (r) at given intervals called lags (L):

$$r_L = \frac{\left[(n-L)(\sum Y_i Y_i + L) - \sum Y_i \sum Y_i \ + \ L\right]/(n-L)(n-L-1)}{\left[(n\sum_{i=1}^{n} Y_i^2 - (\sum_{i=1}^{n} Y_i)^2 - \right]/\, n(n-1)} \qquad (1)$$

Program AUTOCR listed in Davis (1973) was entered in the Sigma VI and the raw quantitative data was run through lag 17. Subroutine TSPLOT (Davis, 1973) produced correlograms from the output of AUTOCR.

Poisson Distribution and Return Time. Two different tests for the Poisson relation (a distribution of rare discrete events) were done:

1) Kolmogorov-Smirnov distribution comparison.

2) $X^2$ goodness of fit probability.

Both tests were performed on the nominal data set. Davis (1973) describes the fo11owinq procedure for comparing a given distribution to a Poisson distribution by use of the Kolmogorov-Smirnov statistic.

1) Transform the data into:

$$Y_i = t_i / T \tag{2}$$

$T_i$ = time from beginning of series to the $i^{th}$ event.

T = total length of the time series.

2) Determine KS+, KS-:

$$KS_+ = (\sqrt{n_{\max}})\left|(1/n - Y_i)\right| \tag{3}$$

$$KS_- = (\sqrt{n_{\max}})\left|(Y_i - (i-1)/n)\right| \tag{4}$$

$$KS = \max\left|KS_+, KS_-\right| \quad \text{(sic.)} \tag{5}$$

This writer modified equation to:(see Pollard, 1977)

$$KS = \max{}_{difference}\left|KS_+ - KS_-\right| \tag{6}$$

3) This value is compared to the KS critical level for 95% confidence:

$$KS_{(0.05)} = 1.36/n \tag{7}$$

The hypotheses for the test are:

$H_O$: no difference from Poisson
$H_A$: different from Poisson

Betsy Armstrong (in Armstrong and Armstrong, 1978) describes a chi-square test of the Poisson distribution as a predictor of 1arge avalanches covering one mile or more of Highway 550 in the San Juan Mountains of Colorado. Assuming the large events on the Peaks to be of similar magnitude, a chi-square test was run on the nominal data set:

The Poisson probability (P) is defined as:

$$P = e^{-\lambda} \lambda^{r} / r! \tag{8}$$

e= base e of natural logs
$\lambda$= mean
r!= number of cases factorial

P was calculated for two cases, the 0 major event per year case, and the 1 major event per year case (the maximum resolution allowable in this study).

The expected probability is found by:

$$P_{\exp} = (P)(n) \tag{9}$$

Expected probability was calculated for each case. This is compared to the number of observed events or non-event years by the chi-square distribution:

$$X^{2} = (O - E)^{2} / E \tag{10}$$

O = observed
E = expected

The chi-square value can then be equated to a probability value for the Poisson distribution as a predictor of major avalanche events. A theoretical return period (T) can be calculated by (Haan, 1977):

$$T = 1/P \tag{11}$$

This can be compared to the observed value.

Similarity Analysis Methods

The path plots from the raw data set show a certain degree of visual similarity. Several tests and analyses were run to quantify the similarity.

Spearman's Rho. - A non-parametric version of Pearson product moment correlation:

$$r_{jk} = \text{Covariance}/s_j s_k \tag{12}$$

Spearman's Rho uses the ranks of the data rather than actual values. The Minitab II program on Sigma VI did the computations.

Kolmogorov-Smirnov Test. - The so called KS statistic is a non-parametric test of distribution similarity which is form sensitive (Miller and Kahn, 1962). Pollard (1977) suggests caution when using the KS test on discrete data. He claims the significance is lower than the nominal rate and the chance of a type II error is increased. He recommends accepting the null hypothesis only when the test statistic is well below the nominal critical value. As a result, the .01 level critical values appear to be the clearest discriminators. Their use solves close tolerance rejection problems for these data. In this study the raw quantitative data are grouped into five-year class intervals (Table 12) and plotted on a cumulative frequency diagram. The maximum difference between any two path plots in question ($d_n$ max) is calculated.

The value N:

$$N = n_1 n_2 / n_1 + n_2 \tag{13}$$

is used to enter a graph of critical level values. The selected critical level value is compared to $d_n$ max with the following hypothesis:

$H_0$: no difference in distribution forms

$H_A$: different distribution forms

<u>Cross-Association.</u> Cross-association is a nominal data equivalent of cross correlation. For this study only one match point was compared (match point 51 or year to year correspondence). The nominal data for each pair of paths is compared for the number of matches (i.e. event year to event year) or mismatches (i.e. non-event year to event year). The chi-square test for goodness of fit is then applied:

$$P = {}^{x}1K\,{}^{x}2K / n_1 n_2 \tag{14}$$

${}^{x}1k$ = number of observations in the k state of sequence 1
${}^{x}2K$ = number of observations in the k state of sequence 2
n = total observations in sequence

P is calculated for two states (match and mismatch). The expected number of matches is:

$$X^2{}_{mat} = (P)(n) \tag{15}$$

The expected number of mismatches is:

$$X^2{}_{mis} = (1 - P)(n) \tag{16}$$

The total chi-square:

$$X^2_{tot} = X^2_1 + X^2_2 \tag{17}$$

This value is compared to $X^2_{(.05,\ 1)}$ with the hypotheses:

$H_O$: no difference from random sequences

$H_A$: different from random sequences

<u>Coefficient of Similarity.</u> This equation provides a simple test of relative association using the nominal data set (Sokal and Sneath, 1963):

$$S_{ss} = (p+n)/(p+n+m) \tag{18}$$

$S_{ss}$= coefficient of similarity
p = number of matches
n = number of negative matches
m = number of mismatches

```
                             AUTOCORRELATION
         -1.0  -.8  -.6  -.4  -.2  .0   .2   .4   .6   .8  1.0
           +----+----+----+----+----+----+----+----+----+----+
LAG (YEARS)
 1  -.259                     XXXXXXX
 2  -.152                       XXXXX
 3  -.006                           X
 4   .275                           XXXXXXXX
 5  -.142                       XXXXX
 6  -.138                        XXXX
 7   .093                           XXX
 8   .086                           XXX
 9  -.044                          XX
10  -.088                         XXX
11   .008                           X
12  -.139                        XXXX
13   .168                           XXXXX
14  -.076                         XXX
15   .037                           XX
16  -.015                           X
17   .246                           XXXXXXX
```

Figure 76. Correlogram for Beard Canyon Path,

```
                       AUTOCORRELATION
           -1.0 -.8  -.6  -.4  -.2   .0   .2   .4   .6   .8  1.0
             +----+----+----+----+----+----+----+----+----+----+

LAG (YEARS)

 1  -.140                         XXXXX
 2  -.138                          XXXX
 3   .147                             XXXXX
 4   .170                             XXXXX
 5   .154                             XXXXX
 6  -.138                          XXXX
 7   .126                             XXXX
 8   .167                             XXXXX
 9   .052                             XX
10  -.097                           XXX
11   .056                             XX
12  -.018                             X
13   .164                             XXXXX
14  -.082                           XXX
15  -.160                         XXXXX
16   .153                             XXXXX
17   .059                             XX
```

Figure 77.   Correlegram for Dunnam Canyon Path.

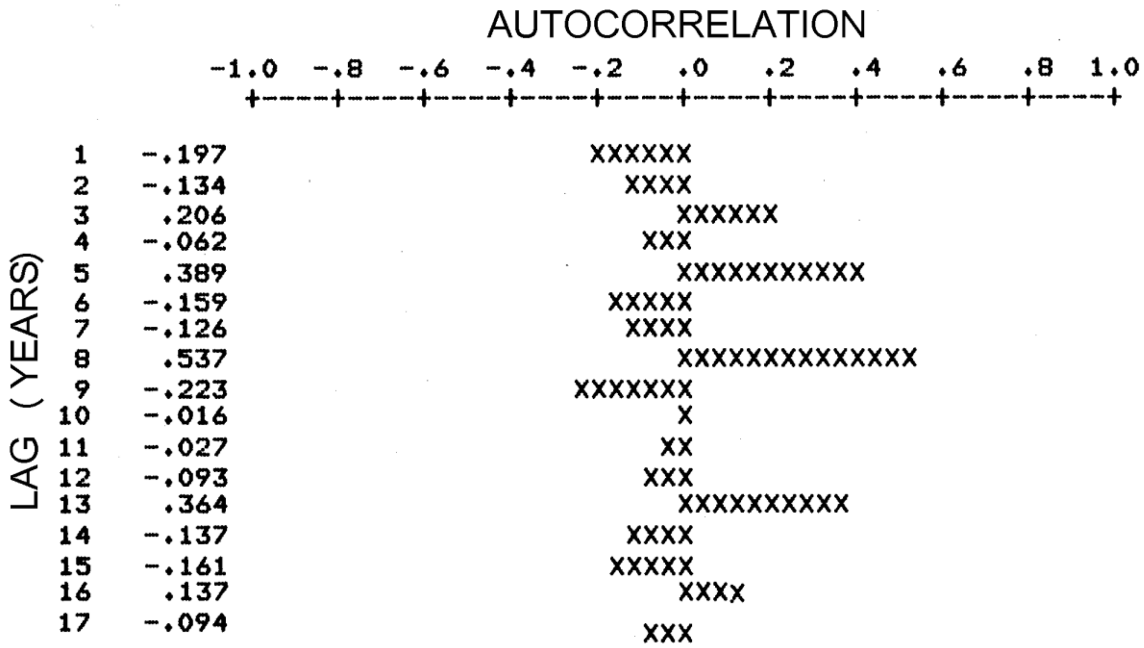


Figure 78. Correlogram for Snowslide Spring Canyon Path.

AUTOCORRELATION

```
            -1.0  -.8  -.6  -.4  -.2   .0   .2   .4   .6   .8  1.0
               +----+----+----+----+----+----+----+----+----+----+
 1   -.003                              X
 2   -.105                           XXXX
 3   -.006                              X
 4   -.247                        XXXXXXX
 5    .048                              XX
 6   -.013                              X
 7    .010                              X
 8    .213                              XXXXXX
 9   -.146                          XXXXX
10   -.114                           XXXX
11   -.080                            XXX
12   -.126                           XXXX
13    .137                              XXXX
14    .001                              X
15   -.103                           XXXX
16    .072                              XXX
17    .080                              XXX
```

LAG (YEARS)

Figure 79. Correlogram for Allison Clay Path.

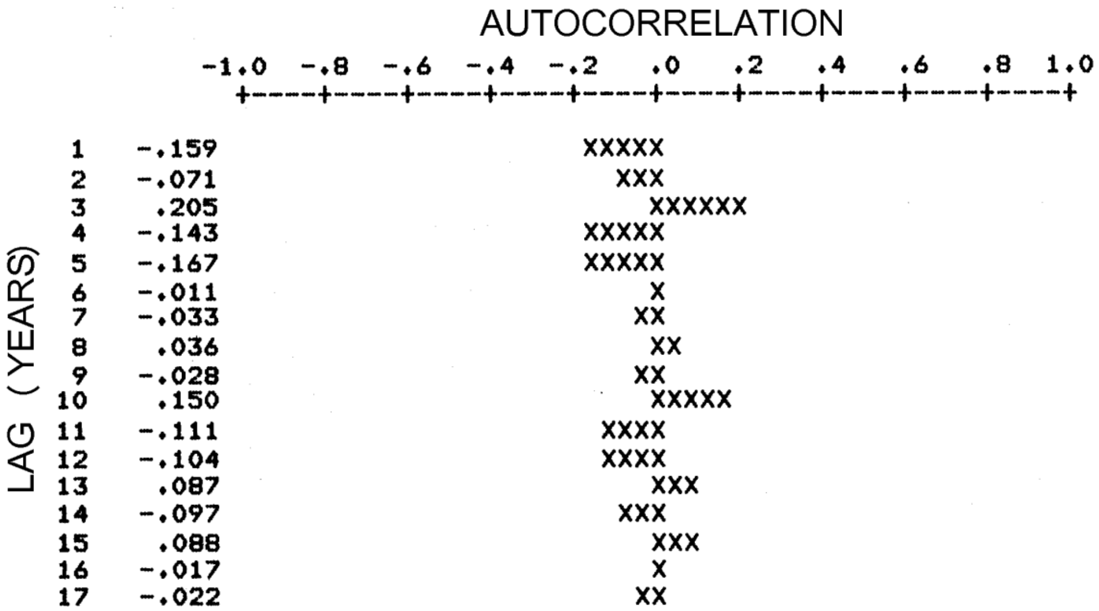


Figure 80. Correlogram for Crossfire Path.

```
                          AUTOCORRELATION
          -1.0  -.8  -.6  -.4  -.2   .0   .2   .4   .6   .8  1.0
            +----+----+----+----+----+----+----+----+----+----+
  1    .166                          XXXXX
  2    .028                          XX
  3    .255                          XXXXXXX
  4    .254                          XXXXXXX
  5    .292                          XXXXXXXX
  6    .102                          XXXX
  7    .150                          XXXXX
  8    .081                          XXX
  9   -.058                         XX
 10    .090                          XXX
 11    .208                          XXXXXX
 12   -.011                          X
 13    .047                          XX
 14   -.025                         XX
 15   -.013                          X
 16    .128                          XXXX
 17    .051                          XX
```

LAG (YEARS)

Figure 81. Correlogram for Flagstaff snowfall.

# Results

## Analysis of Trends

| Path | df | S.D. | R | F |
|---|---|---|---|---|
| Beard | 49 | 13.8 | -1.7 | 0.15 |
| Dunnam | 49 | 16.2 | 6.3 | 4.38 |
| Snowslide | 49 | 10.1 | 3.7 | 2.90 |
| Allison Clay | 49 | 7.5 | -0.1 | 0.93 |
| Crossfire | 49 | 7.5 | -1.2 | 3.91 |

**Table 5. Regression Results**

**above and below k=0**

| Path | Obs runs | Exp runs | Abv/Blw | Signif. | Conclusion at .05 |
|---|---|---|---|---|---|
| Beard | 25 | 20.37 | 13/38 | .0832 | Cannot reject, random |
| Dunnam | 25 | 20.37 | 13/38 | .0832 | Cannot reject, random |
| Snowslide | 25 | 21.31 | 14/37 | .1885 | Cannot reject, random |
| Allison Clay | 19 | 17.08 | 10/41 | .3831 | Cannot reject, random |
| Crossfire | 17 | 14.49 | 8/43 | .1719 | |

**Table 6. Runs Test Results**

## Analysis of Cycles

**see Figures 76-81 for correlograms**

| Path | +Peaks | -Peaks |
|---|---|---|
| Beard | 4,13,17 | 1-2,5-6, 12 |
| Dunnam | 3-5,7-8,13,16 | 1-2,6,15 |
| Snowslide | 3-5,8,12,16 | 1-2,6,9,14-15 |
| Allison Clay | 8,13 | 2,4,9-10,12,15 |
| Crossfire | 3,10 | 1,4-5,11-12 |
| Flag Snow | 1-5,7,10-11,16 | 0 |

**Table 7. Autocorrelation Results**

| Path | KSmax | KS(.05) | Conclusion |
|---|---|---|---|
| Beard | .215 | .1904 | Reject H |
| Dunnam | .275 | .1904 | Reject H |
| Snowslide | .235 | .1904 | Reject H |
| Allison Clay | .216 | .1904 | Reject H |
| Crossfire | .117 | .1904 | Cannot Reject H |

**Table 8. Results of Poisson by Kolmogorov-Smirnov**

| | 0 events | event | |
|---|---|---|---|
| P | .7903 | .1860 | |
| Expected Frequency | 40.31 | 9.48 | |
| Observed Frequency | 39.00 | 12.00 | |
| $x^2$ | .0462 + | .6698 | = .7124 |
| Probability of Poisson Fit 70% | | | |
| Expected Return Time 5.38 yrs.<br>Observed Return Time 4.25 yrs. | | | |

**Table 9. Results of Poisson by Chi Square**

Analysis of Similarity

| | Beard | Dunnam | Snow-slide | Allison Clay | Cross-fire | Control |
|---|---|---|---|---|---|---|
| Dunnam | .540 | | | | | |
| Snowslide | .561 | .538 | | | | |
| Allison Clay | .484 | .484 | .466 | | | |
| Crossfire | .321 | .276 | .505 | .519 | | |
| Control | -.101 | -.072 | .047 | .238 | -.275 | |
| Flag Snow | .345 | .453 | .368 | .210 | .130 | .119 |

**Table 10. Results of Spearman's Rho**

| Path 1/Path 2 | Coefficient |
|---|---|
| Beard/Dunnam | .80 |
| Beard/Snowslide | .78 |
| Beard/Allison Clay | .75 |
| Beard/Crossfire | .75 |
| Dunnam/Snowslide | .86 |
| Dunnam/Allison Clay | .86 |
| Dunnam/Crossfire | .75 |
| Snowslide/Allison Clay | .84 |
| Snowslide/Crossfire | .80 |
| Crossfire/Allison Clay | .84 |

**Table 11. Coefficients of Similarity**

Table 12

Cumulative Frequency Data For Kolmogorov-Smirnov Tests

| Yr. Group | Beard | Dunnam | Snowslide | Allison | Crossfire |
|---|---|---|---|---|---|
| 0-5 | .0389 | .1167 | .0857 | .0143 | .0444 |
| 5-10 | .1492 | .3167 | .1959 | .1286 | .1111 |
| 10-15 | .2987 | .5167 | .3959 | .2429 | .2667 |
| 15-20 | .4156 | .6500 | .5429 | .3286 | .3222 |
| 20-25 | .5584 | .7500 | .6694 | .4571 | .5111 |
| 25-30 | .6883 | .8333 | .7714 | .5571 | .6111 |
| 30-35 | .7662 | .9000 | .8205 | .6286 | .6556 |
| 35-40 | .8442 | .9500 | .8990 | .7143 | .7667 |
| 40-45 | .9351 | .9883 | .9388 | .7571 | .8333 |
| 45-50 | 1.0130 | 1.0167 | 1.0000 | .9857 | 1.0444 |

Table 13

Kolmogorov-Smirnov Tests

| Path 1 / Path 2 | $n_1$ | $n_2$ | N | $d_n$ max | KS .05 | KS .01 | Conclusion |
|---|---|---|---|---|---|---|---|
| Beard/Dunnam | 77 | 60 | 33.72 | .2344 | .230 | .260 | Cannot reject $H_0$, paths similar |
| Beard Snowslide | 77 | 235 | 58.59 | .1273 | .173 | .200 | Cannot reject $H_0$, paths similar |
| Beard/Allison Clay | 77 | 70 | 36.67 | .1780 | .207 | .257 | Cannot reject $H_0$, paths similar |
| Beard/Crossfire | 77 | 90 | 41.50 | .1111 | .202 | .248 | Cannot reject $H_0$, paths similar |
| Dunnam/Snowslide | 60 | 245 | 48.20 | .1208 | .191 | .225 | Cannot reject $H_0$, paths similar |
| Dunnam/Allison Clay | 60 | 70 | 32.31 | .3214 | .232 | .280 | Reject $H_0$, paths differ |
| Dunnam/Crossfire | 60 | 90 | 36.00 | .3278 | .218 | .265 | Reject $H_0$, paths differ |
| Snowslide/Allison Clay | 245 | 70 | 30.63 | .2143 | .235 | .280 | Cannot reject $H_0$, paths similar |
| Snowslide/Crossfire | 245 | 90 | 65.82 | .2207 | .165 | .195 | Reject $H_0$, paths differ |
| Crossfire/Allison Clay | 90 | 70 | 39.38 | .0762 | .209 | .250 | Cannot reject $H_0$, paths similar |

Table 14

Cross-Association $X^2$ Tests

| Path 1 / Path 2 | Match / Mismatch | P | $X^2_{mat}$ | $X^2_{mis}$ | $X^2_{tot}$ | $X^2_{.05}$ | Conclusion |
|---|---|---|---|---|---|---|---|
| Beard/Dunnam | 41/10 | .62 | 2.78 | 4.54 | 7.32 | 3.84 | Reject $H_0$, paths similar |
| Beard/Snowslide | 40/10 | .61 | 2.54 | 3.97 | 6.51 | 3.84 | Reject $H_0$, paths similar |
| Beard/Allison Clay | 38/13 | .65 | 0.71 | 1.32 | 2.03 | 3.84 | Cannot reject $H_0$, paths differ |
| Beard/Crossfire | 38/13 | .67 | 0.43 | 0.87 | 1.30 | 3.84 | Cannot reject $H_0$, paths differ |
| Dunnam/Snowslide | 44/7 | .61 | 5.34 | 8.35 | 13.69 | 3.84 | Reject $H_0$, paths similar |
| Dunnam/Crossfire | 38/13 | .67 | 0.43 | 0.87 | 1.30 | 3.84 | Cannot reject $H_0$, paths differ |
| Snowslide/Allison Clay | 43/8 | .64 | 2.14 | 5.85 | 7.99 | 3.84 | Reject $H_0$, paths similar |
| Snowslide/Crossfire | 41/10 | .65 | 1.86 | 3.45 | 5.31 | 3.84 | Reject $H_0$, paths similar |
| Crossfire/Allison Clay | 43/8 | .71 | 1.27 | 3.12 | 4.39 | 3.84 | Reject $H_0$, paths similar |
| Dunnam/Allison Clay | 44/7 | .65 | 3.55 | 6.60 | 10.15 | 3.84 | Reject $H_0$, paths similar |

# Chapter 5

## RECENT AVALANCHE EVENTS

A snow avalanche is the culmination of a very complex interaction of processes. To estimate the avalanche hazard on any given slope or snowpack, the forecaster considers several parameters called “contributory factors" (Perla and Martinelli, 1976):

1) Old snow depth and condition.
2) Old snow surface.
3) New snow depth.
4) New snow type.
5) New snow density.
6) Snowfall and precipitation intensity.
7) Snowpack settlement.
8) Wind speed and direction.
9) Temperature trends.

For illustrative purposes however, avalanches will be considered to result from an oversimplified twofold cause. Avalanches will start if a snowpack, resting on a sufficiently steep slope, is loaded (or weakened) to the point of failure.

With respect to the snowpack failure can be externally or internally induced. Although other causes can produce external overloads they are generally caused by rapidly accumulating amounts of new snow, resulting in what is called the “direct action” avalanche. If old snow layers are also involved, the event is termed a “climax" event. About 90 percent of the avalanche events in the San Juan Mountains of Colorado are either climax or direct action types (Armstrong and Ives, 1976). Internal failure results from metamorphic weakening within the snowpack producing what is called the "delayed action" avalanche.

If a particular snowpack is stressed beyond its limit of plastic deformation, it will assume one of two basic modes of failure depending on the cohesiveness of the snow involved. The "point release", or loose snow avalanche, occurs in the absence of significant cohesion. These slides are characterized by small initial starting points and fan-shaped flow patterns. Small point releases, referred to as "sluffs", are relatively harmless; but much larger point releases can occur, especially during the spring thaw. The "slab" event, in contrast, occurs when an entire area of the snowpack fails as a unit. The cohesion of the snow is such that the flow consists largely of chunks. "Hard slab" events occur in snow so hiqh1y cohesive (rammsonde values over 10kg) that the blocks are still well defined in the runout zone. "Soft slab" events occur in less cohesive snow where the blocks are poorly defined, or non-existent, in the runout zone (Figures 82-87).

## Methods

During the avalanche seasons from 1977 to 1981, many ski trips (and some fixed-wing aircraft overflights) were made to observe recent slide activity in the study area. Reports were gathered by members of the San Francisco Mountain Avalanche Project and by other knowledgeable skiers. The information was compiled into tabular form (Tables 15-18). The observations are presented as follows:

Figure 82. Slab crowns over 1 meter thick in Telemark Path on January 13, 1980 (Bruce Grubbs photo).

Figure 83. Fresh debris in the runout zone of Skeaky Pete Path (Bruce Grubbs photo).

Figure 84. Sneaky Pete Path loads from a clear area just beyond the right ridge. The starting zone is located in the rocky bowl above the skier (Bruce Grubbs photo).

Figure 85. Large blocks from a spring wet cycle slab avalanche in Telemark Path on May 28, 1979.

Figure 86. Meter thick blocks litter the trees near Corner Path on January 13, 1980 (Bruce Grubbs photo).

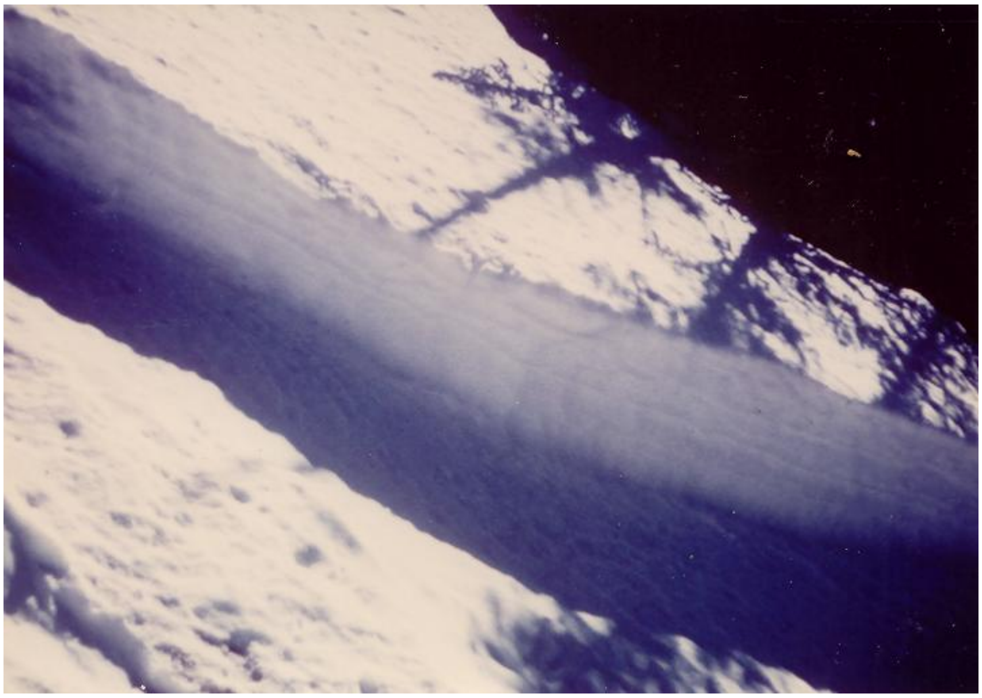

Figure 87. Wet slab crown fracture about ½ meter thick, Telemark Path, June, 1979.

1) Column #1 - Path name and identification number (See Appendix 3).

2) Column #2 - Event number for the particular path.

3) Column #3 - Event Classification.

Type of release:

HS = Hard slab
SS = Soft slab
WS = Wet slab
L = Loose
WL = Wet Loose

Type of trigger:

N = Natural
AS = Artificial-Skier
AE = Artificial-Explosive
AA = Artificial-Artillery
AO = Artificial-Other

Size of event:

1 = Sluff, any event running less than 150'
2 = Small, relative to overall path.
3 = Medium
4 = Large
5 = Major

Running surface:

O = Old snow surface
G - Ground

4) Column #4 - Date observed.

5) Column #5 – Observer.

6) Column #6 - Best estimate of event date.

## Results

The results are listed in Tables 15-18. Figure 88 represents a time series plot of all events with either a known date or an estimated date.

Table 15

Reported Event Chronology 1977-78 Season

| Path (NO.) | EVENT | CLASSIFICATION | DATE OBSERVED | OBSERVER | DATE OF EVENT |
|---|---|---|---|---|---|
| Allison Clay (450) | 1 | SS-N-2-0 | 1/28/78 | Dexter | 1/20 to 1/22/1978 |
| Angel Food (590) | 1 | SS-N-3-0 | 1/22/78 | Werma | 1/20 to 1/22/1978 |
| Determination (600) | 1 | SS-N-4-0 | 1/22/78 | Werma | 1/20 to 1/22/1978 |
| Hill 8593 (no number) (Hart Prairie) | 1 | SS-AS-1-0 | 1/23/78 | Pundt | 1/23/1978 |
| Humphreys Cirque (200) | 1 | DL-N-1-0 | 2/22/78 | Dexter | mid February 1978 |
| | 2 | L-N-2-0 | 4/4/78 | Walters | early March 1978 |
| Jay's Slide (80) | 1 | WL-N-1-0 | 4/15/78 | Pundt | early April 1978 |
| Sickle Moon (60) | 1 | L-N-2-0 | 3/12/78 | Pundt | early March 1978 |
| Silverton (90) | 1 | SS-N-3-0 | 1/22/78 | Werma | 1/20 to 1/22/1978 |
| | 2 | SS-N-4-0 | 1/29/78 | Dexter | 1/23 to 1/25/1978 |
| | 3 | Wl-N-1-0 | 4/15/78 | Pundt | early April 1978 |
| Snowslide (170) | 1 | SS-N-2-0 | 4/4/78 | Walters | early March 1978 |
| Telemark (100) | 1 | SS-N-3-0 | 1/22/78 | Werma | 1/20 to 1/22/1978 |
| | 2 | SS-N-4-0 | 1/29/78 | Dexter | 1/23 to 1/25/1978 |
| | 3 | SS-N-3-0 | 1/29/78 | Dexter | post #2 |
| | 4 | WL-N-1-0 | 4/15/78 | Pundt | early April 1978 |
| Sneaky Pete (70) | 1 | WL-N-4-0 | ? | ? | ? |

Table 16

Reported Event Chronology 1978-79 Season

| Path (NO.) | EVENT | CLASSIFICATION | DATE OBSERVED | OBSERVER | DATE OF EVENT |
|---|---|---|---|---|---|
| Anasazi (355) | 1 | SS?-N-4-0 | | Dexter | |
| Beard (220) | 1 | L-N-1-0 | 1/21/79 | Dexter | 1/19/79 |
| | 2 | L-N-2or3 | | Dexter | |
| Crossfire (360) | 1 | SS?-N-4-0 | | Dexter | |
| Jay's Slide (80) | 1 | L-N-1-0 | | Dexter | |
| | 2 | WS-N-3-0 | 5/28/79 | Hughes | 5/28/79 |
| Roadway (110) | 1 | WS-N-3-0 | 5/28/79 | Hughes | 5/28/79 |
| Silverton (90) | 1 | SS-N-2or3-0 | 1/21/79 | Dexter | 1/19/79 |
| | 2 | WS-N-2-0 | | Walters | |
| Snowslide (170) | 1 | WS-N | 6/79 | Walters | late June 1979 |
| Lew Canyon (410) | 1 | SS-N-1-0 | 1/1/79 | Wheeler | late Dec. 1978 |
| Telemark (100) | 1 | SS-N-4-0 | 1/21/79 | Walters | 1/19/79 |
| | 2 | HS-N-4-0 | | Dexter | |
| | 3 | HS-SS-N-4-0 | | Pundt | |
| | 4 | SS-N-4-0 | | Grubbs | |
| | 5 | WS-N-3-0 | 5/28/79 | Hughes | 5/28/79 |
| | 6 | WS-N-2-0 | 6/79 | Walters | late June 1979 |

Table 17

Reported Event Chronology 1979-80 Season

| Path (NO.) | EVENT | CLASSIFICATION | DATE OBSERVED | OBSERVER | DATE OF EVENT |
|---|---|---|---|---|---|
| Beard (220) | 1 | ?-N-4 | 5/80 | Walters | probably 1/11 to 1/13/80 |
| Corner (120) | 1 | SS-N-3or4 | 1/13/80 | Dexter | 1/11 to 1/13/80 but before Telemark |
| Dunnam (210) | 1 | ?-N-4 | 8/80 | Pundt | probably 1/11 to 1/13/80 |
| Inner Basin (150) | 1 | SS or HS-N-4-07 | 1/13/80 | Dexter | 1/12 or 1/13/80 |
| Roadway (110) | 1 | SS or HS-N-3or4 | 1/13/80 | Dexter | 1/11 to 1/13/80 but before Telemark |
| Humphreys Cirque (200) | 1 | SS-N-2 | 1/23/80 | Dexter | ? maybe storm after 1/11 to 1/13/80 |
| | 2 | SS-N-1 | 2/1/80 | Walters | |
| Sneaky Pete (70) | 1 | SS or HS-N-4-G? | 1/13/80 | Dexter | 1/11 to 1/13/80 |
| Telemark (100) | 1 | SS or HS-N-4-G | 1/13/80 | Dexter | 1/12 or 1/13/80 |
| | 2 | SS or HS-N-3 | 1/23/80 | Dexter | probably left SZ and storm after 1/11 to 1/13/80 |
| | 3 | SS-N-3or4-0 | 2/1/80 | Grubbs | late Jan 1980 |
| Snowslide (170) | 1 | SS or HS-N-3-G | 1/13/80 | Dexter | 1/12 or 1/13/80 |

**Table 18**

**Reported Event Chronology 1980-81 Season (Interim)***

| PATH (NO.) | EVENT | CLASSIFICATION | DATE OBSERVED | OBSERVER | DATE OF EVENT |
|---|---|---|---|---|---|
| Telemark | 1 | HS-N-4-0 | 4/5/81 | Grubbs | 4/3 to 4/4/1981 |

* As the observations of the 1980-81 season were not completed as of the submission date for this paper, the single reported event was not used in any statistical treatment.

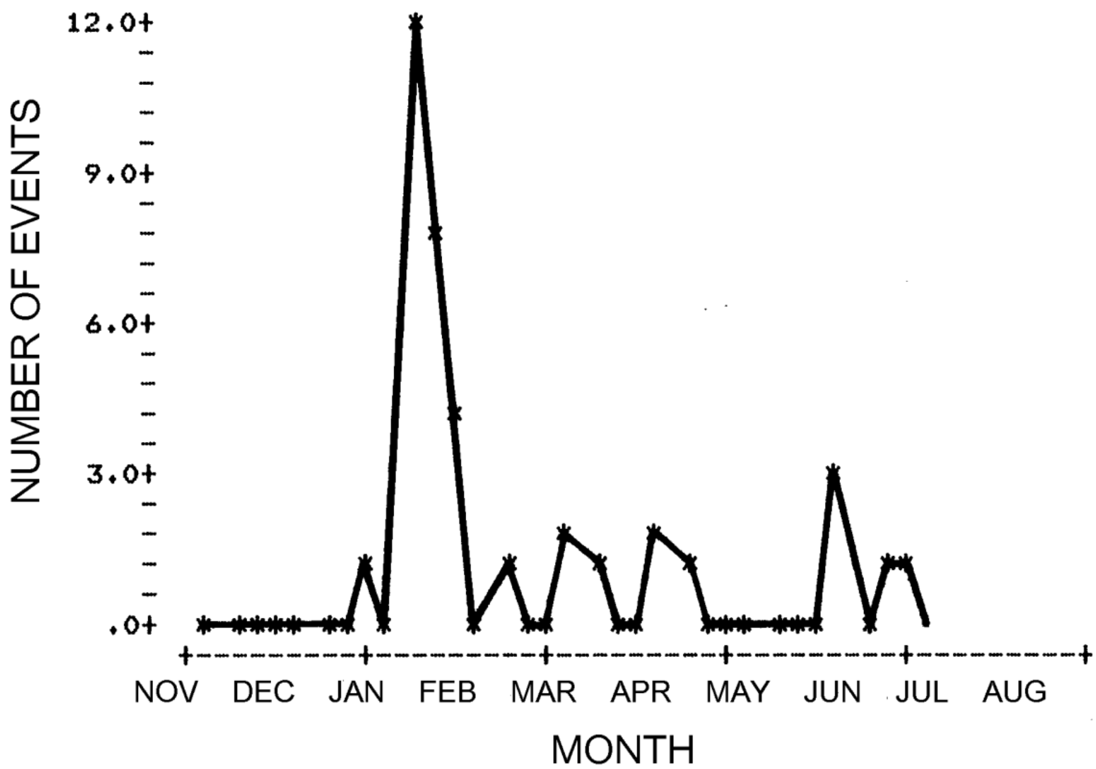


Figure 88. Total number of observed events from winter 1977-78 through winter 1979-80 as a function of time.

# Chapter 6

## CONCLUSIONS

Snow avalanche activity is more common on the San Francisco Peaks than previously thought. To roughly estimate the total number of events on the Peaks over the last fifty-one years two techniques can be applied: 1) the average number of observed events per year (15 events with a standard deviation of 3 events) can be multiplied by the study period (51 years) to give an estimate of 765 events. This figure is most likely an underestimate, 2) another estimate makes use of the assumption that the number of events which did significant damage (i.e. exceeded the 10% random damage value) to trees in any of the five ring study paths is proportional over time to the total number of events. Of the 46 events listed in tables 15-17, only two events (4% of the total) would have been recorded by methods used in the ring study. If this 4% value is extrapolated to the 58 events recorded in the ring study, a value of 1,450 events is obtained. It thus appears safe to estimate at least 1,000 avalanche events (of all sizes) have occurred on the Peaks over the last 50 years. This value is presented, not to quantify the absolute number of events, but rather to impart a feel for the amount of avalanche activity that does occur in an area not generally regarded as avalanche prone.

The lack of historical documentation of such events is attributed to two causes: 1) no one was in a position to observe the actual events, 80% of which are storm related; 2) the physical evidence of most (size 3-4) avalanches is mainly in the form of snow debris (Figure 83). Wind can alter this debris to non-descript mounds within 1 or 2 days (Figure 41). Winter travelers who happened to cross the wind altered debris have had no idea what it was. This left only the rare tree-damaging event to communicate the presence of avalanche activity.

## Annual Avalanche Patterns

Winter begins in earnest when the succession of predominately type B Pacific storms begins to move regularly into Arizona. Much snow is transported by the southwest storm flow into north and east starting zones. Duncklee's (ca. 1974) estimate of early season loading of west slopes due to the prevailing easterly flow is not substantiated by this study. The west slopes appear to load most heavily from southerly storm flow moving snow across the west ridges into the starting zones (seen in Figure 18). A minor amount of west and south slope loading also occurs due to snow redistribution by high speed north or east winds following the storm system.

A plot of the recently observed events (Figure 88) suggests a large number are coincident with the onset of rapid snow accumulation over a weak early season snowpack (Figure 50). Following this unloading of major deep-seated instability, the number of events falls off to a mid-winter level. These mid-winter events result from: 1) remnant pockets of deep-seated instability released by additional snowload, 2) direct action events from a new snow instability (e.g. rimed particles), or possibly, 3) a reformed deep-seated instability (never observed in the three tabulated seasons).

Generally, the snowpack on the Peaks appears to bond quickly due to the lack of persistent low temperatures. A notable period of low avalanche activity occurs around late April or early May due to rapidly warming weather (Figure 88). By late May and June (Figure 53) temperatures have risen sufficiently to allow significant amounts of free water to penetrate the snowpack. This condition gives rise to the spring avalanche cycle. Other weather and snowpack conditions can produce variations in the above pattern, but this sequence prevails on the average. Additional work with small-scale artificial release methods is needed to assess stabilization rates.

Avalanche events appear to occur in at least 66 paths of which 23 have been observed to run either historically or as listed in Tables 15-18. Paths located within the Inner Basin run more frequently than paths located on other portions of the mountain. The single most active path (by far) appears to be Telemark (#100) which produced 4.3 events per year during the 3 tabulated years.

## Long Term Avalanche Patterns

In light of recent observations Beard's estimate of avalanche return times (2-3 years) is low. It must be kept in mind, however, that his estimates are most likely based on tree damage. In this case his estimate agrees favorably with the 4.25 year mean return time (per path) for events producing vegetation damage. It must be remembered that this estimation technique excludes the majority of events which occupy only the high frequency channel.

The largest event in recent years ran in Dunnam Canyon (#210). This slide uprooted, or clipped off, large numbers of mature Engelmann spruce and corkbark fir. Estimates by Breed (1977) indicate at least a 100 year return period for an event of this size. Ring counts done in the course of this study suggest a 200 year return period could be safely assigned to this event. The only other paths which show this magnitude of overrun are Allison Clay (#450) in 1932, and Snowslide (#170) also in 1932. In addition, several notably large events occurred in the following paths; Beard Canyon (#220, in 1980, 1970 and 1952); Snowslide (#170, in 1980, 1973, 1965, and 1952); Allison Clay (#450, in 1973); Crossfire (#360, in 1973, 1968, 1958, and 1932);Dunnam canyon (#210, in 1980); and Telemark (#100, in 1980). Although the sampling methods used in this study were not specifically so designed, they suggested a relationship between event magnitude and proportions of damaged trees. Further study into the event magnitude versus amount of damage relationship is needed.

Regression analyses and runs tests do not support the notion of any time related trend in the data. $R^2$ values are very low and F values are scattered over a wide range. Only one F value passed the $F_{(.05,49,1)}$ test and this is attributed to chance. Although cycles are difficult to interpret, a three-to-five year cycle is indicated in most of the autocorrelation tests. Positive correlation peaks occur at lags 3-5.7-8, 13, 16-17. A similar autocorrelation pattern exists for Flagstaff snowfall.

The attempted fit of a Poisson distribution to the observed event patterns was rejected at the 95% probability level by the Kolmogorov-Smirnov test. The chi-square goodness of fit test gave a 70% probability that the Poisson relation would fit the observed event distribution. It is interesting to note that this agrees closely with the results of a similar test applied to large avalanche events in the San Juan Mountains of Colorado (B. Armstrong in Armstrong and Armstrong, 1978). Thus, the Poisson appears to be only a first approximation of large avalanche event distribution. The Poisson prediction for return times of large events on the Peaks is 5.38 years (per path). This underestimates the observed return time of 4.25 years per path).

Unlike the paths included in Potter's (1969) Absaroka Wyoming study, all the paths in this study display similar event distributions. This is indicated by the relatively close grouping in the Spearman's Rho and coefficient of similarity analyses. This result is attributed to the close proximity of the paths to each other. The variation within the grouping is most likely explained by loca1 differences in aspect and loading characteristics. With a few exceptions, the paths within the Inner Basin display greater event distribution similarity with each other than with paths on the outside portions of the mountain.

Path pairs which display notable disparity by failing either the Kolmogorov-Smirnov test or the cross-association test are: 1) Dunnam/Allison Clay, 2) Dunnam/Crossfire, 3) Snowslide/Crossfire, 4} Beard/Allison Clay, 5} Beard/Crossfire. Again it is noted that the largest disparity in event pattern is found between paths with dissimilar aspect.

Due to the difficulty in scaling between avalanche events and Flagstaff snowfall (Figure 69), Spearman's Rho shows only a weak correlation between events and Flagstaff snowfall. A cross-association comparison around a certain + or - value of snowfall is planned and the results are expected to show a relatively high association. This result is anticipated from field observations both here and in the San Juan Mountains (Armstrong and Ives, 1976). These observations show a high percentage of new snow related events.

Finally, the control transects suggest a non-avalanche damage level of up to 10%. The control transects correlate poorly in time with the paths. This suggests that tree ring analyses do indeed reflect avalanche related damage within the avalanche paths.

## REFERENCES CITED

Aitchison, S. W., 1977, The San Francisco Peaks: A Biologic Sky-island; in: Plateau, v. 49, n. 5, p. 2-9.

Arizona Daily Sun, "Avalanche Damage Seen", 8 September, 1973.

Armstrong, R.L. and Armstrong, B.R., 1978, Evaluation and Prediction of Avalanche Hazard, San Juan Mountains, Colorado: Institute of Arctic and Alpine Research Final Report, Boulder, Colorado, 131 p.

Armstrong, R.L. and Ives, J.D., 1976, Avalanche Release and Snow Characteristics, San Juan Mountains, Colorado: Institute of Arctic and Alpine Research Occasional Paper No. 19, Boulder, Colorado, 131 p.

Beschta, R.L., 1976, Climatology of the Ponderosa Pine Type in Central Arizona: University of Arizona Agricultural Experiment Station Technical Bulletin No. 228, 24 p.

Breed, W.J., 1977, The San Francisco Peaks: A Geologist's Perspective; in: Plateau, v. 49, n. 5, p. 24-32.

Burrows, C.J. and Burrows, V.L., 1976, Procedures for the Study of Snow Avalanche Chronology Using Growth Layers of Woody Plants; Institute of Arctic and Alpine Research Occasional Paper No. 23, Boulder, Colorado, 54 p.

Colton, H.S., 1930, San Francisco Peaks; Museum Notes, v. 3 n. 3 p.1-4.

____________, 1958, Precipitation About the San Francisco Peaks, Arizona: Museum of Northern Arizona Technical Series No.2, 18 p.

Davis, J.C., 1973, Statistics and Data Analyses in Geology; John Wiley and Sons, New York, New York, 550 p.

Dean, J.S., 1980, Personal Communication; Tucson, Arizona.

Duncklee, J.P., ca. 1974, Man-Land Relationships on the San Francisco Peaks, unpublished report, 108 p.

Haan, C.T., 1977, Statistical Methods in Hydrology; Iowa State University Press, Ames, Iowa, 378 p.

Hidore, J.J., 1976, Workbook of Weather Maps; W.C. Brown Co., Dubuque, Iowa, 81 p.

Holm, R. F. 1974, Volcanic Geology of the Inner Basin, San Francisco Peaks Volcano, Arizona; G.S.A. Abstracts with programs, v.6, n.5, Boulder, Colorado, p. 448-449.

Ives, J.D. et. al., 1973, Development of Methodology for Evaluation and Prediction of Avalanche Hazard in the San Juan Mountain Area of Southwestern Colorado; Interim Report for the Division of Atmospheric Water Resources Management, Bureau of Reclamation, 122 p.

LaChapelle, E.R., 1969, Field Guide to Snow Crystals; University of Washington Press, Seattle, Washington, 101 p.

Lawrence, D.B., 1950, Estimating Dates of Recent Glacier Advances and Recession Pates by Studying Tree Growth Layers; Transactions, American Geophysical Union, v. 31, n. 2, p. 243-248.

Martinelli, M. Jr., 1974, Snow Avalanche Sites: Their Identification and evaluation; U.S. Department of Agriculture Information Bulletin No. 360, 26 p.

Mellor, M., 1968, Avalanches; Cold Region Science and Engineering, Part III-A3d, U.S. Army Corps of Engineers, Hanover, New Hampshire, 215 p.

Merriam, C.B., 1890, Results of a Biological Survey of the San Francisco Mountain Region and Desert of the Little Colorado River in Arizona; U.S. Department of Agriculture North American Fauna No. 3, 128 p.

Miller, R.L. and Kahn, J.S., 1962, Statistical Analysis in the Geological Sciences; John Wiley and Sons, New York, New York, 483 p.

Perla, R.I. and Martinelli, M. Jr., 1976, Avalanche Handbook; U.S. Department of Agriculture Handbook No. 489, 238 p.

Pewe, T.L. and Updike, R.G., 1976, San Francisco Peaks: A Guidebook to the Geology; Museum of Northern Arizona, Flagstaff, Arizona, 80p.

Pollard, J.B., 1977, A Handbook of Numerical and Statistical Techniques; Cambridge University Press, Cambridge, England, 349 p.

Potter, N., 1969, Tree Ring Dating of Snow Avalanche Tracks and the Geomorphic Activity of Avalanches, Northern Absaroka Mountains, Wyoming; U.S. Contributions to Quaternary Research, G.S.A. Special Paper No. 123, p. 141-165.

Pundt, A., 1981, Personal Communication; Flagstaff, Arizona.

Robinson, H.H., 1913, The San Francisco Volcanic Field, Arizona; U.S. Geological Survey Professional Paper No. 76. 213 p.

Ruffner, J .A. and Bair, F.E., 1979, The Weather Almanac; Avon Books, New York, New York. 728 p.

Sellers, W.D. and Hill, R.H., 1974, Arizona Climate; University of Arizona Press, Tucson, Arizona, 616 p.

Sigafoos, R.S. and Hendricks, E.L., 1961, Botanical Evidence of the Modern History of Nisqually Glacier, Washington; U.S. Geological Survey Professional Paper No. 387-A, 20 p.

Society of Physics Students, 1975, unpublished data; Northern Arizona University, Flagstaff, Arizona.

Sokal, R.R. and Sneath, P.H.A., 1963, Principles of Numerical Taxonomy; W.H. Freeman and Co., San Francisco, California, 359 p.

Sorenson, P.W., 1974, Climate of Flagstaff, Arizona; National Oceanic and Atmospheric Administration Technical Memorandum NSW WR-95, 43 p.

Stokes, M.A. and Smiley, T.L., 1968, An Introduction to Tree Ring Dating; University of Chicago Press, Chicago, Illinois, 73 p.

Wardrop, A.B., 1965, The Formation and Function *of* Reaction Wood; Cellular Ultrastructure of Woody Plants, Syracuse University Press, Syracuse, New York, p. 371-389.

Wilson, E.D., 1962, A Resume of the Geology of Arizona; Arizona Bureau of Mines.

# APPENDIX 1

## Example of a Damage Versus Time Plot

| Sample No. | 1962 | 1961 | 1960 | 1959 | 1958 | 1857 | 1956 | 1955 | 1954 | 1953 | 1952 | 1951 | Year |
|---|---|---|---|---|---|---|---|---|---|---|---|---|---|
| 095 | | | | | R | | | | | | | | |
| 096 | | | | | E/W | | | | | | | | |
| 097 | | | | | R | | | | | | | | |
| 098 | | E | → | → | R | | | | | | | | |
| 099 | | | | | | | | | | | | | |
| 100 | | | | | | | | | | | | | |
| 101 | | R | | | | | | | | | | | |
| 102 | | | | | R/S | | | | | | | | |
| 103 | | | | | R | | | | | | | | |
| 104 | | | | | R | | | | | | R | | |

## Damage Code

| | |
|---|---|
| Reaction Wood | R |
| Scar | S |
| Scar ring | O |
| Ring width change | W |
| Colonization | C |
| Epicormic | E |
| Decay | D |
| Terminal year | T |
| Maximum year (Minimum return) | M |

# APPENDIX 2

## Tree Ring Specimen Information

| Path \ Species | Picea Englmannii | Abies Lasiocarpa | Abies Concolor | Pinus Aristata | Pinus Flexilis | Unknown |
|---|---|---|---|---|---|---|
| Beard | 17/28 | 0/0 | 1/2 | 0/0 | 0/0 | 0/0 |
| Dunnam | 8/12 | 4/4 | 1/1 | 0/0 | 0/0 | 0/0 |
| Snowslide | 60/78 | 6/6 | 0/0 | 0/0 | 0/0 | 0/0 |
| Allison Clay | 21/28 | 4/7 | 0/0 | 2/3 | 0/0 | 0/0 |
| Crossfire | 30/38 | 1/1 | 0/0 | 0/0 | 0/0 | 0/0 |
| Control | 16/16 | 2/2 | 0/0 | 0/0 | 0/0 | 1/1 |

Number of trees/Number of Specimens

---

| | Number of trees | Number of Specimens |
|---|---|---|
| Total used to date paths | 155 | 208 |
| Total used in control | 19 | 19 |
| Total used for master chronology | 12 | 12 |
| Total not used | 3 | 8 |
| Total collected | 189 | 247 |

# APPENDIX 3

## Path Nomenclature

| Reference Number | Path Name | Events Observed |
|---|---|---|
| 001 | Boulderfield | |
| 010 | Dice | |
| 020 | Hidden | |
| 030 | Baby Peaks | |
| 040 | Black Bear | |
| 050 | Telescope | |
| 060 | Sickle Moon | * |
| 070 | Sneaky Pete | * |
| 080 | Jay's Slide | * |
| 090 | Silverton/Offchute | * |
| 100 | Telemark | * |
| 110 | Roadway | * |
| 120 | Corner | * |
| 130 | Study Plot | |
| 140 | Blowout Basin | |
| 150 | Inner Basin | * |
| 160 | Survey Post | * |
| 170 | Snowslide Canyon | * |
| 175 | Core Ridge Group | * |
| 180 | Riser | |
| 190 | Spring Slide | |
| 200 | Humphreys Cirque | * |
| 210 | Dunnam Canyon | * |
| 220 | Beard Canyon | * |
| 230 | Cutoff | |
| 240 | Zipper | |
| 260 | Crisco | |
| 270 | Cliffband | |
| 280 | Squeeker | |
| 290 | Aspen | |
| 300 | Bear Jaw Canyon | |
| 310 | Stabilizer | |
| 320 | Dike | |
| 325 | Reese Canyon (?) | |
| 330 | Aubineau Canyon | |
| 340 | Hohokam | * |
| 350 | Sinagua | * |

| Reference Number | Path Name | Events Observed |
|---|---|---|
| 355 | Anasazi | * |
| 360 | Crossfire | * |
| 370 | Northridge | |
| 380 | Rockpile | |
| 390 | Noname | |
| 400 | White Horse | |
| 405 | Night Mare | |
| 410 | Lew Canyon | * |
| 420 | Pipeline | |
| 430 | Maybe Not | |
| 440 | Philomena Spring | |
| 450 | Allison Clay | * |
| 460 | Bomber | |
| 470 | Gadzooks Gully | |
| 480 | Rustler/Low Point | |
| 490 | Shiprock | * |
| 500 | Upper Bowl | |
| 510 | Shot Hole | |
| 520 | Parallel | |
| 530 | Solitude | |
| 540 | Watson | |
| 550 | Snake Eye | |
| 560 | Monte Vista | |
| 570 | Meadow | |
| 580 | Kachina | |
| 590 | Angel Food | * |
| 600 | Determination | * |
| 610 | Outside | |
| 620 | Waterboard | |

66 paths total

23 with events

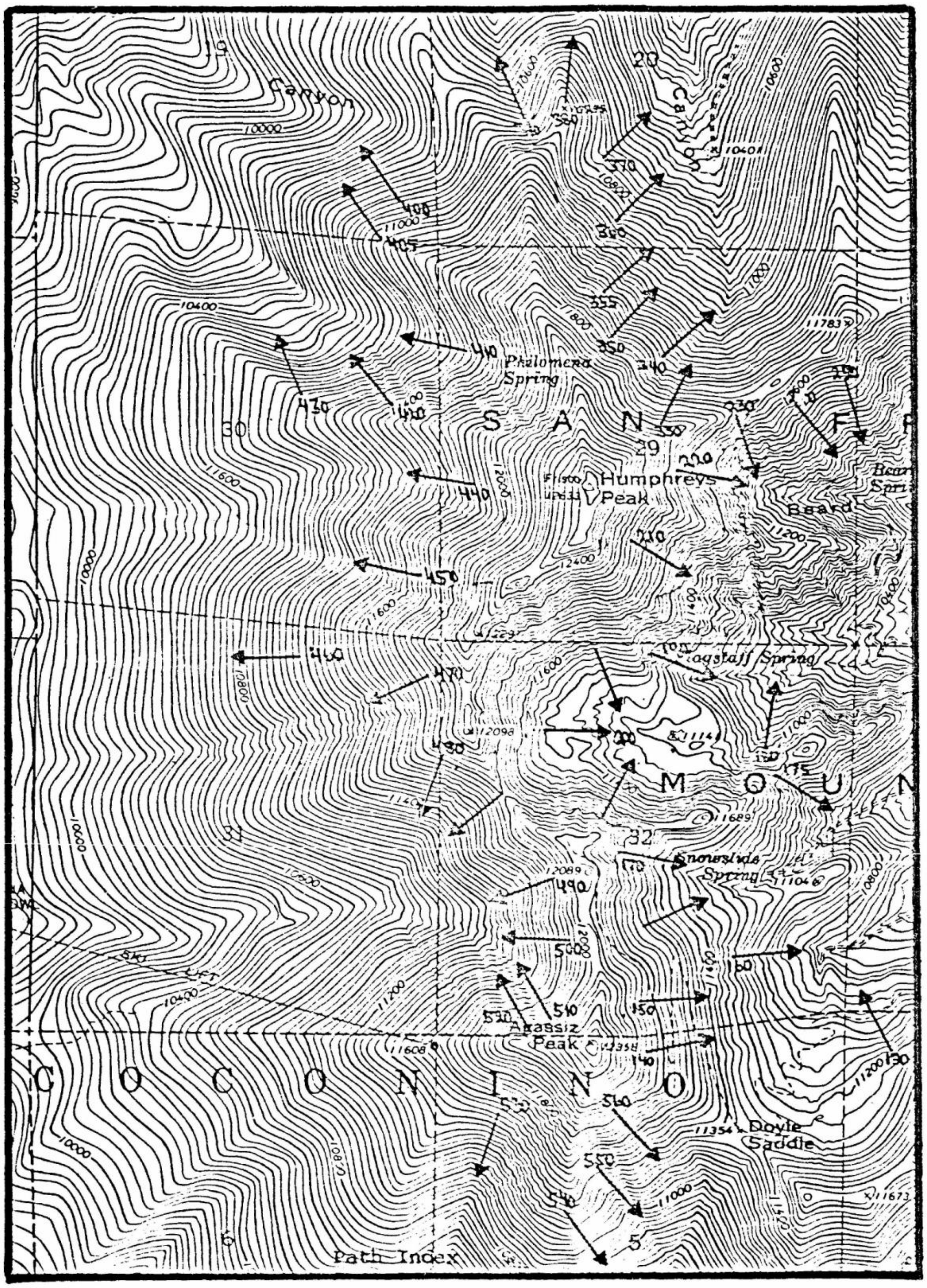
Canyon
Philomena Spring
S A N F
Humphreys Peak
Beard
Flagstaff Spring
M O U N
Snowslide Spring
Agassiz Peak
C O C O N I N O
Doyle Saddle
Path Index

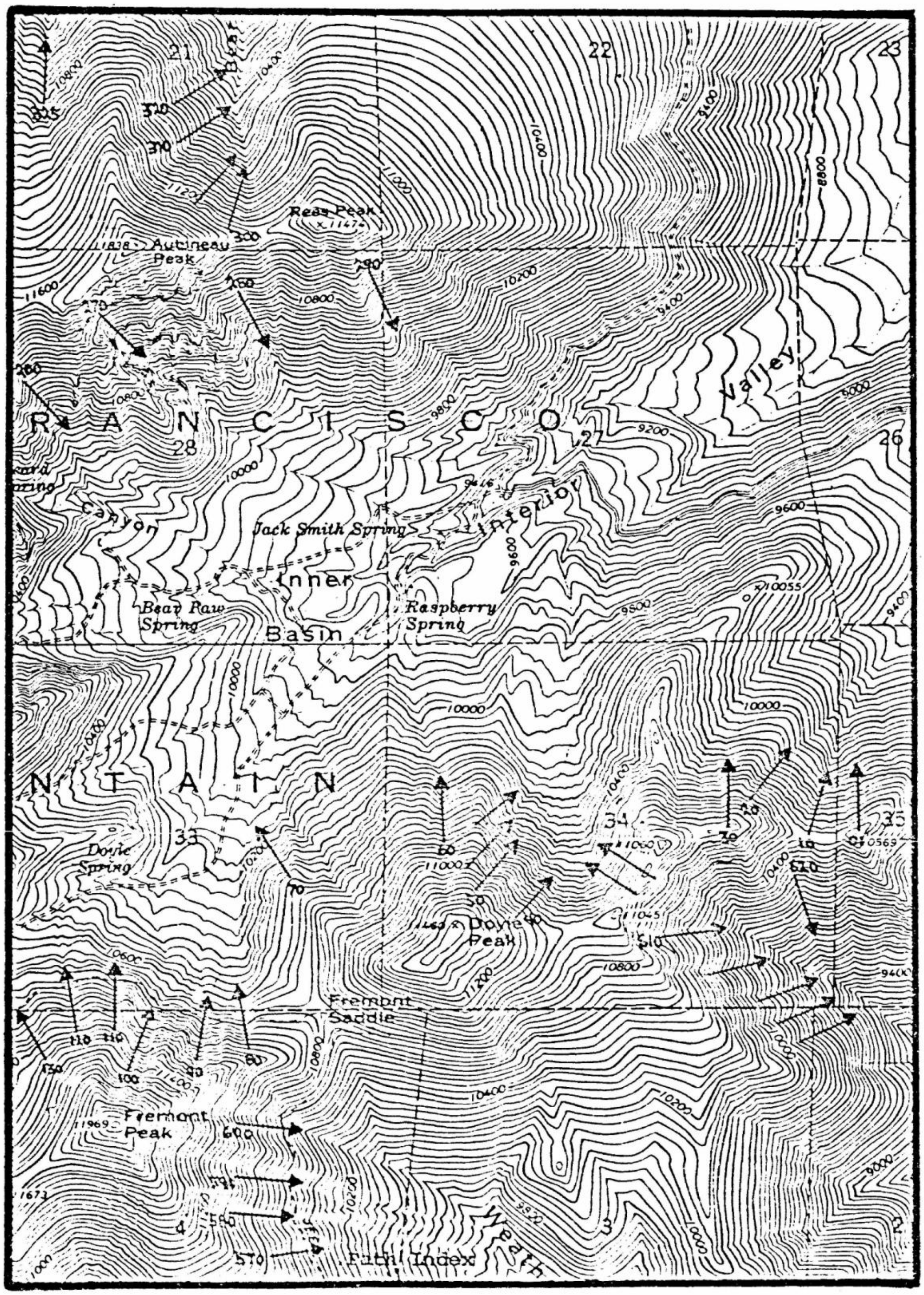
Autineau Peak
Reas Peak
R A N C I S C O
N T A I N
Canyon
Jack Smith Spring
Interior
Inner Basin
Bear Paw Spring
Raspberry Spring
Valley
Doyle Spring
Doyle Peak
Fremont Saddle
Fremont Peak
Fifth Index
21
22
23
28
27
26
33
34
35
4
3
2

HAND-DRAWN MAP OF
SAN FRANCISCO PEAKS
SNOW AVALANCHE ZONES
ORIGINALLY INCLUDED
WITH THE THESIS

1981

UNITED STATES
DEPARTMENT OF THE INTERIOR
GEOLOGICAL SURVEY

# AVALANCHE TERRAIN MAP

BY LEE DEXTER

HUMPHREYS PEAK QUADRANGLE
ARIZONA–COCONINO CO.
7.5 MINUTE SERIES (TOPOGRAPHIC)

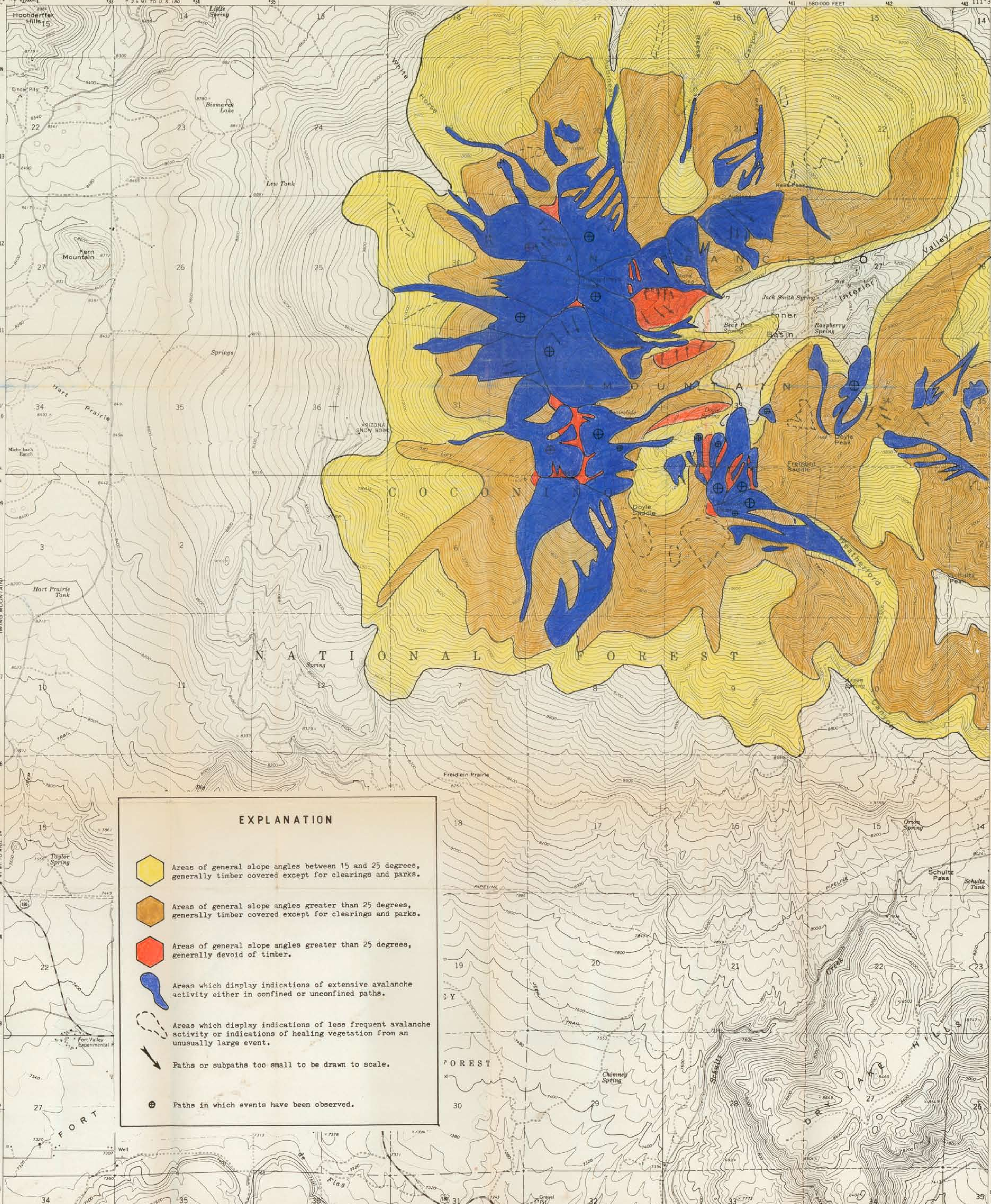


(BELLEMONT) 3654 III NE

(FLAGSTAFF WEST) 3654 II NW — FLAGSTAFF (U. S. 66) 4.8 MI.

(FLAGSTAFF EAST) 3654 II NE

INTERIOR—GEOLOGICAL SURVEY, RESTON, VIRGINIA—1974

Mapped, edited, and published by the Geological Survey

Control by USGS and USC&GS

Topography by photogrammetric methods from aerial photographs taken 1964. Field checked 1966

Polyconic projection. 1927 North American datum
10,000-foot grid based on Arizona coordinate system, central zone
1000-meter Universal Transverse Mercator grid ticks, zone 12, shown in blue

Fine red dashed lines indicate selected fence lines

GN MN 0°24' 7 MILS 14½° 258 MILS

UTM GRID AND 1966 MAGNETIC NORTH DECLINATION AT CENTER OF SHEET

SCALE 1:24 000

1 MILE — 7000 FEET — 1 KILOMETER

CONTOUR INTERVAL 40 FEET
DOTTED LINES REPRESENT 20-FOOT CONTOURS
NATIONAL GEODETIC VERTICAL DATUM OF 1929

ARIZONA
QUADRANGLE LOCATION

ROAD CLASSIFICATION
Medium-duty — Light-duty
Unimproved dirt
U. S. Route

THIS MAP COMPLIES WITH NATIONAL MAP ACCURACY STANDARDS
FOR SALE BY U. S. GEOLOGICAL SURVEY, DENVER, COLORADO 80225, OR RESTON, VIRGINIA 22092
A FOLDER DESCRIBING TOPOGRAPHIC MAPS AND SYMBOLS IS AVAILABLE ON REQUEST

HUMPHREYS PEAK, ARIZ.
N3515—W11137.5/7.5
1966
AMS 3654 I SW—SERIES V898

# GIS-PRODUCED MAP OF SAN FRANCISCO PEAKS SNOW AVALANCHE ZONES

2006

**Major Snow Avalanche Zones Map**
**for the San Francisco Peaks, Coconino County, Arizona**
**L.R. Dexter ©**

This document provides a descriptive key and metadata statement for an accompanying map of the same name. The map is made available as a public service to enhance the awareness of snow avalanches on the San Francisco Peaks. The map is designed to illustrate areas of potential major snow avalanche activity. Since avalanches can occur on very short and localized slopes, this map does not show every possible location where an avalanche can occur. In addition, the original study was limited to elevations above 8000'.  A good example of avalanche terrain not included on this map can be found along the Lockett Meadow Road where heavy snow years have produced small slab avalanches on slopes above the road.

This map is designed with any eye toward backcountry use. The areas where major avalanches are known (or presumed) to occur are shown in light blue. The remaining colors indicate slope angles with light green areas representing the more shallow-angled slopes, yellow areas indicating intermediate-angled slopes, and pink areas showing the steeper slopes. These slope classifications are useful when traveling through terrain where small clearings in the vegetation could be potential avalanche slopes that are too small to be included as a distinct major avalanche path:

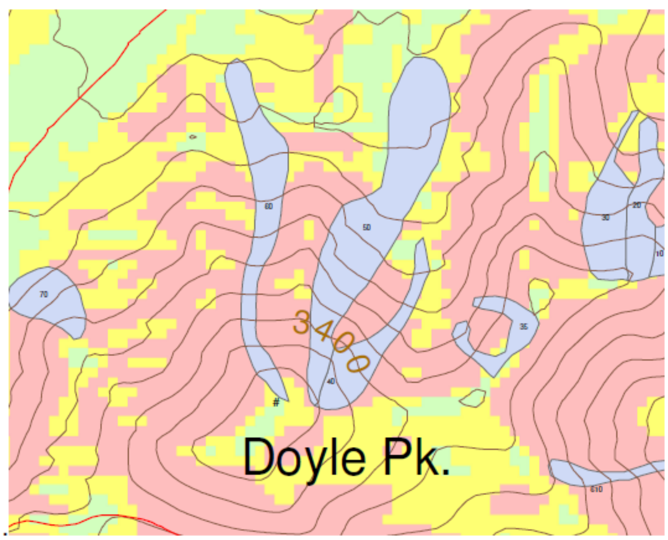


- Light Blue – Recognized major avalanche path
- Pink Zone – Slopes steeper than 25 degrees
- Yellow Zone – Slopes between 25 and 15 degrees
- Light Green Zone – Slopes shallower than 15 degrees

Slopes in the pink category conservatively contain all the major avalanche path starting zones. Any open area in the pink zone should be considered a potential avalanche starting zone under the right weather and snowpack conditions.

Slopes in the yellow category contain occasional starting zones (especially for smaller paths) along with the tracks and runouts of the larger avalanche paths. Slopes in the green category define the typical lower limit of avalanche activity on the “Peaks” but can contain the extreme lower portions of runout zones for some of the larger avalanche paths.

It must be emphasized that the coding used on this map is different from that found on the typical snow avalanche zone maps created for developed areas such as ski resorts. These developed-area avalanche maps typically include three or four color-coded hazard zones as shown below from a Swiss example:

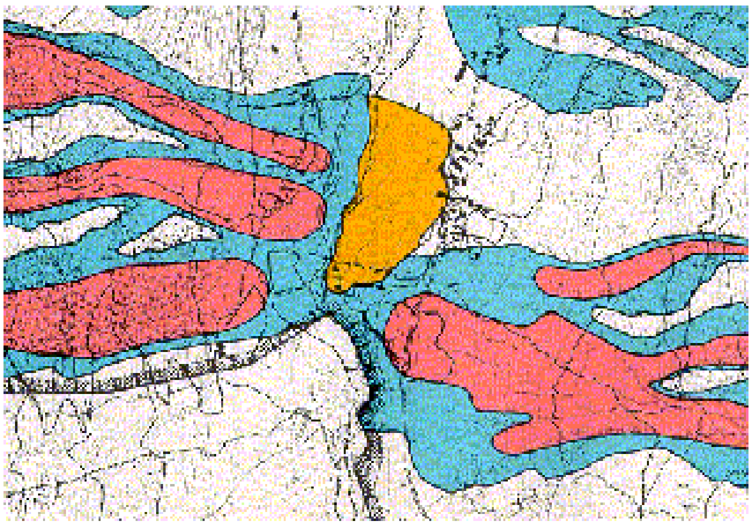

- Red Zone – No habitable structures allowed
- Blue Zone – Directly protected structures only
- Yellow Zone – Avalanches rare or of low impact
- White (green) Zone – No avalanche restrictions

These hazard maps are oriented toward structural placement and require engineering studies to delineate the various zones with any degree of confidence. Please keep the differences between the map types in mind.

The “Peaks” avalanche map is the culmination of work done beginning in the mid-1970s and continuing to this day. The map was compiled by Leland Dexter with field assistance from Arthur Pundt, Ken Walters, and other members of the San Francisco Mountain Avalanche Project or SFMAP (see History of Avalanche Studies on the San Francisco Peaks). The original map was produced as a limited number of hand-drawn copies for inclusion with Dexter’s M.S. degree thesis titled *Snow Avalanches on the San Francisco Peaks, Coconino County, Arizona*. The thesis is available for use at the Cline Library, Northern Arizona University. Recently a digital copy of the full thesis has been produced and is available by request from the author (lee.dexter@nau.edu) or by direct download from the Kachina Peaks Avalanche Center web page (www.kachinapeaks.org).

The data used to create the original map included USGS 7.5' topographic maps, USFS aerial photography, and ground-based field studies. The avalanche path map was created by using an optical zoom-transfer scope (Bausch & Lomb ZT4-H) to superimpose aerial photographs onto a paper USGS 7.5 minute topographic quadrangle. Avalanche paths were subsequently traced onto the paper map using geomorphic and vegetative indicators seen in the photos. Field verification followed and included tree-damage observations, tree-ring avalanche event dates, geomorphic confirmation of path boundaries, and snow avalanche event observations. During the three winter seasons1977-1980, SFMAP members actively scoured the Peaks looking signs for avalanche activity. They recorded an average of seventeen avalanche events per year on the San Francisco Peaks during those years. Backcountry avalanche paths which have produced notably large or frequent natural avalanche activity include Telemark (#100), Snowslide Canyon (#170), Humphreys Cirque (#200), Dunnam Canyon (#210), Crossfire (#360), Allison Clay (#450), and Monte Vista (#560). Many of the avalanche paths located in the Arizona Snowbowl permit area have responded to explosives control.

The numbering and naming system developed by San Francisco Mountain Avalanche Project is used on the map. The path numbers start with #1 (Boulderfield) on the lower eastern slopes of the mountain where avalanche activity is minimal. Numbering progresses counterclockwise around the outer flanks, with an excursion into, and out of, the Inner Basin; and ends up at back at the east side with Waterboard (#620). The numbers increment by 10 so that other paths identified as significant in subsequent years can be inserted between existing numbered paths without having to renumber the entire sequence. Several examples exist of paths inserted in such a fashion (the Core Ridge groups and Cleaver groups for example). For smaller avalanche paths found within the boundaries of a major path, or path group, a decimal numbering system is proposed. As an example, the larger of the two "Core Ridge" formations has a grouping of small chutes collectively called Hardcore South Group (#173) and Hardcore North Group (#177). When it becomes necessary to identify these smaller paths for avalanche purposes, the numbering would become #177.1, #177.2, #177.3 etc. It should be mentioned that naming conventions applied to the summits themselves reflect original and correct spelling (for example Aubineau and not Abineau; Rees and not Reese. These names may disagree with those printed on USGS and USFS maps).

Between 2004 and 2006, Dexter digitized the original map into ArcView/ArcGIS format, adjusted some of the avalanche path boundaries to match newer Digital Ortho Quarter Quad (DOQQ) photography, and updated some of the path names to match conventions developed in more recent years by the Arizona Snowbowl Ski Patrol (provided by B.J. Boyle)(see the attached metadata statement). Updating will continue as a new series of DOQQs are in production at the USGS as of early 2006 and general release is expected soon. Once the avalanche path layer was produced, a USGS Digital Elevation Model (DEM, 10 meter grid spacing) was processed to yield a 50 meter contour layer and a classed slope layer. A USFS trails layer and a summits layer were added to complete the final map. Collar information was added and the map was exported in .PDF format for public use. Two .PDF versions are available. The first is optimized for 8.5 x 11 inch printing and the second is optimized for larger format plotting. There are some companion products available including a path outline map with names labeled directly on the map, a spreadsheet list of path names and numbers, and a metadata statement for the avalanche path GIS layer. Samples of these items are attached below:

Rockpile
Noname
Northridge
Night Mare
Espil
White Horse
Anasazi
Sinagua
Crossfire
Dike
Stabilizer
Liberator
Bear Jaw Canyon
Squeeker
Aspen
Cliffband
Lew Canyon
Pipeline
Maybe Not
Aubineau Canyon
Cohonina
Zipper
Crisco
Cutoff
Philomena Spring
Beard Canyon
Cleaver North Group
Dunnam Canyon
Cleaver South Group
Allison Clay
Spring Slide
Flying Dutchman
Riser
Hardcore North Group
Temptations (Gadzooks)
Humphreys Cirque Group
Sickle Moon
Hidden
Boulderfield
Hardcore South Group
Rustler
Telescope
Baby Peaks
Dice
Sneaky Pete
Sundance
Softcore South Group
Scorpion
Waterboard
Shiprock
Snowslide Canyon
Black Bear
Big Bowl/Lower Bowl
Roadway
Survey Post
Corner
Silverton
Larry's Line
Upper Lightning
Inner Basin
Weatherford
Offchute
Outside
Study Plot
Blowout Basin
Jay's Slide
Telemark
Determination
Monte Vista (Rick's)
Snake Eye
Angel Food
Seven Meadows (Gully One)
Watson
Kachina
Solitude (Gully Two)
Meadow
The Glades (Gully Three)

| PATH_NAME | DEX_NUMBER | MAJOR_GRP |
|---|---|---|
| Boulderfield | 1 | Baby Peaks East |
| Dice | 10 | Baby Peaks East |
| Hidden | 20 | Baby Peaks East |
| Baby Peaks | 30 | Baby Peaks East |
| Scorpion | 35 | Baby Peaks East |
| Black Bear | 40 | Doyle Peak North |
| Telescope | 50 | Doyle Peak North |
| Sickle Moon | 60 | Doyle Peak North |
| Sneaky Pete | 70 | Doyle Peak West |
| Jay's Slide | 80 | Fremont Peak North |
| Silverton | 90 | Fremont Peak North |
| Offchute | 95 | Fremont Peak North |
| Telemark | 100 | Fremont Peak North |
| Roadway | 110 | Fremont Peak North |
| Corner | 120 | Fremont Peak West |
| Weatherford | 125 | Fremont Peak West |
| Study Plot | 130 | Fremont Peak West |
| Blowout Basin | 140 | Agassiz Peak East |
| Inner Basin | 150 | Agassiz Peak East |
| Survey Post | 160 | Agassiz Peak East |
| Softcore South Group | 165 | Core Ridge |
| Snowslide Canyon | 170 | Agassiz Peak East |
| Hardcore South Group | 173 | Core Ridge |
| Hardcore North Group | 177 | Core Ridge |
| Riser | 180 | Humphreys Peak East |
| Spring Slide | 190 | Humphreys Peak East |
| Humphreys Cirque Group | 200 | Humphreys Peak East |
| Dunnam Canyon | 210 | Humphreys Peak East |
| Cleaver South Group | 213 | Humphreys Peak East |
| Cleaver North Group | 217 | Humphreys Peak East |
| Beard Canyon | 220 | Humphreys Peak East |
| Cutoff | 230 | Cliffbands Southeast |
| Zipper | 240 | Cliffbands Southeast |
| Crisco | 250 | Cliffbands Southeast |
| Cliffband | 260 | Cliffbands Southeast |
| Squeeker | 270 | Cliffbands Southeast |
| Aspen | 280 | Cliffbands Southeast |
| Bear Jaw Canyon | 290 | Bear Jaw Canyon |
| Liberator | 300 | Bear Jaw Canyon |
| Stabilizer | 310 | Bear Jaw Canyon |
| Dike | 320 | Bear Jaw Canyon |
| Aubineau Canyon | 330 | Aubineau Canyon |
| Cohonina | 340 | Aubineau Canyon |
| Sinagua | 350 | Aubineau Canyon |
| Anasazi | 355 | Aubineau Canyon |
| Crossfire | 360 | Aubineau Canyon |
| Espil | 365 | Aubineau Canyon |
| Northridge | 370 | North Ridge |
| Rockpile | 380 | North Ridge |
| Noname | 390 | North Ridge |
| White Horse | 400 | Humphreys Peak West |
| Night Mare | 405 | Humphreys Peak West |
| Lew Canyon | 410 | Humphreys Peak West |
| Pipeline | 420 | Humphreys Peak West |
| Maybe Not | 430 | Humphreys Peak West |
| Philomena Spring | 440 | Humphreys Peak West |
| Allison Clay | 450 | Humphreys Peak West |
| Flying Dutchman | 460 | Humphreys Peak West |
| Temptations (Gadzooks) | 470 | Humphreys Peak West |
| Rustler | 480 | Snow Bowl |
| Sundance | 490 | Snow Bowl |
| Shiprock | 495 | Snow Bowl |
| Big Bowl/Lower Bowl | 500 | Snow Bowl |
| Larry's Line | 510 | Snow Bowl |
| Upper Lightning | 520 | Snow Bowl |
| Seven Meadows (Gully One) | 525 | Agassiz Peak Southside |
| Solitude (Gully Two) | 530 | Agassiz Peak Southside |
| The Glades (Gully Three) | 535 | Agassiz Peak Southside |
| Watson | 540 | Agassiz Peak Southside |
| Snake Eye | 550 | Agassiz Peak Southside |
| Monte Vista (Rick's) | 560 | Agassiz Peak Southside |
| Meadow | 570 | Fremont Peak East |
| Kachina | 580 | Fremont Peak East |
| Angel Food | 590 | Fremont Peak East |
| Determination | 600 | Fremont Peak East |
| Outside | 610 | Baby Peaks East |
| Waterboard | 620 | Baby Peaks East |

## *San Francisco Peaks Avalanche GIS Layer Metadata*

***LAYER/DATA SET NAME:*** Avalanche06

***DATA CREATOR/CUSTODIAN SECTION:***

1. *Contact Person:* Leland R. Dexter (Creator)
2. *Contact Telephone:* 928-523-6535
3. *Contact Email:* lee.dexter@nau.edu
4. *Contact Mailing Address 1:* Department of Geography, NAU Box 15016
5. *Contact Mailing Address 2:* Northern Arizona University
6. *Contact City:* Flagstaff
7. *Contact State:* AZ
8. *Contact ZIP Code:* 86011

***DATA IDENTIFICATION SECTION:***

9. *Layer/Data Set Name:* Avalanche06
10. *Date Created:* December 2004
11. *Date Last Modified:* January 2006
12. *Data Representation Model:* Vector
13. *Data Object Type:* Polygons
14. *Digital Format:* ESRI Shapefile
15. *Thematic Key Words:* San Francisco Peaks, Snow Avalanche, Backcountry Skiing
16. *Data Extent SW corner:* 435500 (E), 3906700 (N)
17. *Data Extent SE corner:* 443500 (E), 3906700 (N)
18. *Data Extent NE corner:* 443500 (E), 3913700 (N)
19. *Data Extent NW corner:* 435500 (E), 3913700 (N)
20. *Data Dictionary:*
    a. Path_name (C), name of the avalanche path given by Dexter, 1981
    b. Dex_number (I), number of the avalanche path given by Dexter, 1981
    c. Major_grp (C), major avalanche path group
    d. Path_type (C), type of path (simple, complex etc.)
    e. Apx_aspect (C), approximate aspect of the path
    f. Load_dir (C), loading direction
    g. Ob_ev78_80 (I), number of observed events from 1978-1980
    h. Ob_ev_yrs (I), number of years with observed events from 1978-1980
    i. Tre_ring_dt (I), years where tree ring indicators show avalanche activity
    j. Data_sourc (C), data source = L.R. Dexter
    k. Yr_mapped (I), year the path was originally mapped
    l. Yr_modifie (I), year the path was re-mapped
    m. Notes (C), any comments
21. *Data Completeness:* Complete as presented by Dexter, 1981, Subject to further field updates.
22. *Data Consistency:* Some objects derived by tablet digitizing were modified by heads-up screen digitizing following DOQQ based features.
23. *Description:* Snow avalanche terrain on the San Francisco Peaks from Dexter, 1981, 2004-6

***SOURCE SECTION:***

24. *Source Name:* Snow Avalanche Zones on the San Francisco Peaks
25. *Source Format:* USGS paper 7.5 minute quadrangle
26. *Source Quality:* Very good, new manuscript
27. *Source Scale:*1:24000
28. *Creator of Source:* L.R. Dexter
29. *Date of Source:* 1981 NAU MS Thesis, revised September, 2004 from DOQQs
30. *Data Conversion Methodology:* Tablet digitizing with heads-up updating from DOQQs
31. *Other Lineage Notes:* Features drawn on a standard 7.5 minute topo base map using an optical zoom-transfer scope and conventional USFS air photos in 1981. Features updated in 2004 with DOQs from the early 1990s.

(Continued)

***PROJECTION SECTION:***

32. *Coordinate System:* UTM, Zone 12, North
33. *Horizontal Datum:* NAD 1927
34. *Vertical Datum:* NAVD 1929
35. *Projection:* Transverse Mercator
36. *Horizontal Units:* Meters
37. *Vertical Units:* Meters

***ACCURACY/PRECISION/RESOLUTION SECTION:***

38. *Horizontal Accuracy:* 2 meters RMS at digitizing time
39. *Horizontal Precision:* 20 meters
40. *Vertical Accuracy:* Unknown
41. *Vertical Precision:* Unknown
42. *Resolution (or RESEL per Tobler, 1987):* RESEL = 858 meters
43. *Minimum Mapping Unit:* 30 meters

***METADATA REFERENCE SECTION:***

28. *Metadata Revision Date*: January 17, 2006

***COMMENTS SECTION:***

44. *Data Set Description:* Snow Avalanches on the San Francisco Peaks, Coconino County, Arizona
45. *Bibliographic Reference:*; See Dexter, L.R. (1981) Snow Avalanches on the San Francisco Peaks, NAU MS Thesis for more details.
46. *Other Comments:* A .PDF copy of a map created using this data layer (combined with others) is available for free public distribution. The original GIS data layer is proprietary.

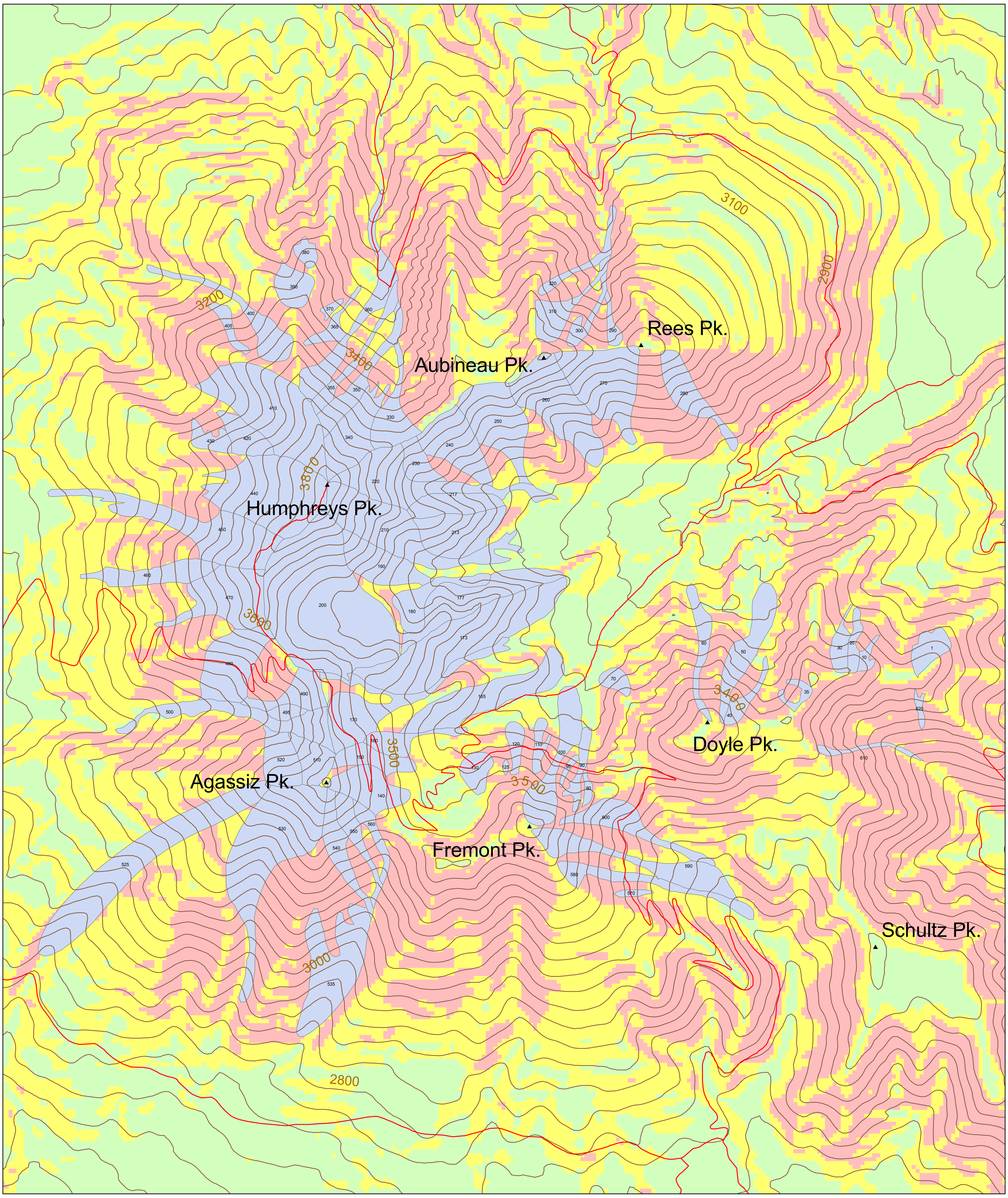


**Legend**

- Summits
- Trails
- Contours

**Slope Angle Class**

- <15 degrees
- 15-25 degrees
- >25 degrees
- Avalanche Paths
- 470 Path Number

# Major Snow Avalanche Zones

## on the San Francisco Peaks
## Coconino County, Arizona

0 1,000 2,000 3,000 4,000 Meters

Contour Interval 50 Meters

N

UTM Zone 12 NAD 1927
Mapping by L.R. Dexter, 1981©
Northern Arizona University.
Based on aerial photos and
ground surveys. Revised 2004-6
based on DOQQ photography
For further details see
Dexter, L.R. ,1981, NAU MS Thesis
Disclaimer: avalanches may occur at locations
other than those shown on this map